CRANFIELD UNIVERSITY

YUFEI LIN

# SYSTEM DIAGNOSIS USING A BAYESIAN METHOD

SCHOOL OF AEROSPACE, TRANSPORT AND MANUFACTURING
IVHM CENTRE

PhD
Academic Year: 2014 - 2017

Supervisors:Prof Ian K. Jennions
Dr Zakwan Skaf

Sep 2017

CRANFIELD UNIVERSITY

SCHOOL OF AEROSPACE, TRANSPORT AND MANUFACTURING
IVHM CENTRE

PhD

Academic Year 2014 - 2017

Yufei Lin

# SYSTEM DIAGNOSIS USING A BAYESIAN METHOD

Supervisors:Prof Ian K. Jennions
Dr Zakwan Skaf
Sep 2017

This thesis is submitted in partial fulfilment of the requirements for the degree of PhD

# ABSTRACT

Today's engineering systems have become increasingly more complex. This makes fault diagnosis a more challenging task in industry and therefore a significant amount of research has been undertaken on developing fault diagnostic methodologies. So far there already exist a variety of diagnostic methods, from qualitative to quantitative. However, no methods have considered multi-component degradation when diagnosing faults at the system level. For example, from the point a new aircraft takes off for the first time all of its components start to degrade, and yet in previous studies it is presumed that apart from the faulty component, other components in the system are operating in a healthy state. This thesis makes a contribution through the development of an experimental fuel rig to produce high quality data of multi-component degradation and a probabilistic framework based on the Bayesian method to diagnose faults in a system with considering multi-component degradation. The proposed method is implemented on the fuel rig data which illustrates the applicability of the proposed method and the diagnostic results are compared with the neural network method in order to show the capabilities and imperfections of the proposed method.



Keywords: fault diagnostic method, probabilistic framework, multi-component degradation, experimental fuel rig, neural network method

# ACKNOWLEDGEMENTS

First, I would like to thank Professor Ian K. Jennions who is my primary supervisor for all the guidance and time he has given during the past three years. It's my honour to be his PhD student.

I am also grateful for the assistance of Dr. Zakwan Skaf, who is my secondary supervisor.

My gratitude extends to Professor Steve King from Rolls-Royce Company for his valuable suggestions and discussions during this research project.

Further acknowledgement is extended to my colleagues in the IVHM Centre, especially to Dr. Mohammad Samie and Dr. Manuel Esperon-Miguez for their technical guidance and encouragement during the construction of the experimental fuel rig.

Last but not least, I would like to thank my parents for letting me study for so long and so far away from home.

This research is funded by the China Scholarship Council (CSC).

# TABLE OF CONTENTS

# LIST OF FIGURES

# LIST OF TABLES

# LIST OF EQUATIONS

# LIST OF ABBREVIATIONS

| | |
|---|---|
| AC | Alternating Current |
| AHU | Air-Handling Unit |
| APU | Auxiliary Power Unit |
| ATA | Air Transport Association |
| AUV | Autonomous Underwater Vehicle |
| CAE | Computer-Aided Engineering |
| CBM | Condition-Based Maintenance |
| CG | Central Gravity |
| CP | Conditional Probability |
| CWT | Continuous Wavelet Transform |
| DAQ | Data Acquisition |
| DPV | Direct-Acting Proportional Valve |
| DWT | Discrete Wavelet Transform |
| ECS | Environmental Control System |
| EKF | Extended Kalman Filter |
| FAA | Federal Aviation Administration |
| FFT | Fast Fourier Transform |
| FTA | Fault Tree Analysis |
| GA | Genetic Algorithm |
| GUI | Graphical User Interface |
| HMM | Hidden Markov Model |
| HVAC | Heating, Ventilation and Air Conditioning |
| IVHM | Integrated Vehicle Health Management |
| LRU | Line-Replaceable Unit |
| LVQ | Learning Vector Quantization |
| MLP | Multi-Layer Perceptron |
| MRO | Maintenance, Repair and Overhaul |
| NI | National Instruments |
| NN | Neural Networks |
| PCA | Principle Components Analysis |
| PDF | Probability Density Functions |
| PHM | Prognostics and Health Management |

| | |
|---|---|
| PLS | Partial Least Squares |
| PNN | Probabilistic Neural Network |
| RUL | Remaining Useful Life |
| SDG | Signed Digraph |
| SVM | Support Vector Machine |
| UAV | Unmanned Aerial Vehicle |
| V&V | Verification and Validation |

# 1 Introduction

This chapter presents an overview of the research project. The research background is introduced in Section 1.1, followed by the research aim and objectives in Section 1.2. The thesis contribution is presented in Section 1.3 while Section 1.4 provides an overview of the research project. The published papers related to this thesis are listed in Section 1.5, followed by the thesis organization in Section 1.6.

## 1.1 Research Background

In the past few decades engineering systems have become increasingly more complex. At the same time, the demands on the reduction in life cycle costs of the engineering systems are increasing. These make MRO (Maintenance, Repair and Overhaul) a more challenging task in industry. For example, in the aviation market, the MRO cost was $64.3 Billion in 2015, and is expected to grow at 4.1% every year until 2025 to $96 Billion (Michaels, 2016). How to reduce this magnitude of cost and increase the safety and availability of the aircraft systems at the same time is a crucial issue faced by the aviation industry.

Current maintenance strategy can be broadly categorized into preventive (scheduled) maintenance and condition-based maintenance (CBM). Preventive maintenance is a kind of traditional maintenance that is regularly conducted on a system or component, while CBM is a relatively modern maintenance that will only be conducted when certain indicators show signs of fault or degradation. Compared with preventive maintenance, CBM includes fault diagnosis and prognosis. It can significantly reduce the maintenance costs, increase the safety and availability of the system.

Fault diagnosis is a main part of CBM. The aim of fault diagnosis is to stop the system and schedule a maintenance task once an abnormality has been detected. So far, a wide range of fault diagnostic methods have been developed, and the research in this field is still very active.

In the literature, there exist three views about the definition of fault diagnosis:

1. Fault diagnosis includes fault isolation and identification (Gustafsson and Gustafsson, 2000; Yu, 2013).
2. Fault diagnosis includes fault detection, isolation and identification (D'Angelo et al., 2014).
3. Fault diagnosis includes fault detection and isolation (Wheeler et al., 2010; Chen and Patton, 2012; Bouzida et al., 2011).

In this thesis, the third definition is adopted.

Fault diagnosis is a relatively mature subject when applied at the component level. However, for some engineering systems such as an aircraft, it is desirable to diagnose faults at the system or sub-system level for effective maintenance, i.e. identifying a specific LRU (Line-Replaceable Unit) that needs to be removed or repaired. A faulty LRU can be replaced by a healthy one without disassembling the faulty one when the airplane is on the ground. The airplane continues its mission and the availability of the airplane is only influenced by the time required to remove the faulty one and install a healthy LRU. The faulty LRU is then sent to the workshop where it will be disassembled, repaired and tested before it is ready for working in another airplane.

However, in an engineering system, all components start to degrade from the first day of service and do not degrade equally, yet the previous research implicitly assumes that apart from the faulty component, all other components are operating in a healthy state. In this backdrop, this thesis addresses the problem of how to diagnose a fault in a system by considering multi-component degradation through the development of a probabilistic framework using the Bayesian method. The proposed framework is validated using data generated from an experimental fuel rig and the results are compared with a well-known method.

## 1.2 Research Aim and Objectives

The aim of this research project is to develop a fault diagnostic methodology for complex systems with multi-component degradation.

In order to achieve this aim, the following objectives are established:

1. To conduct a full literature review on current fault diagnostic methods.
2. To develop a probabilistic framework from the classical Bayesian approach, considering multi-component degradation.
3. To design, construct and validate an experimental fuel rig in order to produce benchmark datasets from a complex system.
4. To validate the proposed framework using data generated from the experimental fuel rig.
5. To compare the proposed Bayesian method with another well-known method, in order to show the capabilities and imperfections of the proposed Bayesian method.

## 1.3 Thesis Contributions

From the point a new engineering system runs for the first time, all of its components start to degrade. However, previous research assumes that apart from the faulty component, all other components in the system are operating in a healthy state, which could lead to a wrong diagnostic result. Considering this problem, this thesis paves a way to diagnose a fault in a system while other components are degrading through the development of a probabilistic framework.

Because there is no publicly available dataset, an experimental fuel rig is designed, constructed and validated to obtain reproducible data on multi-component degradation. A simulation model of the fuel rig is also developed in order to test the performance of the rig system.

## 1.4 Overview of the Research Project

The Gantt chart for the whole research project is shown in Figure 1-1.

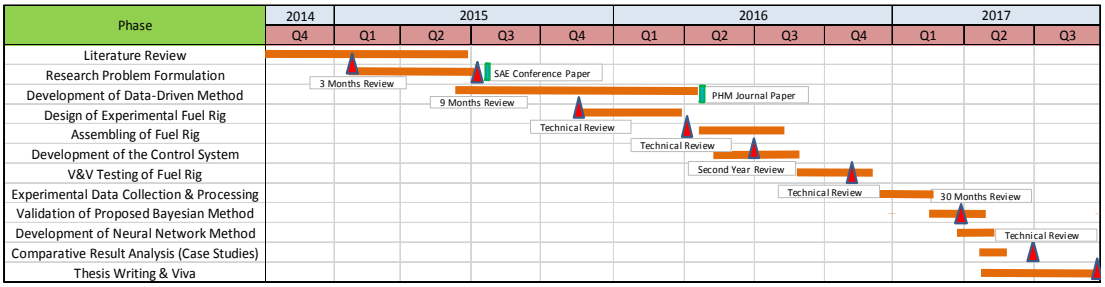


**Figure 1-1 Gantt chart for the whole research project**

The 3-year research project was conducted in three phases. During phase one, a full literature review was undertaken which provided an opportunity to formulate the research problem and identify the research aim and objectives. This study has resulted in the publication of a conference paper (Lin et al., 2015). After that, a probabilistic framework was developed based on the data-driven Bayesian method and the results were published in the PHM Journal (Lin et al., 2017). During phase two, an experimental fuel rig was developed in order to generate the degradation data for validating the proposed Bayesian method. The whole development process included the design, construction and V&V testing of the rig system. After completing the development of the experimental fuel rig, experiments were conducted to generate the data for validating the proposed Bayesian method, followed by the development of the neural network method in order to compare with the proposed Bayesian method. During phase three, the validation of the proposed Bayesian method and the neural network method was completed, followed by the comparative result analysis.

## 1.5 Published Papers

### Journal Paper

Yufei Lin, Skaf Zakwan, Ian K. Jennions, A Bayesian approach to fault identification in the presence of multi-component degradation, International Journal of Prognostics and Health Management, Vol 8. 004, 2017.

### Conference Paper

Yufei Lin, Skaf Zakwan, Ian K. Jennions, A Survey on Operational Safety Assessment in the Aviation Industry and its Link to IVHM, SAE AeroTech Conference, September 2015.

## 1.6 Thesis Organization

The organization of this thesis is shown in Figure 1-2:

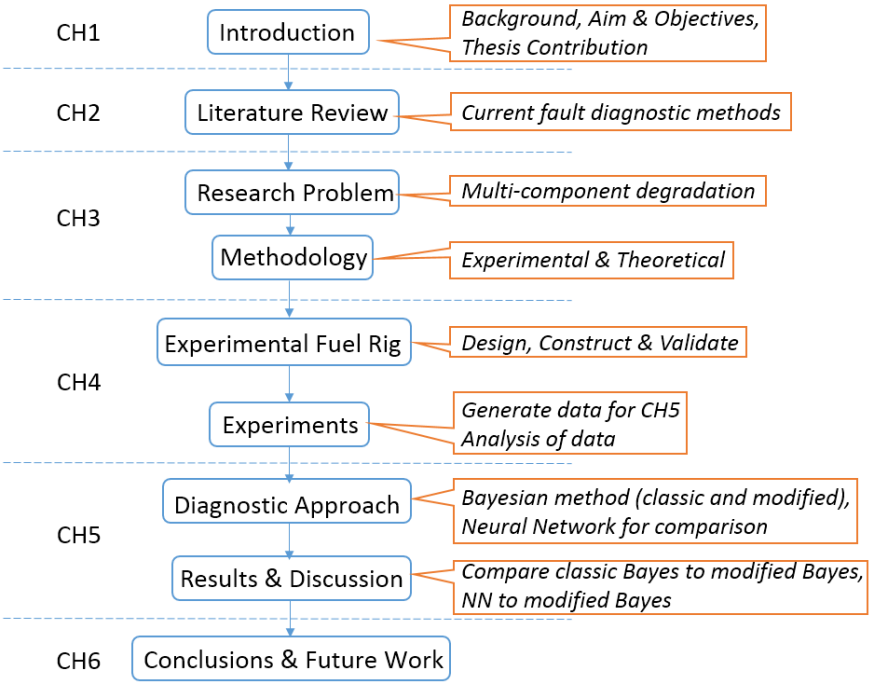


**Figure 1-2 Organization of the thesis**

Chapter 1 introduces the background of this research. The aim and objectives are laid out and the thesis contributions are presented.

Chapter 2 introduces current fault diagnostic methods. A detailed literature review and the gaps identified from the current methods are presented.

Chapter 3 focuses on the research problem formulation and the layout of the research methodology.

Chapter 4 describes the design, construction and verification and validation (V&V) testing of the experimental fuel rig in details. All these have placed the rig in a state where it could be used for research. The experiments conducted for the implementation of system diagnosis are also introduced.

Chapter 5 describes the data-driven Bayesian method (both classic and modified) and introduces a neural network method in order to compare with the proposed method. The metrics that are used to assess the performance of a diagnostic method are also introduced, followed by five different application scenarios that are used to validate the proposed Bayesian method and compare the diagnostic results. The discussion on the diagnostic results obtained from the five application scenarios is presented in the end.

Chapter 6 summarizes the research presented in this thesis and outlines the future work that needs to be done on this research.

# 2 Literature Review

This chapter aims to carry out an extensive literature review on current fault diagnostic methods and identify the relevant gaps in the knowledge.

Before moving on to the review of current fault diagnostic methods, it should be addressed that this thesis is focused on the diagnosis of single/individual fault. The methods for diagnosing multiple/combined faults is out of the scope of this research, but as some of the methods for multiple/combined faults can also be used for single/individual fault, they are covered in this literature review as well.

As mentioned in the previous chapter, fault diagnosis is a relatively mature subject when applied at the component level. The number of methods focus on diagnosing fault at the component level is significantly high compared with the methods applied on system or subsystem level diagnosis, but as the methods for component level diagnosis have many aspects in common with the methods for system or subsystem level diagnosis, they are put together in this literature review.

## 2.1 Review of Current Fault Diagnostic Methods

In general, current fault diagnostic methods can be divided into two classes: qualitative and quantitative, as shown in Figure 2-1. Qualitative methods include two subcategories: graph theory methods (Boukhobza et al., 2008) and expert system methods (Zhang and Roberts, 1991; Wu et al., 2012). Graph theory methods can be divided into signed digraph (SDG) method (Yang et al., 2012) and fault tree method (William, 2010). Quantitative methods include two subcategories as well: model-based methods and data-driven methods. Model-based methods (Yang et al., 2011; Meskin et al., 2013; Poon et al., 2015) include observer/filter-based method (Zhang and Pisu, 2014; Amoozgar et al., 2013; Caliskan et al., 2014), parameter estimation method (Rajaraman et al., 2004) and parity relation method (Willsky, 1976; Chen and Patton, 2012). Data-driven methods include signal processing method (Bouzida et al., 2011), machine learning method (Kankar et al., 2011; Ghate and Dudul, 2011; Vanini et al., 2014; Du et al., 2014; Tayarani-Bathaie et al., 2014; Ali et al., 2015; Chen

et al., 2013; Saimurugan and Nithesh, 2016; Jaber and Bicker, 2016; Rahmoune et al., 2017), fuzzy logic method (Mohammadi and Montazeri-Gh, 2015), statistical method (Yuwono et al., 2016) and hybrid method (Macgregor, 1989; Gertler and McAvoy, 1997; Jackson et al., 2005; Muralidharan and Sugumaran, 2012). The following subsections will present a detailed review of the fault diagnostic methods mentioned above.

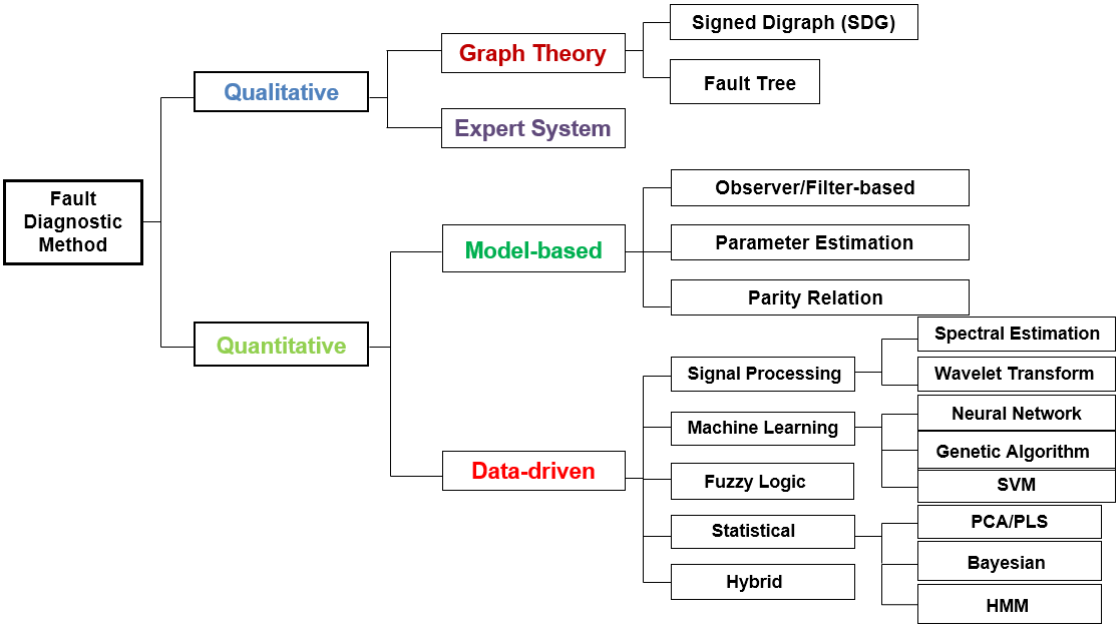


**Figure 2-1 Classification of current fault diagnostic methods**

### 2.1.1 Qualitative Methods

#### Graph Theory Method

Signed Digraph (SDG) Method

The SDG method has been widely used for fault diagnosis as it provides an efficient way to represent the relationships and interactions between different system variables. It does not need complete quantitative description of the system and can be developed from operator's experience. More specifically, a digraph contains a group of nodes and edges, in which the nodes represent the system variables (such as pressure, flow rate, temperature, etc.) and the edges represent the interrelationships between different variables. When a fault occurs in the system, the corresponding node will be highlighted and the possible faulty

component will be determined through a back-tracing from the highlighted node. Recently, Liu et al. (2014) proposed a hierarchical method of fault diagnosis based on the SDG which can improve the search efficiency of fault sources. The advantage of the SDG method is that it can deal with uncertainties, noise and incomplete system information, however, assumption of qualitative linearity, inability to perform multiple fault diagnosis and poor resolution are remains weakness.

### Fault Tree Method

Fault tree method is a conventional graph theory method developed by Bell Telephone Laboratory in 1961. It is a top down method in which a system level failure condition is analysed using Boolean logic. Due to its ease of use in representing the interaction of component faults in a system, fault tree method has been widely adopted in industries (Aslansefat et al., 2014; Chen et al., 2017; Zhang et al., 2016). More specifically, the starting points of a fault tree are the component faults in consideration, and the end point is the undesired or unsafe system state. The occurrence probability of the undesired or unsafe system state is the sum of probabilities from independent paths (there might be alternative logical paths through which a fault could propagate according to the rules of combinations). Although the fault tree could be very comprehensive, the weakness of it is that it has a huge table of probabilities and combinations in causal chains when dealing with a complex system such as aircraft system (Vesely et al., 2010). It produces too many redundancies that are difficult to handle in some cases.

Recently, the fault tree method has been used for optimizing maintenance planning (Rodrigues et al., 2015): based on the system architecture information and the remaining useful life (RUL) estimation of each component in the system, an overall system-level RUL can be estimated. In this way, the proposed method can improve the maintenance planning efficiency by identifying the impact of each component on the whole system degradation

level and neglecting the failure of a component that does not have a significant impact on the system. The workflow of this work is shown in Figure 2-2.

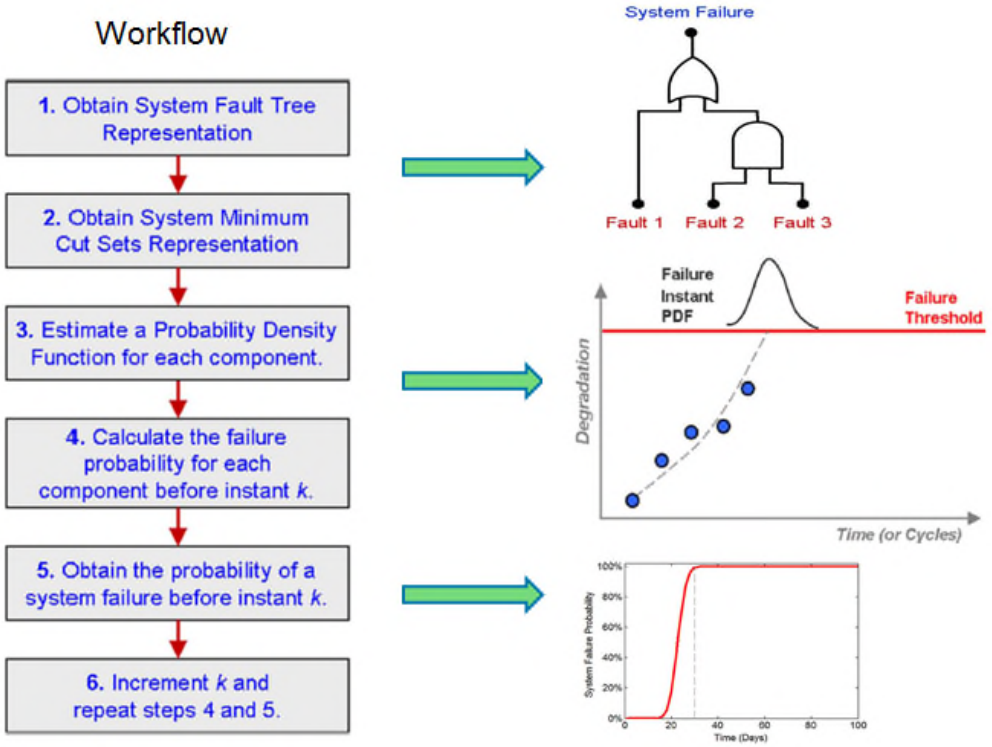


**Figure 2-2 Workflow (Rodrigues et al., 2015)**

### Expert System

Expert system method has been used for fault diagnosis for a long time (Liao, 2005). It is essentially an artificial intelligence method. The expertise of the target system is stored in the knowledge base, and maintainers will apply the extracted rules into failure situations. Initial attempts at using expert system method for fault diagnosis was found in Niida (1985). Recently, Zhi-Ling et al. (2012) applied expert system method to diagnose faults in wind turbine gearbox based on fault tree analysis. They developed a web-oriented expert system in C# which can save the fault diagnosis time. Regarding system level diagnosis, Schein and Bushby (2006) proposed a rule-based expert system method for heating, ventilation and air conditioning (HVAC) systems which takes component interdependence into account. The weakness of expert system

method is that it cannot diagnose a fault that has not been stored in the knowledge base. Moreover, because the experts' personal experience and judgement play a vital role in the fault diagnostic process, sometimes the result may be bias or conservative.

### 2.1.2 Quantitative Methods

#### Model-based Method

The model-based method has been the subject of interest for a long time in the realm of fault diagnosis. It usually uses a model of the target system or component to generate comparative measurements to detect fault, as shown in Figure 2-3. To be able to detect the deviations from the actual measurements, the model-based method first needs to define a baseline based on the system or component model. To create an accurate baseline, the model must be accurate enough to simulate the system or component performance which makes the model-based method more challenging to implement in complex systems. In addition, the model-based method is specific for each system. If the target system is modified then remodelling is usually required.

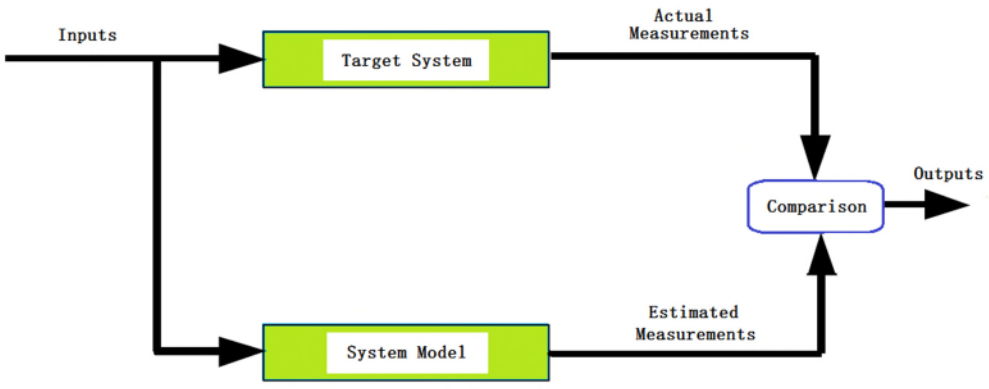


**Figure 2-3 Diagram for model-based method**

So far, a lot of work has been done using the model-based method for fault diagnosis, especially for real-time applications. Chen and Patton (2012) wrote a book about robust model-based fault diagnostic methods for dynamic systems which contains many methods and corresponding applications. Meskin et al.

(2013) proposed a real-time model-based method for fault diagnosis of aircraft jet engines. The proposed method can diagnose not only the single fault but also multiple concurrent faults in the engine. Poon et al. (2015 & 2017) proposed a real-time model-based fault diagnostic method for switching power converters. Their method can diagnose component and sensor faults, and operate in parallel with the converters. Sidhu et al. (2015) used adaptive nonlinear model-based method for fault diagnosis of Li-ion batteries such as over charge and over discharge which can cause significant model parameter variation. In terms of system level diagnosis, the model-based methods have been used for generating fault propagation models. Saha (2008) developed a model-based reasoning architecture for helicopter power-train modules. The proposed method can diagnose the inaccessible component's fault from observable system level behaviour.

The main advantage of model-based methods is that they can diagnose the fault with limited operating data. Moreover, they can diagnose unknown failure modes. The common weakness of model-based methods is that they need an accurate system model and their flexibility is limited as they work on a specific system model.

Kalman Filter

Kalman filter is a typical model-based method. It is a recursive filter of Gaussian least squares technique which has been widely used in the realm of fault diagnosis (Chen and Patton, 2012). A general Kalman filter model is shown in Eq. (2-1) and (2-2):

$$z_k = H_k x_k + v_k \quad \textbf{(2-1)}$$

$$x_k = \Phi_k x_{k-1} + B_k u_k + w_k \quad \textbf{(2-2)}$$

where $z_k$ is the measurement vector, $H_k$ is the system matrix, $x_k$ is the current state vector, $v_k$ is the measurement noise, $\Phi_k$ is the transition matrix which defines how state vector varies with time, $B_k$ is the control matrix, $u_k$ is the

control vector, $w_k$ is the process noise. Eq. (2-1) represents an estimation of the current measurement using current system state and Eq. (2-2) represents estimation of current system state using previous state and control inputs. When an initial condition is assumed, a successive estimate of the system state will be provided.

Recently, Amoozgar et al. (2013) applied Kalman filter to diagnose actuator faults in an unmanned quadrotor helicopter. Saravanakumar et al. (2014) used Kalman filter to diagnose sensor fault for wind turbine generators. Their proposed method can diagnose incipient faults and deal with the modelling/parametric uncertainties. Caliskan et al. (2014) utilized Kalman filter to detect actuator faults in a Boeing 747 model. Besides the conventional Kalman filter, extended Kalman filter (EKF) is also used to diagnose fault (Nadarajan et al., 2016; Delgado-Aguiñaga et al., 2016; Wu et al., 2016). It can reduce the approximation errors associated with the conventional Kalman filter. The weakness of Kalman filter is that it requires prior knowledge of the system and the initial condition can dramatically influence the result.

Parameter Estimation Method

The parameter estimation method is another typical model-based method. It usually deals with the fault that occurs as time dependent parameter drifts. A typical model used by the parameter estimation method is described as follows:

$$y(t) = f(u(t), \theta) \quad \textbf{(2-3)}$$

where parameter θ will be estimated when the measurements y(t) and u(t) become available, and θ in turn is related to the physical parameter φ of the system by θ=g(φ). Based on this relationship, the change in the physical parameter φ can be calculated which is related to a certain fault in the system. Based on the parameter estimation method, Rajaraman et al. (2004) developed an algorithm for fault diagnosis of nonlinear system with uncertainty in

parameters. The proposed methodology is able to achieve an accurate fault diagnostic result with no historical operational data.

The weakness of the parameter estimation method is that it often requires the availability of an accurate system model and has very high computational complexity when dealing with a complex system.

Parity Relation Method

The parity relation method is an open-loop technique that uses the residual (parity vector) generated by the system model to diagnose a fault. When the system is in a healthy state, the residual is zero, and the non-zero residual means a fault has occurred in the system. Recently, Laamami et al. (2015) proposed a fault diagnosis approach for nonlinear systems based on the parity relation method. Zhong et al. (2015) applied the parity relation method to fault diagnosis of linear time-varying systems with unknown input. Odendaal and Jones (2014) proposed an optimised parity relation method for fault diagnosis of aircraft control surface actuators. Hwang and Huh (2015) used the parity relation method for fault diagnosis of electromechanical brake systems. Same as other model-based methods, the parity relation method requires the availability of an accurate system model to generate the residual for fault diagnosis which makes it difficult to work with complex systems.

**Data-driven Method**

The data-driven method has been recognized as a very useful tool to extract knowledge from huge amounts of system monitoring data. Compared with the model-based method, the data-driven method does not require a system model for making diagnostic decisions and therefore is more flexible and adaptable. However, its use for fault diagnosis is still faced with some challenges. The main challenge is that its efficacy is highly dependent on the quantity and

quality of the system monitoring data. In the literature, a wide range of data-driven methods can be found for fault diagnosis.

*Signal Processing Method*

Signal processing methods are mainly used in fault diagnosis of the mechanical components (such as bearings, gearbox and rotors). The fault is reflected in the measured signals, and a diagnostic result is obtained based on the symptom (extracted features from the measure signals) analysis and prior knowledge of the symptoms under the healthy conditions. Typical signal processing methods include spectral estimation method and wavelet transform method.

Spectral Estimation Method

The spectral estimation method is a proven technique in the realm of fault diagnosis (Picón et al. 2009; Choqueuse and Benbouzid, 2015; Nasrolahzadeh et al., 2016; Trachi et al., 2016). Current spectral estimation method is usually conducted based on the fast Fourier transform (FFT) which is used to obtain the frequency spectrum from a signal. The variations of certain components in the frequency spectrum are related to a fault and thus can be used as the fault feature for fault diagnosis. So far, the FFT method has been successfully applied to diagnose a variety of faults (Liu et al., 2010; Xu and Zhou, 2016; Sapena-Bañó et al., 2015).

Wavelet Transform Method

The fundamental principle of the wavelet transform method is decomposing a signal into a series of frequency channels. In this way, the wavelet transform method is able to grasp both the time and frequency information in a signal and extract the features that vary in time. Generally, the wavelet transform method can be categorized into the continuous wavelet transform (CWT) and discrete wavelet transform (DWT), both have been widely used in the realm of fault

diagnosis (Singh et al., 2009; Bouzida et al. 2011; Gritli et al., 2013; Cabal-Yepez et al., 2013; Jaber and Bicker, 2016; Wang et al., 2014).

The main weakness of the signal processing methods is that their performances are highly dependent on the quality and quantity of the system monitoring data which is a common weakness of the data-driven methods.

*Machine Learning Method*

Neural Network (NN) Method

The neural network method is perhaps the most well developed machine learning method for complex systems. The networks are made up of simple processing units based on the structure of the human biological nervous system. A simple example of the processing unit is shown in Figure 2-4. The inputs are multiplied by synaptic weights and then added together. The sum is mapped to the output via activation function which determines whether the unit fires or not. Usually, the form of activation function is sigmoid or piecewise-linear.

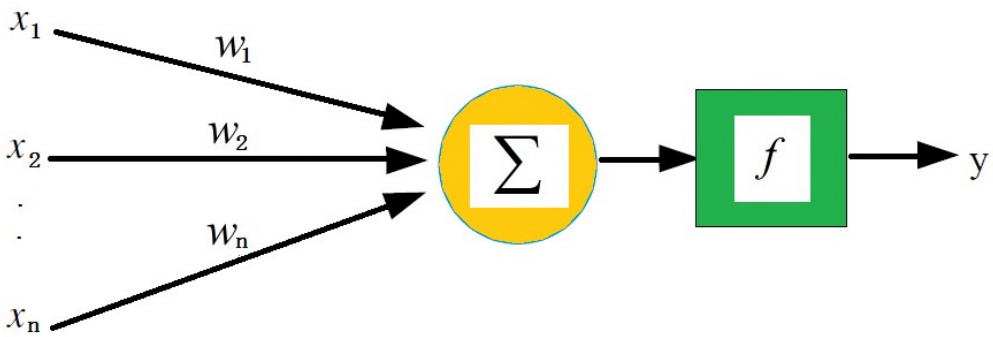


**Figure 2-4 Example of the processing unit**

To implement the neural network method, the first step and perhaps the most important step is training. So far, there already exist many training methods for the neural network, such as the back-propagation method (Jang et al. 1997, Maki and Loparo, 1997) by which the network's actual outputs can be compared

with the desired outputs, and the difference will be used to modify the synaptic weights.

After the training process, a neural network will be able to diagnose fault based on sensor readings. Due to its powerful adaptive learning and nonlinear function approximation capability, neural network method has drawn considerable attention in the realm of fault diagnosis. There exist many types of neural network used for fault diagnosis such as probabilistic neural network (PNN) (Romessis and Mathioudakis, 2002; Malik and Mishra, 2015; Zhang et al., 2014; Song et al., 2011; Dai et al., 2014; Loboda and Olivares, 2015), learning vector quantization (LVQ) neural network (Malik and Mishra, 2015; Liu et al., 2009; Zhou et al., 2013), multi-layer perceptron (MLP) network (Waqar and Demetgul, 2016; Kamal and Yu, 2014; Payganeh et al., 2012), deep neural network (Jiang et al., 2016), dynamic neural network (Abed et al., 2014) and auto-associative neural network (Palmé et al., 2011).

In terms of system level diagnosis, Hare et al. (2015) applied neural network method to the environmental control system (ECS) of an aircraft and proposed a system level fault diagnostic method which allows for systematic elimination of healthy components through the hierarchical view of the system. Their proposed method reduced the false alarm and the computational complexity by eliminating healthy components in the system. Lee et al. (2004) developed an online subsystem level fault diagnostic method for a building's air-handling unit (AHU) using neural networks.

The advantage of neural network method is that it does not need a system model, only operating data is used to train the network. Moreover, it can handle the complex relationship between inputs and outputs, work in the presence of faulty sensors or missing information and tolerate noise. The main weakness of the neural network method is that it usually needs a significant amount of operating data and takes a long training time.

Genetic Algorithm (GA)

The genetic algorithm has been described as a search algorithm based on the mechanics of natural genetics. It imitates the process of evolution to diagnose the fault. During the fault diagnostic process, first, the actual sensor reading will be compared with the expected sensor reading corresponding to the current operating conditions. Then the deviations will be combined into an objective function:

$$J(x) = \sum_{i=1}^{n} \frac{[s_i - h_i(x)]^2}{(es_i\sigma_i)^2} \quad \textbf{(2-4)}$$

where n represents the total number of the sensor reading, $s_i$ is the ith sensor reading, $h_i$ is the ith simulated sensor reading, $es_i$ is the expected sensor reading corresponding to the current operating condition, $\sigma_i$ is noise. Through minimizing the objective function, genetic algorithm will find the degraded operating point corresponding to the actual sensor reading. The workflow of the genetic algorithm is shown in Figure 2-5.

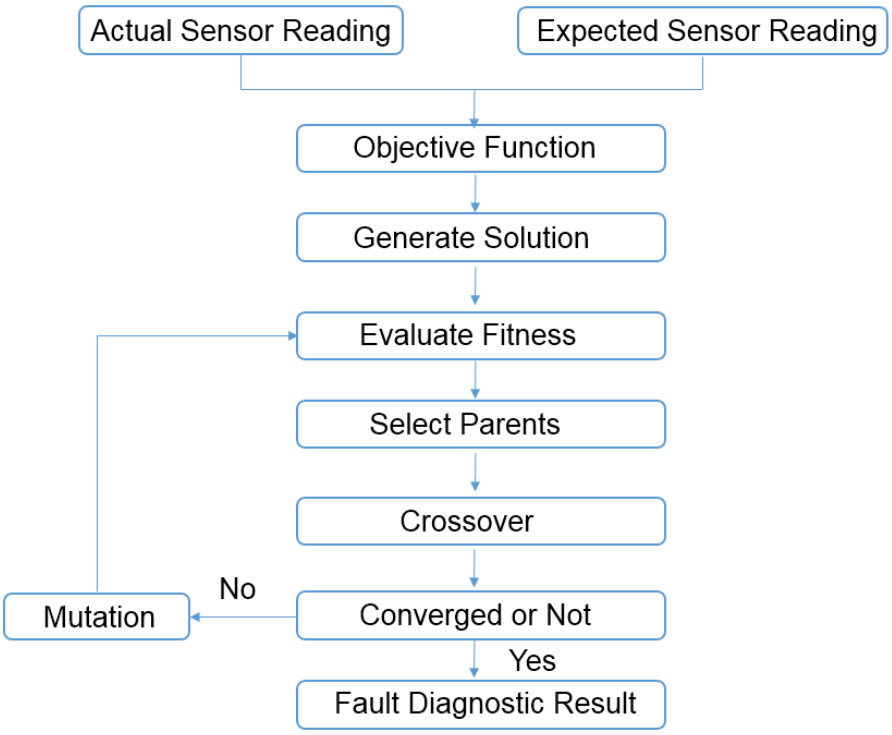


**Figure 2-5 Diagnostic process based on Genetic Algorithm**

So far, there already exists a lot of applications using the genetic algorithm to diagnose fault (Lu et al., 2015; Nguyen et al., 2014). Recently, Wu et al. (2016) proposed a new diagnostic framework based on genetic algorithm to diagnose multiple parametric faults in power electronic circuits. Cerrada et al. (2016) used the genetic algorithm for fault diagnosis in spur gears. The weakness of genetic algorithm is that it relies on the quantity of historic data and will take a long convergence time when dealing with several degraded components.

### Support Vector Machine (SVM)

Support vector machine method is a computational learning method based on statistical learning theory. It was proposed by Vapnik and Vapnik (1998) and has become popular in machine learning area due to its excellence of generalization capability compared with the traditional methods such as the neural network method. In the realm of fault diagnosis, the SVM method is used for recognizing patterns from acquired signal, and then those patterns are classified according to the occurrence of certain faults in the machine. So far, many works have been done on fault diagnosis using the SVM method. Yin et al. (2014) used the SVM method to diagnose satellite fault based on a hybrid voting mechanism. Their proposed method can deal with the problem of multiple faults, small samples and enormous parameters. Santos et al. (2015) proposed an SVM-based method for fault diagnosis in wind turbines. Tyagi (2008) and Zhang et al. (2015) used the SVM method to diagnose the rolling element bearings' faults. Seryasat et al. (2010) proposed a multi-class SVM method to diagnose multiple faults of the ball bearing. Armaki and Roshanfekr (2010) developed an SVM-based method for fault diagnosis of broken rotor bar in an induction motor. For further reading, more articles can be found in (Demetgul, 2013; Ozturk, 2016; Ma et al., 2016; Zhang and Zhou, 2013). The high algorithmic complexity is the main weakness of the SVM method.

### Fuzzy Logic Method

The fuzzy logic method was introduced by Zadeh (1973), it is a rule-based method that deals with possibility rather than probability. In the workings of the fuzzy logic method, the imprecise information will be converted to mathematical expressions through a graph representation of the fuzziness between two extremes degree values (usually 0 and 1). After this fuzzification step, inference will be applied and followed by a de-fuzzification process.

The fuzzy logic method has a wide range of applications from simple components to complex engineering systems (Zidani et al., 2008; Zarei et al., 2015; Holbert and Lin, 2012; Sheikh and Patel, 2016; Ramos et al., 2016). Recently, Mohammadi and Montazeri-Gh (2015) used the fuzzy logic method to detect faults in a gas turbine. The results showed that their proposed method can reduce the average estimation error and increase the success rate compared with other diagnostic methods. The advantage of the fuzzy logic method is that it can deal with noise and uncertainties with the use of linguistic expressions. It does not require a system model and therefore has high flexibility. However, difficulties of determining good fuzzy rules and limited capability of learning are the disadvantages of the fuzzy logic method.

*Statistical Method*

Principle Components Analysis (PCA)/ Partial Least Squares (PLS)

The PCA and PLS method are two main techniques used in multivariate statistical process monitoring (MSPM) framework which can avoid the time-consuming and challenging work of building physical models for complex systems. They have been widely applied to the chemical processes and their effectiveness for diagnosing fault is well recognized. More specifically, PCA method aims to extract the principle components that can reflect the change of a system so that the dataset size can be reduced when diagnosing a fault, while PLS method focuses on figuring out the fault in a certain measurement space which is often related to the output variables. In literature, there exists a lot of work using these two methods for fault diagnosis. Chen et al. (2016) used PCA

and PLS method for fault detection of wastewater treatment process. Tao et al. (2013) used PCA method for fault diagnosis of sensors in laboratorial wastewater treatment process. Chiang et al. (2000) applied PCA and discriminant PLS method in fault diagnosis of chemical processes. Xiao et al. (2016) developed a multiway PCA method for fault diagnosis of piercing production of seamless tube. The main weakness of PCA and PLS method is that their efficacy is highly dependent on the quality of system monitoring data, which is the common weakness of data-driven methods.

### Hidden Markov Model (HMM)

A hidden Markov model (HMM) is a statistical model in which the system being modelled is assumed as a Markov process with hidden states (i.e. faulty states which are not directly measurable). A typical HMM is completely defined by five parameters: 1. the number of states in the model; 2. the number of different observations for each state; 3. the initial state distribution; 4. the state transition probability distribution; 5. the observation probability distribution for each state. When applying the HMM to fault diagnosis, the extracted features from complete monitoring history of the system (from the healthy state to the faulty state) will be transformed into the model to obtain the above five parameters.

As the HMM allows for unobserved variables, it has been widely used for fault diagnosis. Recently, Yuwono et al. (2016) applied Hidden Markov Model in automatic bearing fault diagnosis. Alvarez and Lane (2016) used Hidden Markov Model with Gaussian Mixture emissions for fault diagnosis on a simulated AUV platform. Zhang et al. (2016) developed an online fault diagnostic method for electric machine based on the Hidden Markov Model. The main weakness of HMM is that it usually requires a long training time.

### Bayesian Method

The Bayesian method is a statistical method that can update the current probability of an event given new or additional evidence. The applications of Bayesian method have been found in the realm of image processing, medical science, pattern recognition, fault diagnosis and reliability analysis (Chien et al., 2002; Dey and Stori, 2005; Mehranbod et al., 2005; Steinder and Sethi, 2004; Mack et al., 2011). In the realm of fault diagnosis, commonly used Bayesian method includes Naïve Bayesian inference (Sankararaman and Mahadevan, 2013; Fernández-Cantí et al., 2013; Verbert et al., 2017) and Bayesian belief network (Romessis et al., 2001; Kadamb, 2003; Zhao et al., 2013; Askarian et al., 2016; Verron et al., 2010; Romessis and Mathioudakis, 2006; Ahooyi et al., 2014), both of them essentially use probabilistic knowledge from the target system to calculate the probability of certain faults.

The most appealing features of the Bayesian method include:

1. It can deal with simultaneous evidence and combine them together to get a result. Recently, Zhao et al. (2013) developed an intelligent chiller fault diagnostic methodology using a Bayesian method which can make use of conflicting information from the concerned chiller. Jiang et al. (2016) used the Bayesian method to diagnose fault with asynchronous measurements. Asr et al. (2017) developed a Bayesian method for diagnosis of combined faults in rotating machinery.
2. It can deal with uncertainties and non-linear relationship between cause and evidence. Recently, Yu and Rashid (2013) developed a novel dynamic Bayesian network for fault diagnosis of a chemical process. They characterized the causal relationships among the monitored parameters through the probability density functions (PDF) obtained from the process operating data and then used the Bayesian inference rule to calculate the probability of abnormalities. Sankararaman and Mahadevan (2013) also developed a Bayesian method for the quantification of uncertainties in fault diagnosis of the structural frame and hydraulic actuation system. Codetta-Raiteri and Portinale (2015) developed a dynamic Bayesian network for fault diagnosis in autonomous spacecraft (e.g. a Mars rover).

3. Based on statistical data or expert's judgment, it can avoid the difficulty and time-consuming work from building physical models of the target system and therefore become more applicable when an understanding of the principles of system operation is not clear (Jiang et al., 2012; Fernández-Cantí et al., 2013; Askarian et al., 2016; Yu, 2013).

Due to its advantages, the Bayesian method has been used for system level diagnosis. Verbert et al. (2017) used Bayesian method for system level fault diagnosis of HVAC systems through combining knowledge and historic data with the consideration of component interdependency and multiple operating modes. Lee et al. (2010) used Bayesian method for industrial gas turbines fault diagnosis in a steady state. The fault situations could be a single fault happened in one component or multiple faults occurred in more than one component.

The main weakness of Bayesian method is that it usually requires substantial time and effort to obtain the probabilistic knowledge from the target system.

*Hybrid Method*

Besides the methods mentioned above, there also exist many hybrid methods in the realm of fault diagnosis. Li et al. (2012) applied Kalman filter and SVM method to the rolling bearing fault diagnosis, and the detection rate is over 96.5%. Hocine and Ahmed (2016) applied neural network method and genetic algorithm to detect a bearing fault for the electric motor. Lee and Lan (2014) used neural network method and fuzzy logic method to diagnose a fault in dynamic systems. D'Angelo et al. (2011, 2014) proposed a fuzzy/Bayesian formulation for detecting a fault in dynamical systems. Li et al. (2016) used genetic algorithm and SVM for power transformer fault diagnosis. More articles can be found in (Lo et al., 2009; Kobayashi and Simon, 2005; Sampath and Singh, 2006; Wang et al., 2014; Laurentys et al., 2011; Loboda and Yepifanov, 2010; Wang and Chen, 2011; Chen et al., 2013; Tian et al., 2007; Najjar et al., 2013; Li et al., 2013; Unal et al., 2014).

## 2.2 Summary and gaps in the knowledge

Looking at qualitative and quantitative methods, as above, the advantages and disadvantages of current fault diagnostic methods are summarized in Table 2-1. It can be observed that methods in both categories have their own advantages and disadvantages. Qualitative methods suffer from the requirement of sufficient domain knowledge and experience in applied field, which is often found to be very difficult when dealing with complex systems. Quantitative methods, which include model-based methods and data-driven methods require many conditions to be met. Model-based methods require sufficient system information to build a model while data-driven methods have very high dependence on the quantity and quality of the system monitoring data.

**Table 2-1 Summarized advantages and disadvantages of current fault diagnostic methods**

| | Qualitative Methods | Quantitative Methods | |
|---|---|---|---|
| | | Model-based Methods | Data-driven Methods |
| Advantage | Wide application<br>Simplicity | Do not need extensive operating data<br>Able to diagnose unknown failure mode | Adaptable and flexible<br>Do not need system model |
| Disadvantage | Difficult to perform in complex system<br>Require sufficient domain knowledge and experience<br>Cannot cope with unknown failure mode | Require sufficient system information to build model<br>Limited flexibility<br>Hard to perform in complex system | High dependence on the quantity and quality of system operating data<br>High computational complexity |

Also, from the above literature review, it has been proved that compared with the methods applied to diagnose fault at the component level, the number of methods applied to system/subsystem level diagnosis is relatively low. So far, the fault tree method and expert system method under the qualitative category have been successfully applied to the system/subsystem level diagnosis while for the quantitative methods, the Bayesian method and neural network method have been implemented on the system/subsystem level diagnosis.

Both qualitative and quantitative methods, regardless of the component level or system/subsystem level, have not considered multi-component degradation when diagnosing a fault in a system. With this in mind, this thesis proposes a probabilistic framework to incorporate multi-component degradation information when diagnosing a fault in a system. The concept of multi-component degradation will be introduced in the next chapter.

As the Bayesian method has been used for system level diagnosis and can avoid the difficulty and time-consuming work from building physical models of the target system, the proposed probabilistic framework will make use of it which will be introduced in Chapter 5.

The neural network method is chosen to compare with the proposed Bayesian method due to its broad application in the realm of fault diagnosis. The implementation of the neural network method will be introduced in Chapter 5.

# 3 Research Methodology

The previous chapters introduced the necessary information to understand the background of the research and a review of the literature on current fault diagnostic methods. In this chapter, the research problem is described and the methodology to solve it is developed.

## 3.1 Research Problem Formulation

When dealing with the relationship between a sensor reading change and a fault (caused by a faulty component), ambiguity often turns out to be a problem. That is to say, different faults may cause the same sensor reading change (shown in Figure 3-1).

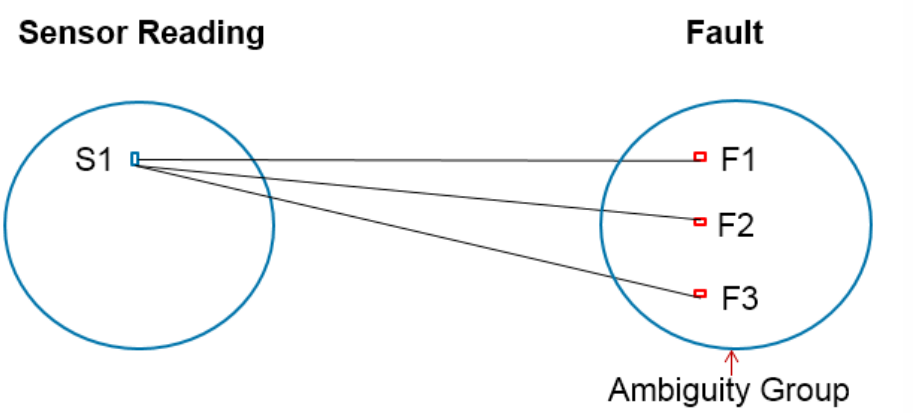


**Figure 3-1 Ambiguity group between sensor reading change and fault**

Under this condition, it is very challenging for us to distinguish different faults in the system. To solve this problem, current fault diagnostic methods usually use information from nearby sensors as reinforcement, shown in Figure 3-2. However, when integrating information from nearby sensors, current methods commonly assume that apart from the faulty component, other components in the system are healthy, i.e. no degradation happens in other components, and the sensory information would not be influenced by other non-faulty components.

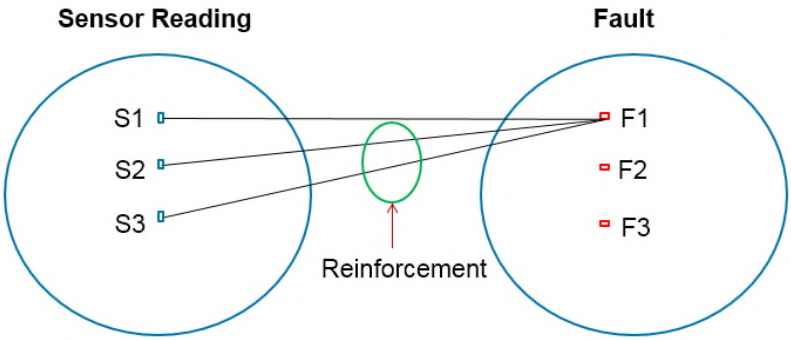


**Figure 3-2 Integrating sensory information for reinforcement**

In order to illustrate this multi-component degradation, a fuel rig test-bed (shown in Figure 3-3) developed in the IVHM Centre at Cranfield University (Niculita et al., 2014) is used.

**Figure 3-3 Photograph of the fuel rig in the IVHM Centre at Cranfield University**

This rig is specifically designed to replicate a number of component degradation faults with high accuracy and repeatability so that it can produce benchmark datasets to evaluate and assess the developed algorithms. It consists of a storage tank that contains water, a motor-driven gear pump with an internal relief valve that provides volumetric flow rate, a solenoid shut-off valve, five direct-acting proportional valves (DPVs), a flow meter and five pressure

sensors. The DPVs can be opened/closed to simulate degradation in the system due to: filter clogging (DPV 1), pump degradation (DPV 2), shut-off valve degradation (DPV 3), pipe leak (DPV 4), nozzle clogging (DPV 5). It can be run in a continuous circular manner. The layout of the fuel rig is shown in Figure 3-4.

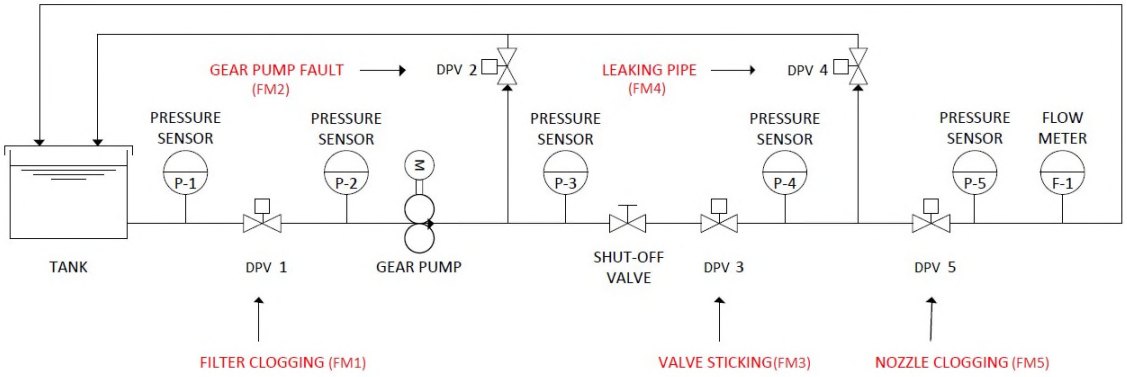


**Figure 3-4 Layout of the fuel rig**

Pressure values (P1-P5) from different points of the system and flow rate (F-1) in the main line are taken to be the indicators of a fault. The sensors' position is shown in Figure 3-4. In order to collect data from the sensors, a system using National Instruments LabVIEW instrumentation has been utilized.

So consider a simple example from the rig: the gear pump is running at 400rpm, and the pipe leaking fault is injected into the system. Figure 3-5 shows the reading change of pressure sensor 4 when the leak happens. The ordinate represents the opening percentage of DPV 4 while the abscissa represents the reading of pressure sensor 4. The red dotted line represents the reading with no leak. The effect of the leak is clearly seen as a reduction in the pressure measured by pressure sensor 4 as the gear pump is running at a constant speed. It should be noted here that if the demand on the pump speed is set by the flow meter (F-1), when the leak happens, the pump speed will increase to keep the flow rate constant through the flow meter (F-1).

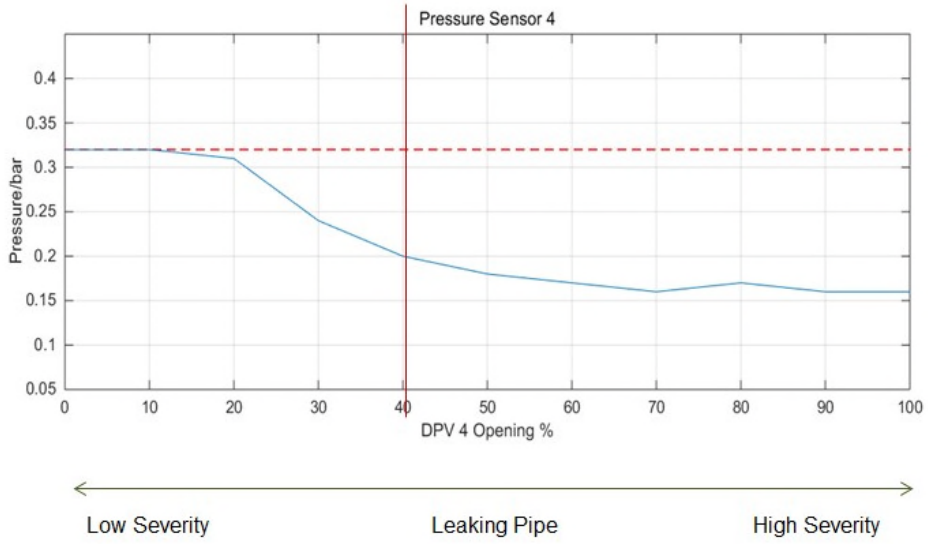


**Figure 3-5 Reading change of pressure sensor 4 with a leaking pipe fault**

However, if at the same time the nozzle has 10% or 20% degradation, the reading of pressure sensor 4 will vary as shown in Figure 3-6.

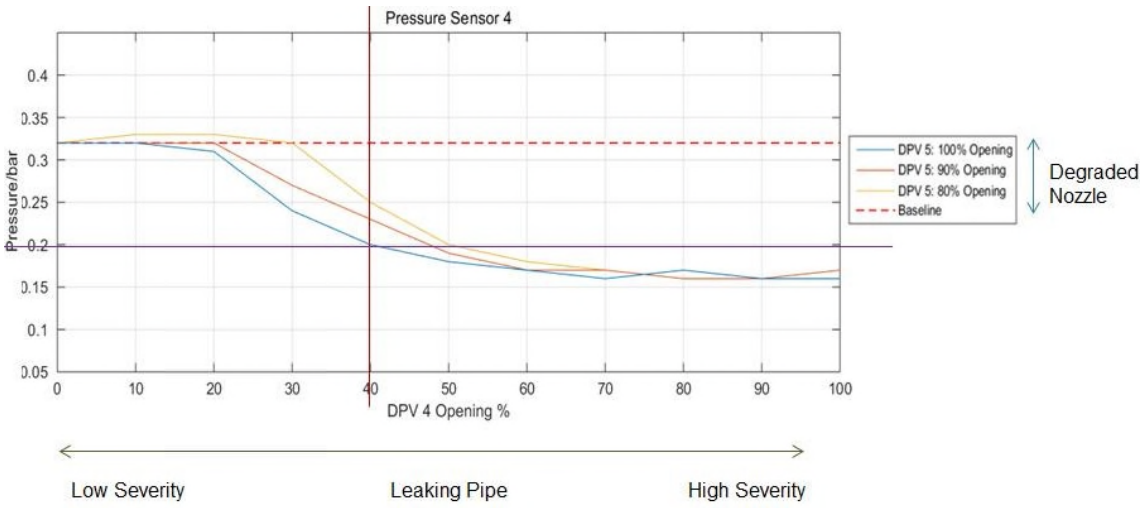


**Figure 3-6 Reading change of pressure sensor 4 when leaking happens in the presence of a degraded nozzle**

The blue line shows the sensor reading when no degradation happens in the nozzle, while the orange and yellow line show the reading change when the nozzle has 10% and 20% degradation respectively. This variation in sensor reading is caused by the degraded nozzle and proves that the sensor reading change is influenced not only by the faulty component, but also by other degraded components in the system. When constructing a diagnostic limit, the

reading of pressure sensor 4 is expected to be around 0.2 bar when the pipe leaking is 40%, if there are no other degraded components in the system. However, due to the degraded nozzle, the reading of pressure sensor 4 does not reach this diagnostic threshold until around 50%, i.e., it does not accurately reflect the severity level of the leaking. Under this condition, the sensory information without considering the influence of the degraded nozzle will lead to a wrong diagnostic result. Since every component starts to degrade from the first day of its service, the above mentioned phenomenon is very likely to happen in reality. In order to solve this problem, it is necessary to consider multi-component degradation when utilizing sensory information for fault diagnosis.

## 3.2 Methodology

Having formulated the research problem the next step is to develop a methodology to structure the research. The layout of the proposed methodology is shown in Figure 3-7 (within the dotted line). The methodology guides the main activities in this research and therefore forms the basis of the thesis. In the following text, each step of the methodology will be presented.

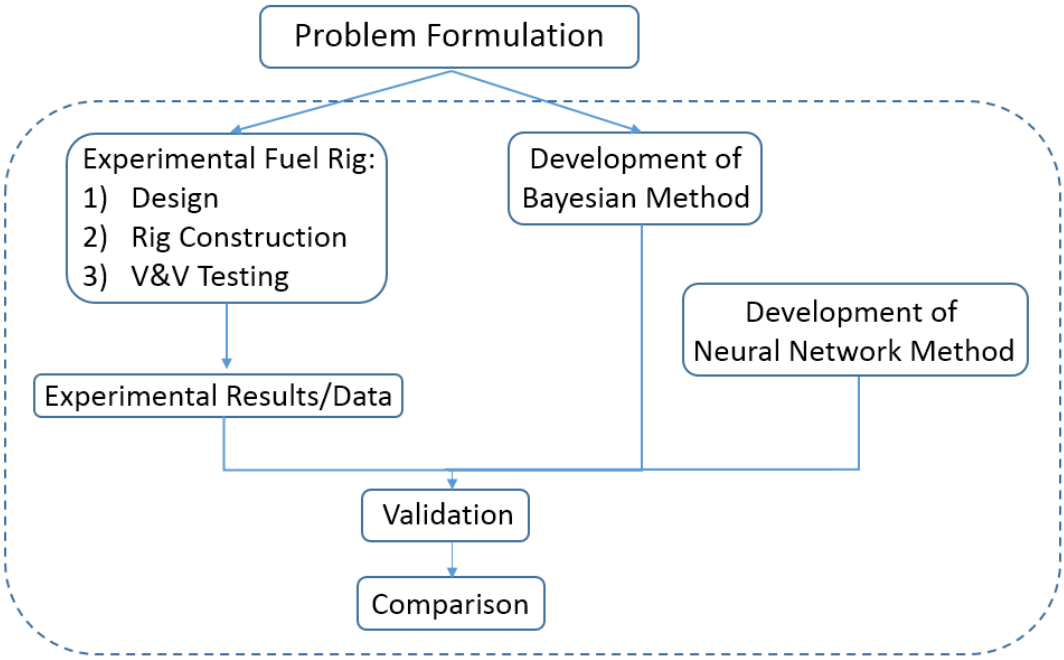


**Figure 3-7 Layout of the research methodology**

**Development of Bayesian Method**

In order to integrate distributed sensory information in a system, the issue as to how best to represent information from a wider range of sources in one framework has to be considered. After reviewing the previous research work by other authors (Chapter 2), a Bayesian method is chosen as the basis of the proposed method for its great capability of dealing with simultaneous evidence and combining information from distributed sensors by offering a probabilistic synthesizing framework, where probability addresses the degree of belief.

The Bayesian method used in this research is drawn from the classic Bayesian method. The main difference made here is that the conditional probability of the sensor reading under a certain degradation level is not only dependent upon the faulty component but also the degraded components in the system. A comprehensive introduction of the proposed Bayesian method is provided in Chapter 5.

**Experimental Fuel Rig**

In order to validate the proposed Bayesian method experimental data is needed. Since there is no publicly available data of multi-component degradation, an experimental rig is required to provide the necessary data.

In the real world, generating degradation data always requires running a system over a long period of time, which is not easy to conduct and costly. Therefore three different approaches are usually taken to generate the degradation data:

1. Accelerated degradation testing. This is usually achieved by conducting the tests under certain severe conditions (e.g. very high speed, extreme loads) which might be out of budget in some cases. It is ideal for the faults provoked by constant degradation such as fatigue, corrosion and creep, etc.
2. Machined components to represent the degradation. By accurately knowing the degraded modes to be studied, the components can be machined to represent the degradation mode. Simulation is usually necessary for this approach.

3. Emulating degradation modes. For some degradation modes, the cause of the degradation can be emulated. For example, a nozzle can be replaced by a direct-acting proportional valve (DPV), which is a valve that can produce an output (flow, pressure) proportional to an electronic control input, so that the clogged nozzle degradation mode can be emulated by gradually closing the valve. This method can generate the reproducible data of degradation and is easy to conduct compared with the accelerated degradation testing.

In this research, the experimental rig is designed based on the third approach for its merits.

A typical system engineering approach is used to successfully develop the rig in the lab. In our case, because an old fuel rig (shown in Figure 3-3) was developed before, the prior knowledge (e.g. selection of the appropriate sensors and actuators) can be very useful for the design of a new fuel rig. The detailed account of the whole development process of the experimental fuel rig is given in Chapter 4.

**Experimental Results/Data**

After completing the development of the experimental fuel rig, experiments will be conducted to generate the data for the validation of the proposed method. The experimental results are covered in Chapter 4 as well.

**Development of Neural Network Method**

The neural network method is developed in order to compare with the proposed Bayesian method. A brief introduction of the neural network method is given in Chapter 2, and the implementation is covered in Chapter 5. It is chosen for its wide application and simplicity.

**Validation and Comparison**

After obtaining the experimental results from the experimental fuel rig, the validation can be conducted to test the applicability and effectiveness of the proposed Bayesian method. Five case studies are presented: 1. Leaking pipe,

2. Clogged filter, 3. Clogged nozzle, 4. Sticking valve, 5. Blocked flow meter. The diagnostic performance of the proposed Bayesian method is assessed by using four metrics, and the results are compared with the classic Bayesian method and neural network method respectively. All the discussion on the results is given at the end of Chapter 5.

## 3.3 Summary

This chapter has outlined the research problem, and the methodology, which will guide the research undertaken within this thesis. In Chapter 4, the whole development process of the experimental fuel rig will be introduced in detail.

# 4 Experimental Fuel Rig

To generate the data for the validation of the proposed method an experimental fuel rig was developed. This chapter introduces the whole development process of the experimental fuel rig and the experimental data produced for Chapter 5. The entire development process (shown in Figure 4-1) starts from a guideline (provided by the IVHM Centre) about experimental work process which outlines the major steps and documentation that should be followed for a successful rig design, construction, verification and test. The design stage (introduced in Section 4.1) includes the investigation of real aircraft fuel systems, the identification of the main functions of aircraft fuel systems, the development of the system design requirements, and ends up with a design review in which the design plan is evaluated by fellow researchers and industrial sponsors. The assembling stage includes the installation of the components on a breadboard and the electrical connection of the equipment. Then the control and measuring system (introduced in Section 4.2) is developed using LabVIEW with NI (National Instruments) modules. The V&V (Verification and Validation) testing stage (covered in Section 4.3) includes the instrument level testing, the component level testing and the system level testing. After finishing the V&V testing, a configuration management (introduced in Section 4.4) document is produced in order to record the description, manufacturer's information, quantity and cost of each component, along with an operating procedure (introduced in Section 4.5) that helps the operators carry out routine operations.

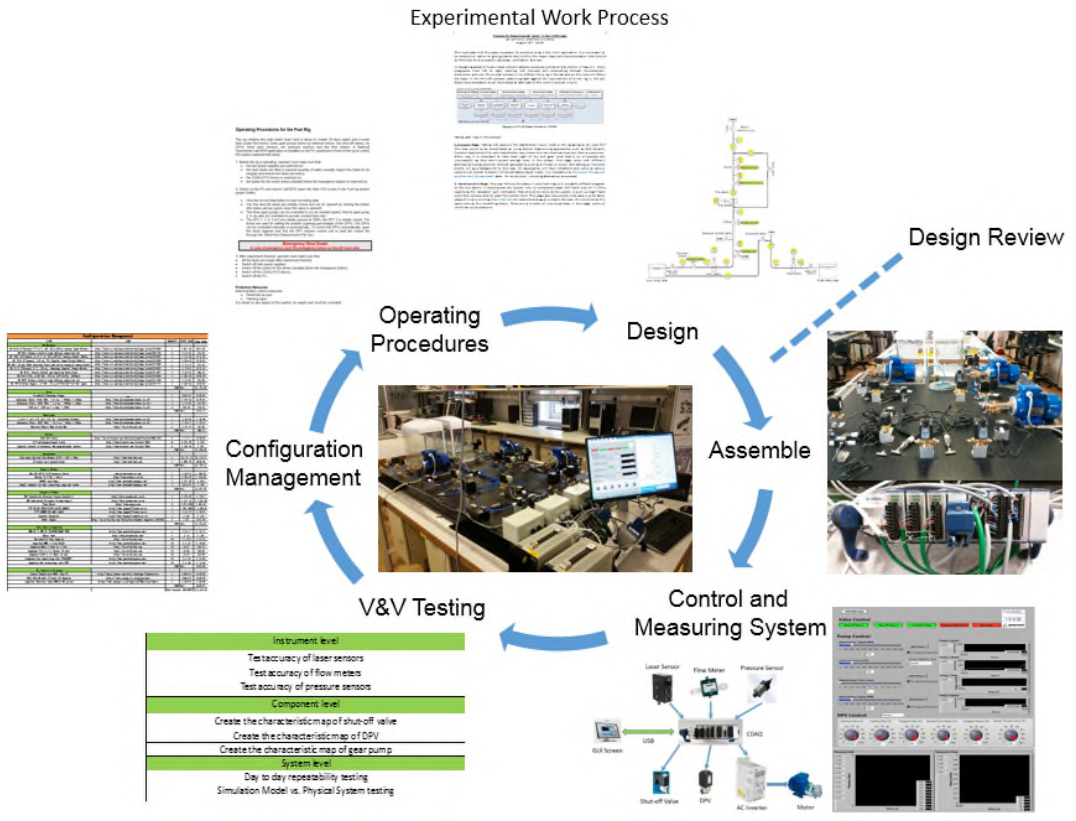


**Figure 4-1 The whole development process of the fuel rig**

## 4.1 Fuel Rig Design

### 4.1.1 Design Requirements

This section introduces the design requirements of the experimental fuel rig which aims to emulate a simplified aircraft fuel system with several common faults. In order to make the fuel rig close to reality, two specific aircraft fuel systems are investigated. This is followed by the identification of the main functions of real aircraft fuel systems. Then the faults that will be injected into the fuel system are described, the corresponding system design requirements are developed.

#### Specific Aircraft Fuel Systems

In the real world, there exist a number of fuel systems ranging from commercial aircraft to military aircraft. In this research, two typical commercial aircraft fuel systems from the Boeing 777 and the Airbus A380 are investigated.

1. The Boeing 777 fuel system

   The Boeing 777 fuel system is designed for twin engines. It contains an integral center tank (configured as two compartments), two integral main tanks and two surge tanks, shown in Figure 4-2. The center tank and main tank are used to feed the engine while the surge tank is used to protect the fuel system from over-pressure situations. The two sections of the center tank and the two main wing tanks are both interconnected by a large diameter pipe that allows the fuel from the heavier wing to flow to the opposite wing to achieve lateral balance, i.e. central gravity (CG) control.

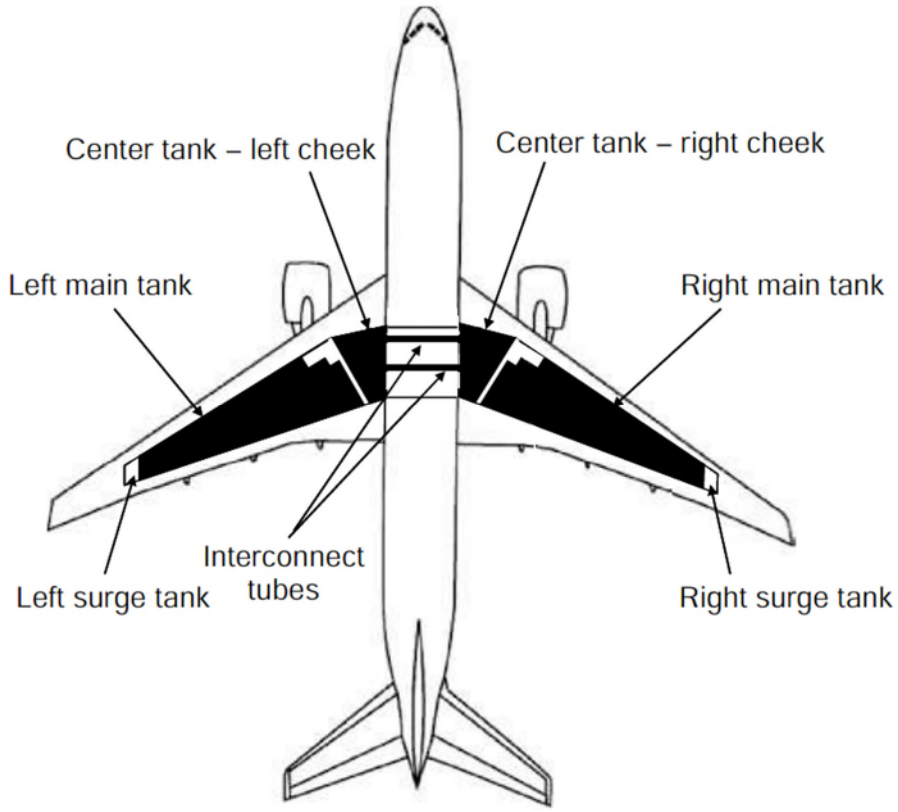


**Figure 4-2 Layout of Boeing 777 fuel system (Langton, et al. 2009)**

All of the pumps and valves are located close to or on the rear spar, shown in Figure 4-3, well away from the engine rotating part and thus well outside the rotor burst zones.

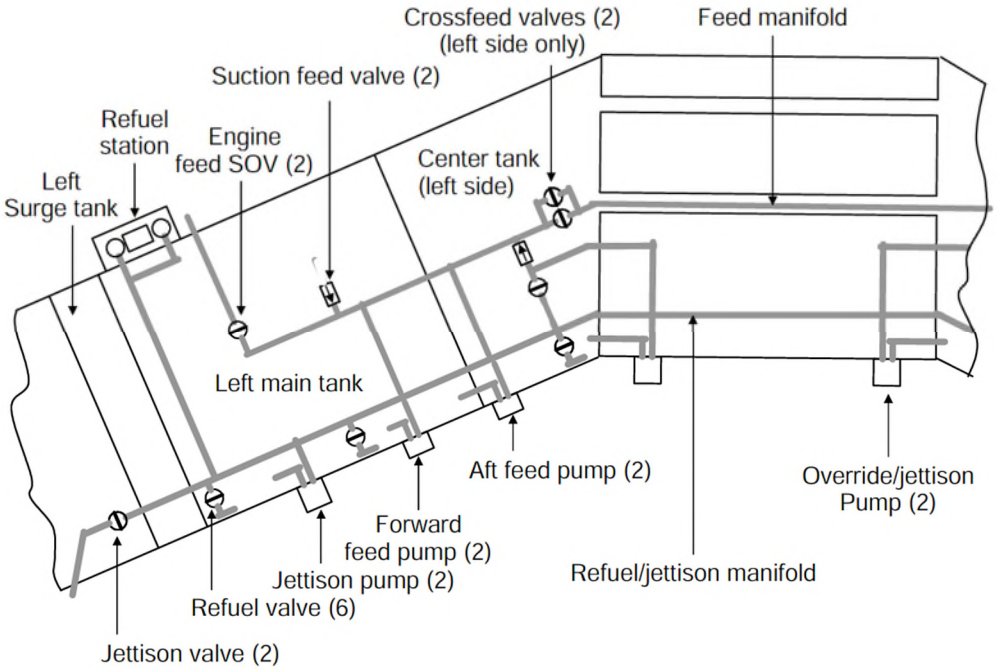


**Figure 4-3 Pumps and valves position in Boeing 777 fuel system**

**(Langton, et al. 2009)**

More specifically, there are altogether six refuel shut-off valves in the Boeing 777 fuel system. Each valve can be opened or closed automatically to meet the required weight in each tank when the auto-refuelling is in process. There are two jettison valves and two jettison pumps which enable the crew to dump fuel overboard in order to reduce the aircraft weight in the event of an emergency. During the flight, the center tank fuel will be used first through two override pumps. Once the center tank is empty, the Forward and Aft feed pumps will automatically take over the feed task (the term ‘Forward’ and ‘Aft’ represent the location of the snorkel inlets). In the loss of both engine feed pumps, the engine will operate in a suction feed mode via two suction feed valves. Also, two crossfeed valves are connected in parallel (this redundant design ensures the availability of the crossfeed function) in order to transfer fuel from the heavier wing to the opposite wing.

2. The Airbus A380 fuel system

   As a generation after the Boeing 777 fuel system, the A380 fuel system is more complex. It is designed for four engines. Compared with B777, A380 fuel system does not have a center tank. It contains a trim tank in the horizontal stabilizer, which can increase the usable fuel on board and achieve optimum CG during climb and cruise, and five tanks (inner engine feed tank, inner transfer tank, mid tank, outer engine feed tank and outer tank) in each wing, shown in Figure 4-4. The wing tanks are vented to the vent tank in each wing while the trim tank is vented via a vent tank next to the trim tank. In addition, three surge tanks are used to accommodate the ground refuel condition. After the aircraft leaves the ground, the fuel transfer pumps will move fuel from the inner and mid tanks to the outer tank for alleviating wing load. The outer tank usually remains full until the end of the cruise phase when the aircraft weight is substantially reduced by fuel consumption and wing load alleviation is no longer necessary.

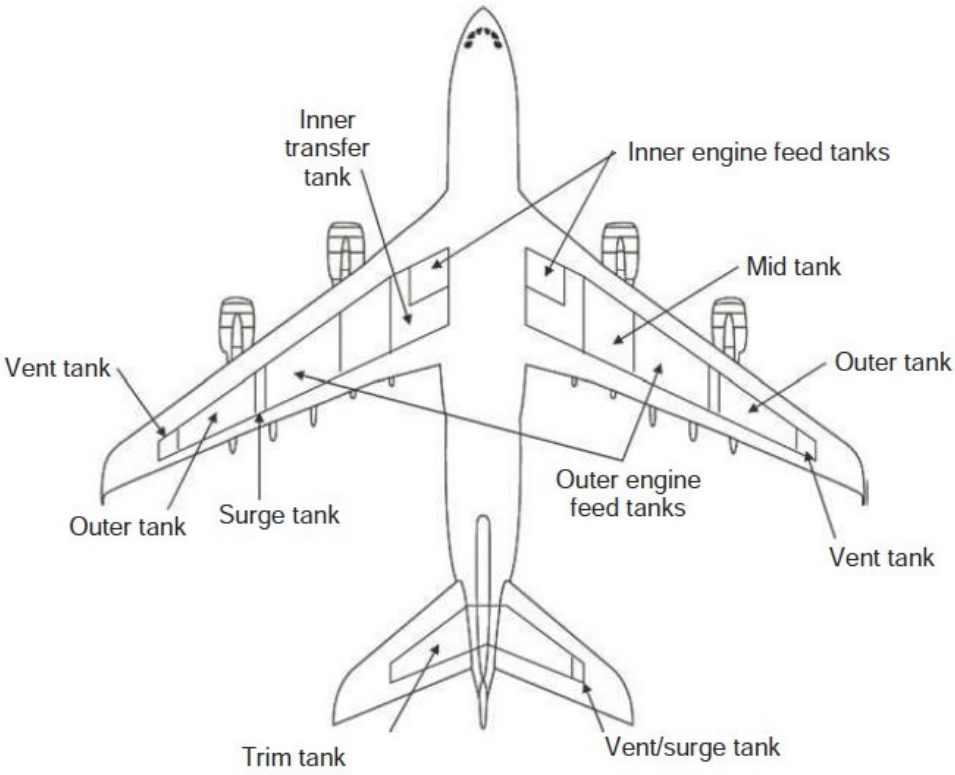


**Figure 4-4 Layout of Airbus A380 fuel system (Langton, et al. 2009)**

Because there are a large number of auxiliary fuel tanks in the A380 fuel system, the number of pumps and valves is correspondingly increased (shown in Figure 4-5) compared with Boeing 777 fuel system. Each engine has two feed pumps that draw fuel from the feed tank. One pump serves as the primary pump while the second pump serves as the back-up pump and will start automatically when the primary pump is not working properly. Also, a low pressure shut-off valve is provided close to each engine. Four crossfeed valves allow fuel crossfeed to any of the four engines when a shutdown of any of the four engines happens thus ensuring that feed tank fuel for a shutdown engine is available to the other remaining engines. The APU has its own boost pump for initial start-up and a low pressure isolation valve is located close to the APU. During the flight, the fuel will be transferred from the mid and inner fuel tanks to the feed tank so that the feed tank remains full until the mid and inner tanks have been depleted. The outer and trim tanks are usually the last auxiliary tanks to be transferred.

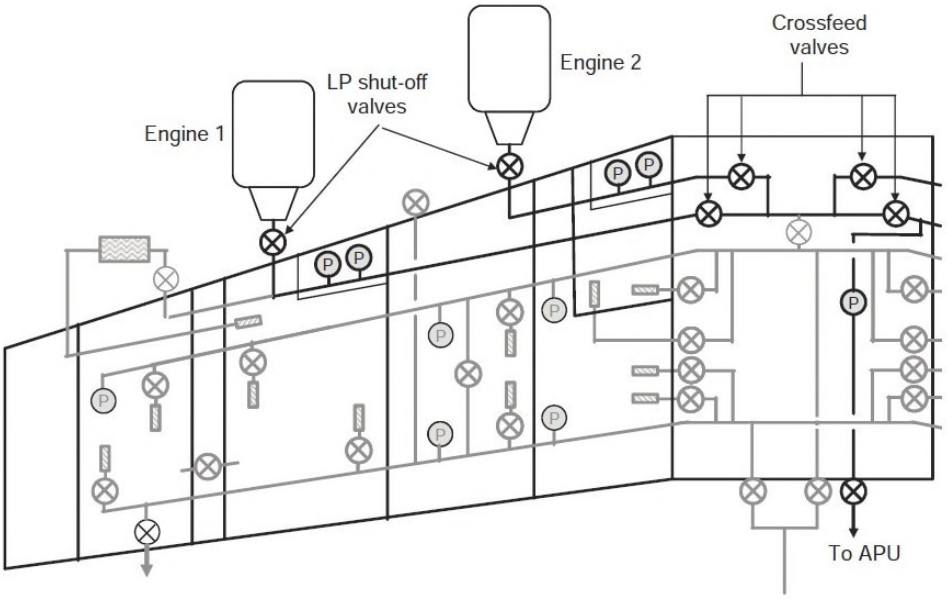


**Figure 4-5 Pumps and valves position in Airbus A380 fuel system**

**(Langton, et al. 2009)**

## Main Functions of Aircraft Fuel System

After investigating two specific aircraft fuel systems, the main functions of a commercial aircraft fuel system are identified. Figure 4-6 (Frost, 2015) shows the main functions of a commercial aircraft fuel system based on the document from ATA (Air Transport Association). The main functions of a commercial aircraft fuel system include:

1. To feed the engine.

   During the flight, the aircraft fuel system must make sure that the fuel on board remains available to the engines. In the case of an engine failure, the aircraft fuel system must also provide the ability to transfer fuel between fuel tanks so that the failed engine's fuel can be used for the remaining engine.
2. To feed the APU (Auxiliary Power Unit).

   The primary function of APU is to provide electrical power when the aircraft is on the ground. In some cases, the APU needs to operate in flight if the engine-driven generator becomes inoperative. During APU

start the aircraft fuel system needs to provide fuel to the APU through the APU pump.

3. To relieve load and keep the lateral balance of the airplane.

   Since the fuel tank is located in the wings, the aircraft fuel system can relieve the wing load to minimize wing bending moment and thus reduce the wing fatigue effects through using the inner tank fuel before the outer tank fuel. Also, by transferring fuel from the heavier wing to the opposite wing, the aircraft fuel system can keep the lateral balance of the airplane.

4. To reduce the aircraft weight by jettison.

   In the event of an emergency, if the pilots decide to return the plane to the ground, the aircraft fuel system needs to reduce the aircraft weight by jettison as the maximum take-off weight is significantly higher than the maximum landing weight for the landing gears.

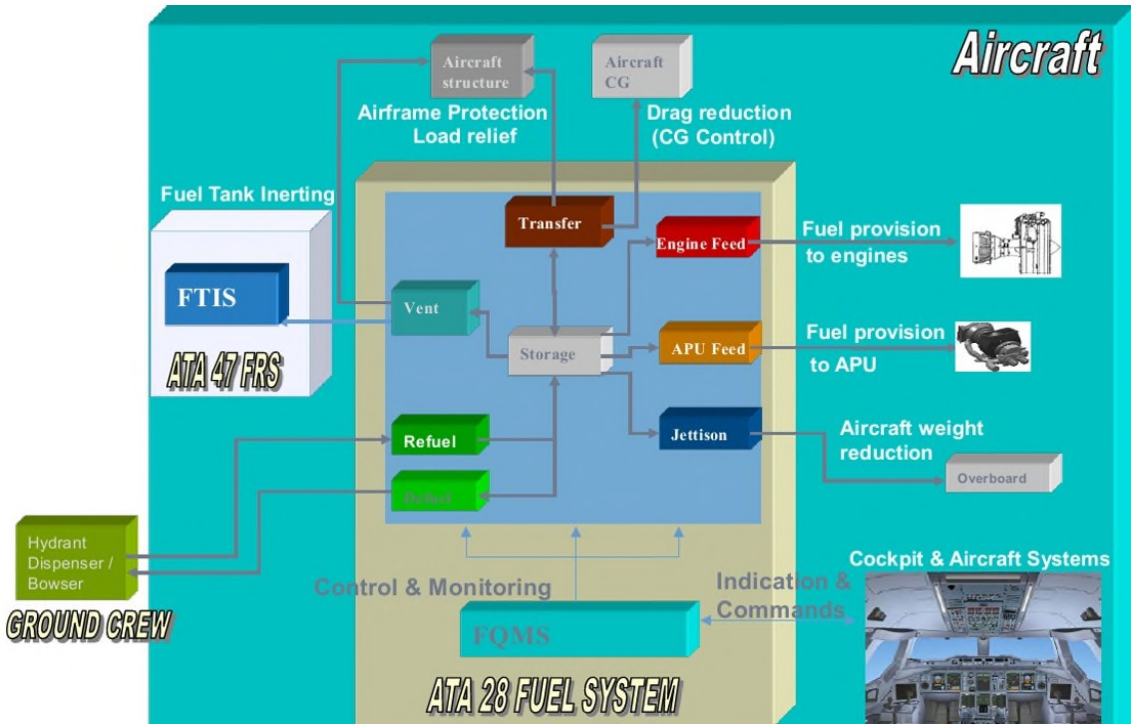


**Figure 4-6 Main functions of an aircraft fuel system (Frost, 2015)**

## Fault Types

For an aircraft fuel system, the faults can be broadly classified into three different types, namely process faults, actuator faults and sensor faults. Process faults include faults which will affect the operational ability of the system itself such as a leaking pipe or cracked joint. Actuator faults include faults that will affect the actuated parts of the system such as pump malfunction or a sticking valve, and sensor faults include faults that will affect the sensor operation. Some faults in the aircraft fuel system are caused by the degradation of components due to fouling (usually caused by adherence of particulate contaminants), erosion (usually caused by hard particles such as dust, dirt and rust ash), or corrosion (usually caused by the chemical reactions). In our case, the faults that will be injected into the fuel system are listed in Table 4-1. They were chosen based on the suggestions from industrial collaborator.

**Table 4-1 The faults injected into the fuel system**

| Fault type | Fault |
|---|---|
| Process fault | Leaking pipe |
| Actuator fault | Sticking valve |
| | Clogged filter |
| | Clogged nozzle |
| Sensor fault | Blocked flow meter |

**System Design Requirements**

Based on the above investigations and the suggestions from industrial collaborator, some basic system design requirements for the experimental fuel rig are developed:

1. The rig system should be able to implement the engine feed function of the aircraft fuel system. This corresponds to the first main function mentioned above.
2. The rig system should be able to simulate the scenario when the fuel needs to be transferred from one tank to another in order to keep the

lateral balance of the airplane during flight. This corresponds to the third main function mentioned above.

3. The rig system should be able to implement the pressurizing function before the fuel enters into the engine. This corresponds to the first main function mentioned above.
4. The rig system should be able to simulate the scenario when the engine requires less fuel than the aircraft fuel system is delivering. This corresponds to the first main function mentioned above.
5. The rig system should be able to emulate the faults (listed in Table 4-1) with different degrees of severity and in any combination. This corresponds to the fault types mentioned above.

### 4.1.2 Design

After developing the system design requirements, the experimental fuel rig was designed as shown schematically in Figure 4-7. To meet each of the design requirements the following are chosen. Numbers correspond to those above.

1. Gear pump 1 serves as the low pressure pump with a control system.
   This design is chosen as it can implement the engine feed function of the aircraft fuel system.
2. Crossfeed line that includes the shut-off valve 2, the gear pump 3 serves as the crossfeed pump with a control system, and the crossfeed valve.
   This design is chosen as it can transfer the fuel from the right wing tank to the left wing tank so that the CG of the aircraft can be maintained during flight.
3. Gear pump 2 serves as the high pressure pump with a control system.
   This design is chosen as it can implement the pressurizing function before the fuel enters into the engine.
4. Spill branch that includes the spill valve and the DPV 6 serves as the engine throttle valve.
   This design is chosen as it can simulate the scenario when the engine requires less fuel from the aircraft fuel system. The DPV 6 can generate

the backpressure when the spill valve is opened so that the remaining fuel can be returned to the high pressure pump inlet.

5. DPV 1 to 5 used to inject the sticking valve fault, leaking pipe fault, clogged filter fault, blocked flow meter fault, and clogged nozzle fault respectively.

   The reason for choosing this design has been discussed in Chapter 3.

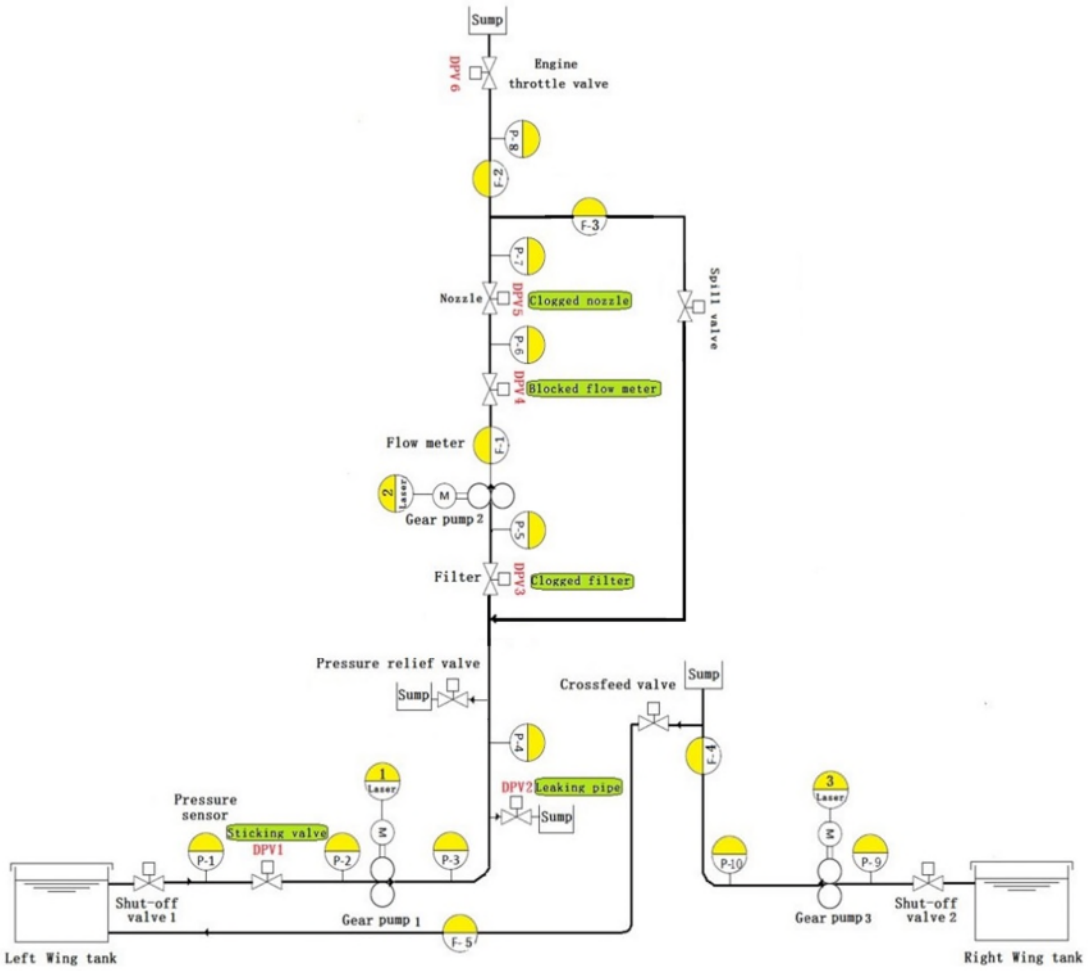


**Figure 4-7 Layout of the fuel rig system**

## 4.2 Fuel Rig Description

This section provides a comprehensive description of the experimental fuel rig which includes the hydraulic system, the control and measuring system, and the fault injection mechanism. A picture of the fuel rig is shown in Figure 4-8. The rig is now in the IVHM Centre Lab at Cranfield University.

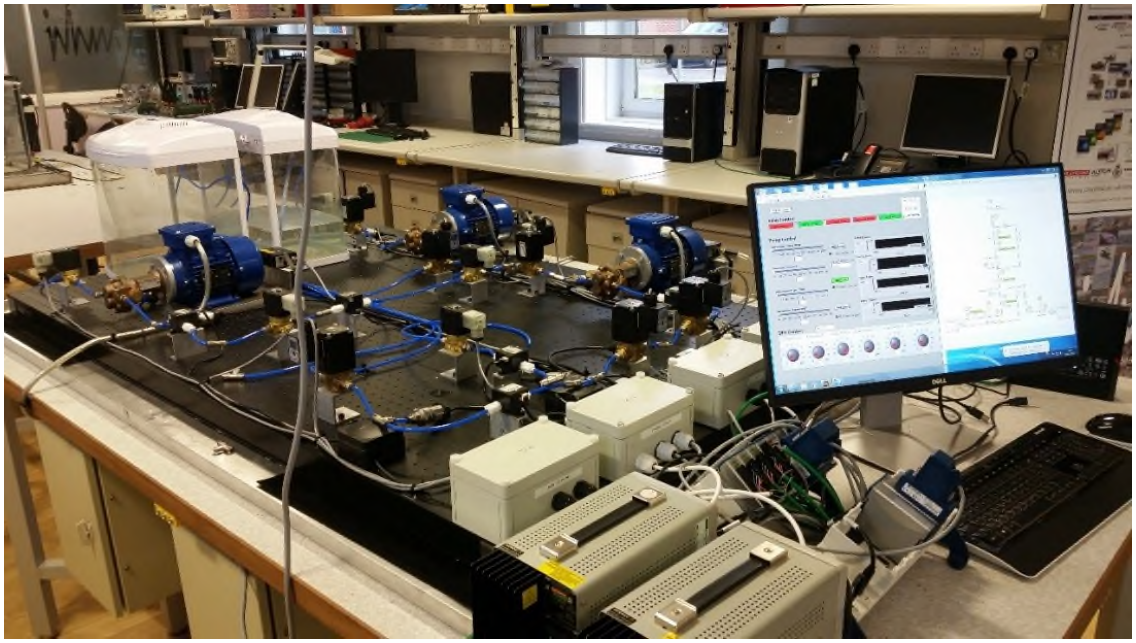

**Figure 4-8 Picture of the fuel rig in the IVHM Centre Lab at Cranfield University**

### 4.2.1 Hydraulic System

In the hydraulic system (schematic shown in Figure 4-7), there are altogether three water tanks (two main tanks representing the left wing tank and right wing tank respectively, and a sump tank representing the engine that receives the fuel from the aircraft fuel system), three gear pumps (each pump is driven by an external motor and has a pressure-relief valve inside in order to prevent overstressing the gears), five shut-off valves and six DPVs. All the components are connected using the pipe with 4mm internal diameter and 6mm outside diameter, and are mounted on an aluminum optical breadboard (1.8m x 1.1m x 5cm) which is above a drip tray in order to catch any unintended leak in the system. A list of specifications is shown in Table 4-2.

**Table 4-2 List of Specifications**

| Item | Description |
|---|---|
| Gear Pump | Oberdorfer-N999R, Bare Shaft, 150 PSI Max, RPM Range: 0-600rpm, 12 teeth |
| Motor | 3-Phase, 0.37kW, 4 Pole, 230/400V, 50H |
| Shut-off Valve | Orifice: 4.5mm, Power Supply: 24V DC, 5.0 MPa Max |
| DPV | Orifice: 3mm, Power Supply: 24V DC, 25 bar Max |
| Pipe | Polyurethane, 4mm internal diameter and 6mm outside diameter |

More specifically, the hydraulic system can be divided into three parts:

1. The main line part which includes the shut-off valve 1, the non-return valve (emulated by the DPV1), the gear pump 1 (serves as the low pressure pump), the pressure-relief valve (a shut-off valve) which is used to perform a function of safety when the overpressure condition happens, a filter (emulated by the DPV3), the gear pump 2 (serves as the high pressure pump), a flow meter (emulated by the DPV4) and a nozzle (emulated by the DPV5).
2. The crossfeed line which includes the shut-off valve 2, the gear pump 3 (serves as the crossfeed pump that can transfer the fuel from the right wing tank to the left wing tank in order to keep maintaining the central gravity of the aircraft during flight), and the crossfeed valve (a shut-off valve).
3. The spill branch which includes the spill valve (a shut-off valve) used to return the fuel when the engine requires less fuel from the aircraft fuel system, the engine throttle valve (DPV6) which is used to generate the backpressure when the spill valve is opened.

### 4.2.2 Control and Measuring System

The control and measuring system, shown in Figure 4-1 and expanded in Figure 4-9, includes ten pressure sensors, five flow meters, three laser sensors, three AC inverters, nine National Instruments (NI) module cards that installed in two NI CDAQ-9172 8 slots USB chassis and the LabVIEW interface (GUI screen) developed on a PC. The specifications of the sensors are summarized in Table 4-3. The sensors are chosen as they are reliable and have very high repeatability. The sensors' position can be seen in Figure 4-7.

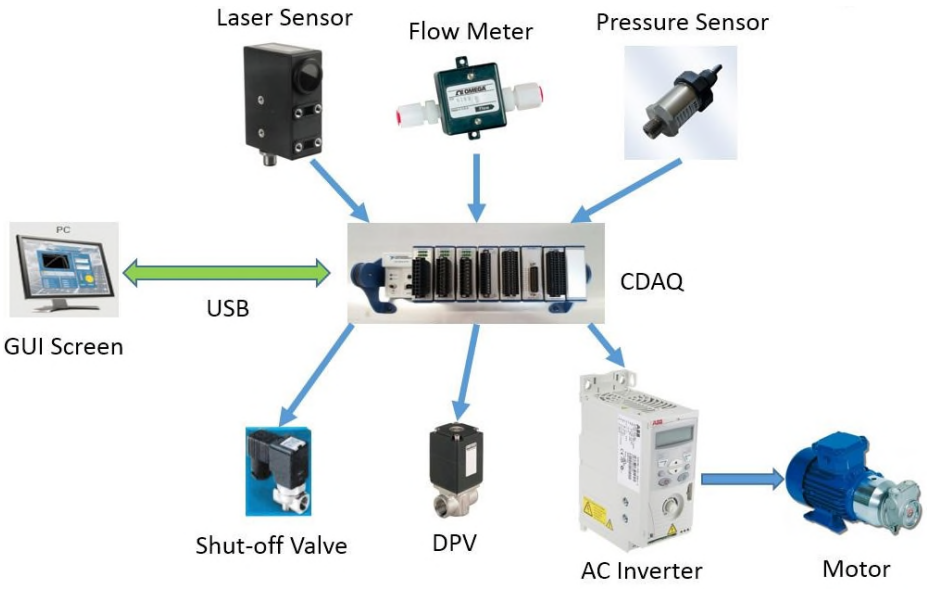


**Figure 4-9 Control and Measuring System**

**Table 4-3 Specifications of the sensors**

| Sensor | Description |
|---|---|
| Absolute Pressure Sensor | Measurement range: 0-5 bar, Output Signal: 0-5V, Quoted accuracy: ±0.25% (full scale), Power Supply: 12.8V DC |
| Gauge Pressure Sensor | Measurement range: 0-4 bar, Output Signal: 0-5V, Quoted accuracy: ±0.25% (full scale), Power Supply: 12.8V DC |
| Flow Meter | Measurement range: 0-2L/min, Output Signal: 0-5V, Quoted accuracy: ±3% (full scale), Temperature sensitivity: ±0.2% per ℃, Reference temperature: 23℃, Power Supply: 12.8V DC |
| Laser Sensor | Sensing range: 0-10 m, Power Supply: 10-30V DC |

The NI modules used in the control and measuring system are chosen for their customizable and accurate features compared with other tools. More specifically, the nine NI module cards selected for the control and measuring system are: NI 9485, NI 9205, NI 9264, three NI 9401 and three NI 9472.

The NI 9485 module is an 8-channel solid state relay sourcing or sinking digital output module. It allows for direct connection to a variety of industrial devices such as valves, motors, etc. In order to control the open/close status of five solenoid shut-off valves in the hydraulic system, the NI 9485 module is chosen to provide access to the solid state relay for switching the voltage applied to the shut-off valve.

The NI 9205 module is a 250 kS/s, 32-channel voltage input module. It is chosen to receive the analogue voltage output from the ten pressure sensors and five flow meters, and convert this information using the calibration forms into digitized information readable on the GUI screen. The sampling rate is 1 kHz within the LabVIEW environment.

The NI 9264 is a 25 kS/s, 16-channel module simultaneously updating analog output module which is chosen to enable the implementation of the six DPVs position control. The DPV position is modified by varying the voltage applied to the solenoid and is open circuit.

The NI 9401 module is a configurable digital I/O interface. It is chosen to receive the output from the laser sensor and convert them into frequency for calculation of the pump speed.

The NI 9472 module is an 8-channel 24V logic, sourcing digital output module which is chosen to provide the signals to the pump inverter (ABB ACS150) in order to implement the pump controls (start pump, stop pump, increase speed, maintain speed, decrease speed). The pump speed input from the control system is 0-5V to the inverter drive, whereby the inverter drive determines the 3 phase motor control.

**GUI screen**

The GUI screen designed for the control and measuring system is shown in Figure 4-10. It is developed using LabVIEW, which is a widely known system engineering software combined with a graphical programming syntax.

The user can open/close the shut-off valves (when the indicator turns green, the valve is opened; when the indicator turns red, the valve is closed), set the pump speed/flow rate through the scroll bar, change the opening percentage of DPVs through the knobs (manually or automatically), monitor the pump speeds, and observe the readings from the ten pressure sensors and five flow meters. Referring to Figure 4-10 the GUI screen is structured in four layers. The top layer contains the valve control unit while the second layer contains the pump control unit. The third layer enables the injection of the fault through the control

of the opening percentage of DPVs. The fourth layer presents the readings from the ten pressure sensors and five flow meters.

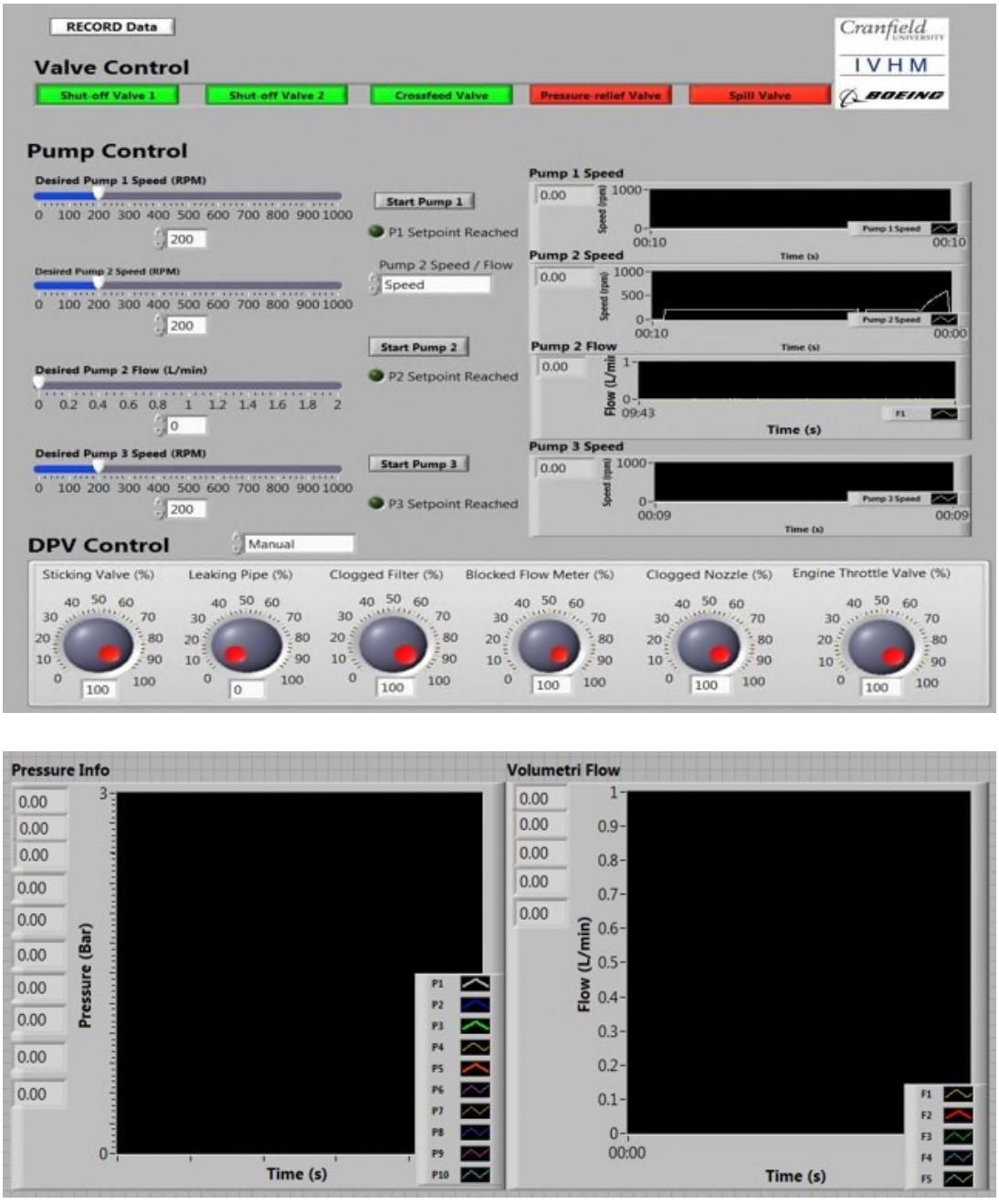


**Figure 4-10 GUI Screen for the Control and Measuring System**

The data file provided by the control and measuring system contains the time of the experiment, the atmosphere pressure and temperature in the lab, the readings from the ten pressure sensors, five flow meters and three laser

sensors, the status of the shut-off valves, and the opening percentage of the DPVs.

### 4.2.3 Fault Injection Mechanism

In order to inject various faults (shown in Table 4-1) with different degrees of severity into the fuel system, five DPVs are used. DPV 1 is used to inject a sticking valve fault into the system. The fully opened DPV 1 is equivalent to a healthy valve while the partially closed DPV 1 is equivalent to a sticking valve with a certain degree of severity. Different degrees of severity can be emulated by varying the opening percentage of the DPV which is controlled by the PC and can be varied from 0% to 100%. DPV 2 is used to inject a leaking pipe fault into the system. The fully closed DPV 2 is equivalent to a healthy pipe while the partially opened DPV 2 is equivalent to a leaking pipe with a certain degree of severity. DPV 3 is used to inject a clogged filter fault into the system. The fully opened DPV 3 is equivalent to a healthy filter while the partially closed DPV 3 is equivalent to a clogged filter with a certain degree of severity. DPV 4 is used to inject a blocked flow meter fault into the system. The fully opened DPV 4 is equivalent to a healthy flow meter while the partially closed DPV 4 is equivalent to a blocked flow meter with a certain degree of severity. DPV 5 is used to inject a clogged nozzle fault into the system. The fully opened DPV 5 is equivalent to a healthy nozzle while the partially closed DPV 5 is equivalent to a clogged nozzle with a certain degree of severity.

## 4.3 Verification and Validation (V&V)

This section describes the verification and validation (V&V) testing of the fuel rig system. The goal in carrying out this V&V testing is to test all the functions of the rig to ensure repeatable and accurate results. To achieve this goal, the following tasks are listed in Table 4-4.

**Table 4-4 V&V Tasks**

| Instrument level |
| --- |
| Test accuracy of laser sensors |
| Test accuracy of flow meters |

| |
|---|
| Test accuracy of pressure sensors |
| Component level |
| Create the characteristic map of gear pump |
| Create the characteristic map of shut-off valve |
| Create the characteristic map of DPV |
| System level |
| Day to day repeatability testing |
| Simulation Model vs. Physical System testing |

### 4.3.1 Instrument Level

#### Laser sensor

In order to test the laser sensor, the pump speed is set incrementally from 100 to 600 rpm through the control system developed in LabVIEW. The frequency output from the laser sensor is measured using an oscilloscope and at the same time sent to the NI module which is connected to a PC. The frequency from both sources turn out to be in excellent agreement, as shown in Table 4-5.

**Table 4-5 Measurements from the oscilloscope and NI module for the laser sensor at different pump speeds**

| Pump Speed (RPM)/Hz | Reading from the Oscilloscope (Hz) | Reading from the NI Module (Hz) |
|---|---|---|
| 100.1/1.67 | 1.67 | 1.67 |
| 200.3/3.34 | 3.34 | 3.34 |
| 300.6/5.01 | 5.01 | 5.01 |
| 400.0/6.67 | 6.67 | 6.67 |
| 499.8/8.33 | 8.33 | 8.33 |
| 599.6/9.99 | 9.99 | 9.99 |

It should be noted that the reading from the laser sensor is precise to five decimal places (e.g. 1.67532) but here only two decimal places are displayed.

#### Flow meter

In order to test the flow meter (turbine wheel type), the five flow meters are connected in series and the readings from all of them are collected for a range of speeds (100-600rpm). The result from 600rpm is selected as an example and shown in Figure 4-11.

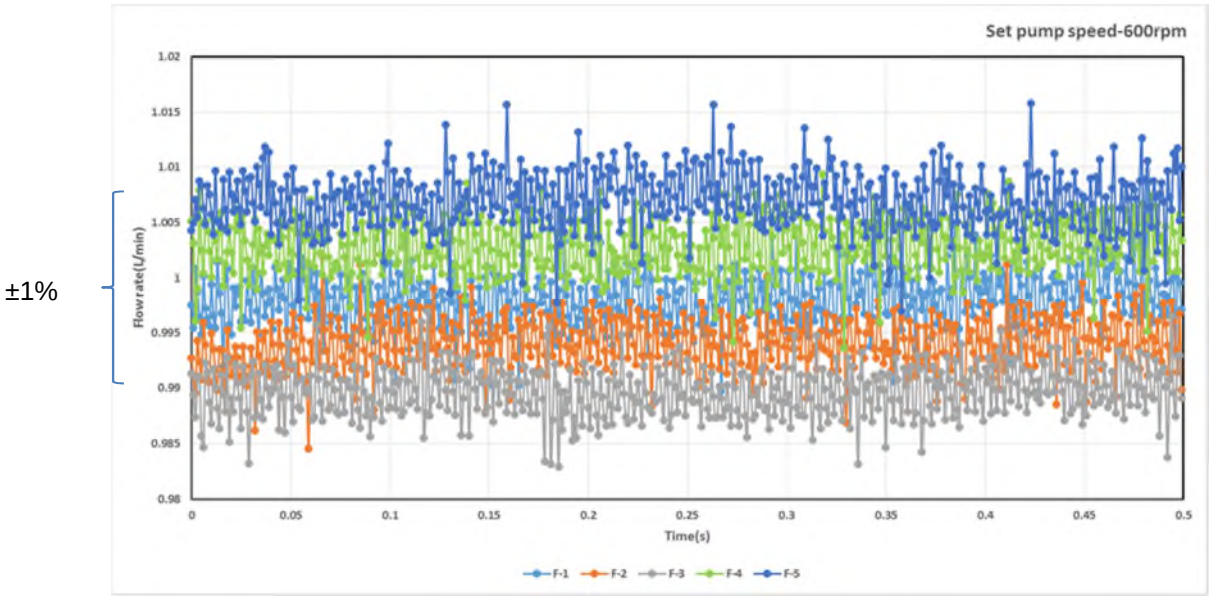


**Figure 4-11 Readings from the five flow meters at 600rpm pump speed**

Table 4-6 shows the discrepancy between different flow meters under different pump speeds.

**Table 4-6 Discrepancy between different flow meters under different pump speeds**

| Set pump speed (rpm) | Flow error (%) |
|---|---|
| 600 | ±1% |
| 500 | ±1% |
| 400 | ±1% |
| 300 | ±2% |
| 200 | ±2% |
| 100 | ±5% |

It can be seen that the discrepancy between different flow meters for 200-600rpm pump speeds is no more than ±2% but when the pump speed is

100rpm (i.e. at low flow rates), the discrepancy between different flow meters is ±5% which is because the flow error is around ±0.01L/min all of the time, so moving away from the full scale flow will increase the discrepancy as a percentage of flow rate.

### Pressure sensor

As the previous pressure sensors, of this type, have been sent away to certify accuracy and the result has proved to be ten times better than the manufacturer's claim. It is, however, expensive and so here only the temporal accuracy of the pressure sensor is tested. The readings from the pressure sensor before a gear pump are collected over a timed interval at 1 kHz. The results from 400rpm are selected as an example and shown in Figure 4-12.

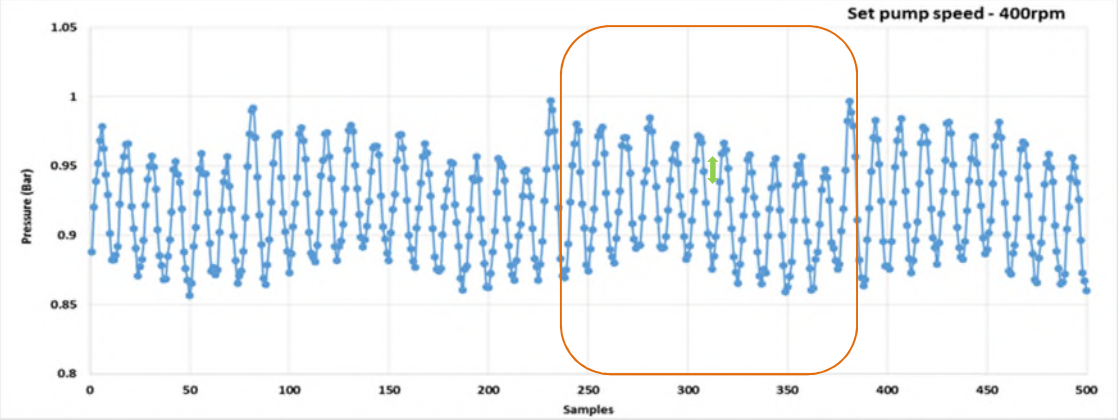


**Figure 4-12 Pressure reading over a timed interval**

From Figure 4-12 it can be seen that the pressure sensor has an excellent measurement accuracy in terms of frequency (better than the 1 kHz collection frequency). Within one period (highlighted by the orange window), there are 12 peaks in the waveform which corresponds to the 12 teeth of the gear pump (consistent with the manufacturer's information).

It also can be seen that for each measuring point, the approximate accuracy in terms of measuring pressure is better than ±0.01bar (highlighted by the green arrow).

It should be noted that the absolute pressure sensor reading ($P_{absolute}$) is corrected using the barometer reading in the lab according to:

$$P_{\text{corrected}} = P_{\text{absolute}} + (P_{\text{STP}} - P_{\text{barometer}}) \quad \textbf{(4-1)}$$

where the $P_{STP}$ is 1.01325 bar.

The gauge pressure sensor reading ($P_{gauge}$) is corrected as:

$$P_{\text{corrected}} = P_{\text{gauge}} + P_{\text{STP}} \quad \textbf{(4-2)}$$

In order to understand over what time period the sensor readings should be averaged, Figure 4-13 illustrates the experimental precision in which the blue dotted line represents the pdf of the pressure sensor reading over 0.3 seconds, the orange dotted line represents the pdf of the pressure sensor reading over 3 seconds and the green dotted line represents the pdf of the pressure sensor reading over 30 seconds. It can be seen that the rig has a very high experimental precision and the sample size does not affect the precision much. So in the following sections, the averaged sensor reading is coming from a series of 3000 samples (3 seconds). In the case studies conducted in Chapter 5, 3000 sensor readings (3 seconds) are selected under each operating condition among which 2700 (i.e. 90%) are being used as historic data while the remaining 10% (0.3 seconds) are used as test data. The test data was sampled randomly from the training data.

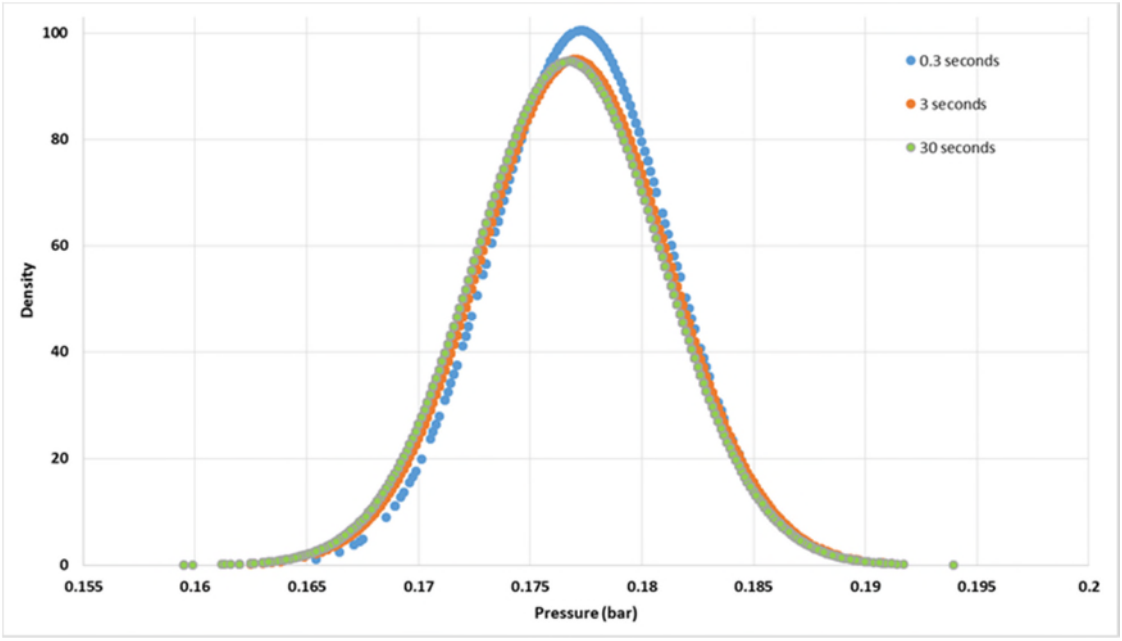


**Figure 4-13 Illustration of experimental precision**

### 4.3.2 Component Level

#### Gear pump

In order to create the simulation model for the gear pump, the pump characteristic map (a chart that describes the correlation between the mass flow and the pressure differential that the pump creates) is needed. The three gear pumps used in the fuel rig are driven by external motors. To create the characteristic map, the pump is connected with a DPV to generate different back pressure to the output (by changing the opening percentage of the DPV) and running at different speeds (from 200rpm to 600rpm). Figure 4-14 shows the characteristic map of the three gear pumps. The ordinate is the flow rate, and the abscissa is the pressure ratio across the pump. The red line represents the gear pump 1 which serves as the low pressure pump, the blue line represents the gear pump 2 which serves as the high pressure pump, and the green line represents the gear pump 3 which serves as the crossfeed pump. The measurement points are averaged over 3 seconds.

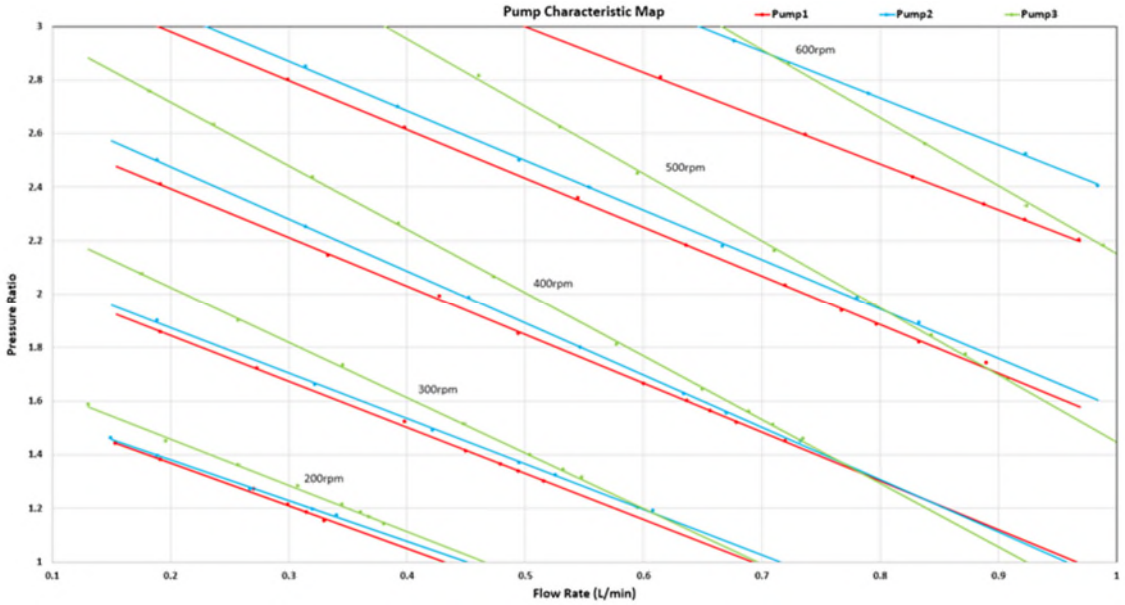


**Figure 4-14 The pump characteristic map**

It can be seen that for different pumps, the characteristics are not identical. This is due to the manufacturing variability and will not influence the experimental results.

It also can be seen that the characteristic curves have high slope so increasing the flow rate will cause a significant reduction in the pressure differential under a certain pump speed.

### Shut-off valve

In order to create the simulation model for the shut-off valve, the valve characteristic map (a chart that describes the correlation between the mass flow through the valve and the pressure drop across the valve) is needed. To create the characteristic map, a gear pump is used to connect with the valve to get different flow rates (by changing the pump speed) through the valve. Figure 4-15 shows the characteristic map of the shut-off valve. The ordinate is the pressure drop across the valve, and the abscissa is the flow rate through the valve. The measurement points are averaged over 3 seconds.

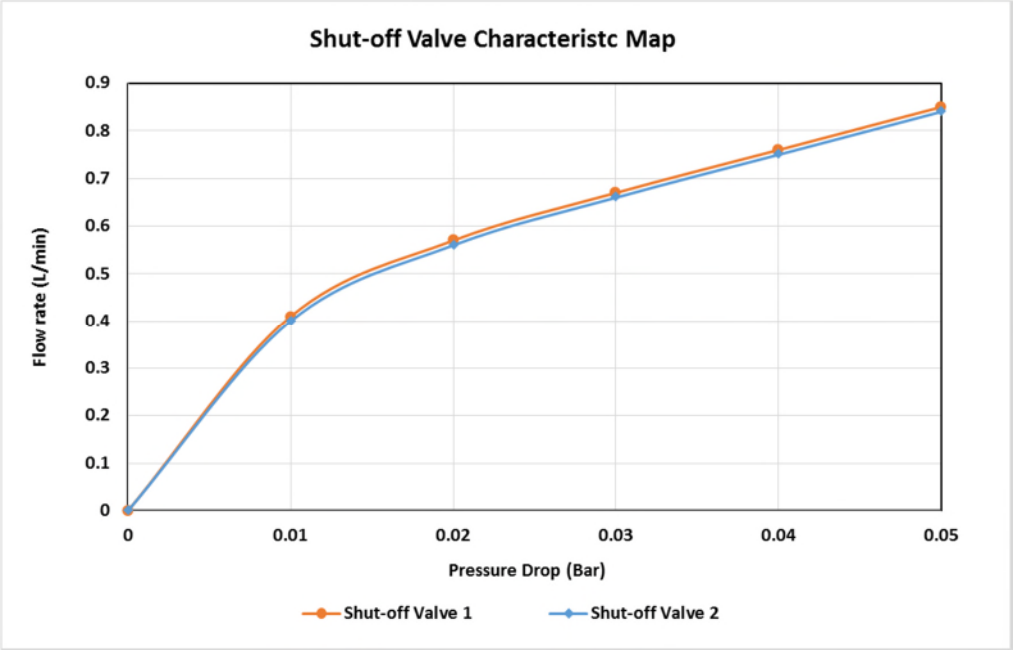


**Figure 4-15 The shut-off valve characteristic map**

It can be seen that as more flow is forced through the valve, the pressure drop gets higher. The characteristic of the flow rate versus pressure drop is linear apart from the zero point. It should be noted here that the maps of the five shut-off valves are not exactly the same. The difference between the characteristics of the five shut-off valves for each measurement point is within 3%.

### Direct proportional valve (DPV)

In the same way as for the shut-off valve, the characteristic map for the DPV is created by using a gear pump to connect with the DPV to get different flow rates (by changing the pump speed) through the valve. Figure 4-16 shows the characteristic map of the DPV when it is opened at 100%, 80% and 50%. The ordinate is the pressure drop across the valve, and the abscissa is the flow rate through the valve. The measurement points are averaged over 3 seconds.

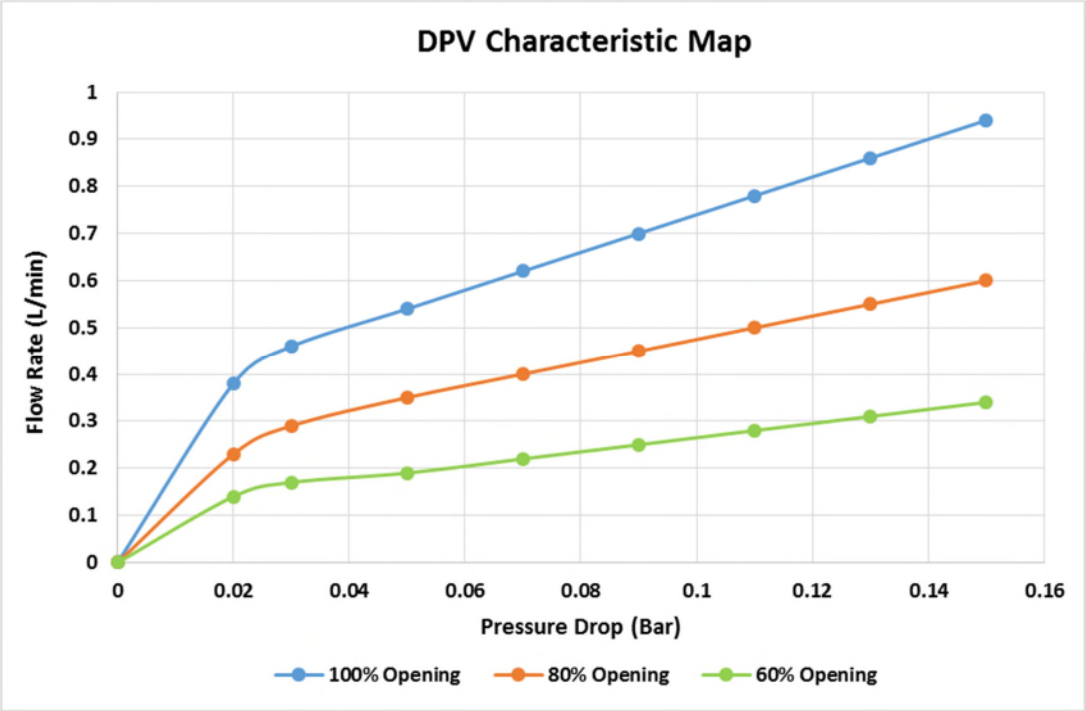


**Figure 4-16 The DPV characteristic map**

It can be seen that the closing of the DPV leads to an increase in the pressure drop across the valve. The characteristic of the flow rate versus pressure drop for a certain opening percentage is linear apart from the zero point. It should be noted here that the maps of the six DPVs are not exactly the same. The difference between the characteristics of the six DPVs for each measurement point is within 3%.

### 4.3.3 System Level

#### Day to Day Repeatability Testing

The testing is conducted by running the fuel rig and collecting readings from all ten pressure sensors (P1-P10) and four flow meters (F1, F2, F4, F5) at different pump speeds (from 200rpm to 600rpm) under steady state conditions. The difference between the averaged pump speed on the rig and the set value of the pump speed in the control system is within ±1rpm. An example of the rig configuration for testing is shown in Table 4-7. This table is seen as an easy way to express the status of all controllable components in the rig. It will be used to describe the rig configuration for the experiments in Section 4.6 as well.

**Table 4-7 Rig configuration for testing**

| Degradation Valves | | | | | Gear Pumps | | | Other Valves | | | | | |
|---|---|---|---|---|---|---|---|---|---|---|---|---|---|
| DPV1 | DPV2 | DPV3 | DPV4 | DPV5 | 1 | 2 | 3 | SOV1 | SOV2 | PRV | SV | CFV | DPV6 |
| 100% Opening | 0% Opening | 100% Opening | 100% Opening | 100% Opening | 400 rpm | 400 rpm | 400 rpm | OPEN | OPEN | CLOSE | CLOSE | OPEN | 100% Opening |

The results from the pressure sensor 1 and flow meter 1 when the pump speed is 400rpm are selected as examples and shown in Figure 4-17 and Figure 4-18 respectively. The sensor readings are labeled with E-1, E-2 and E-3 to represent the result from different days' experiment.

±1.5%

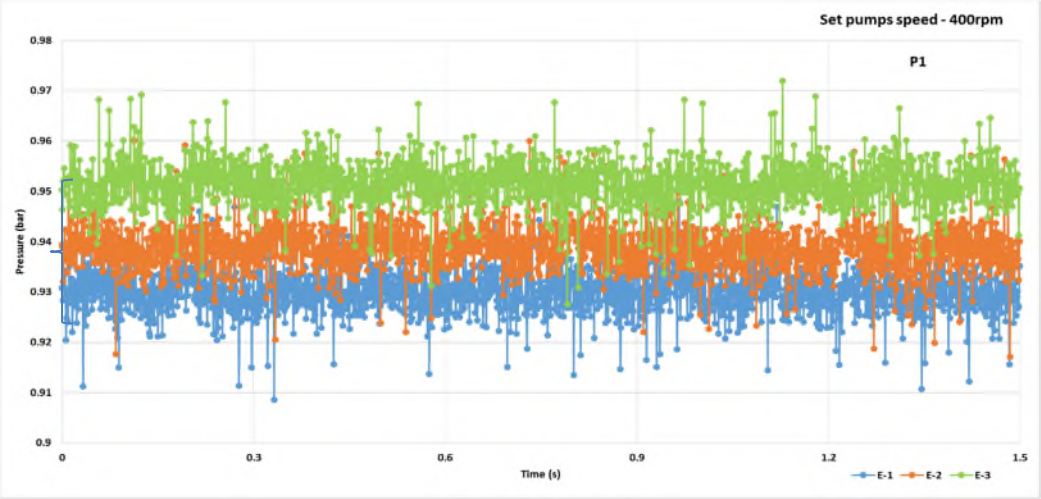


**Figure 4-17 Results from pressure sensor 1 when the pump speed is 400rpm**

±3%

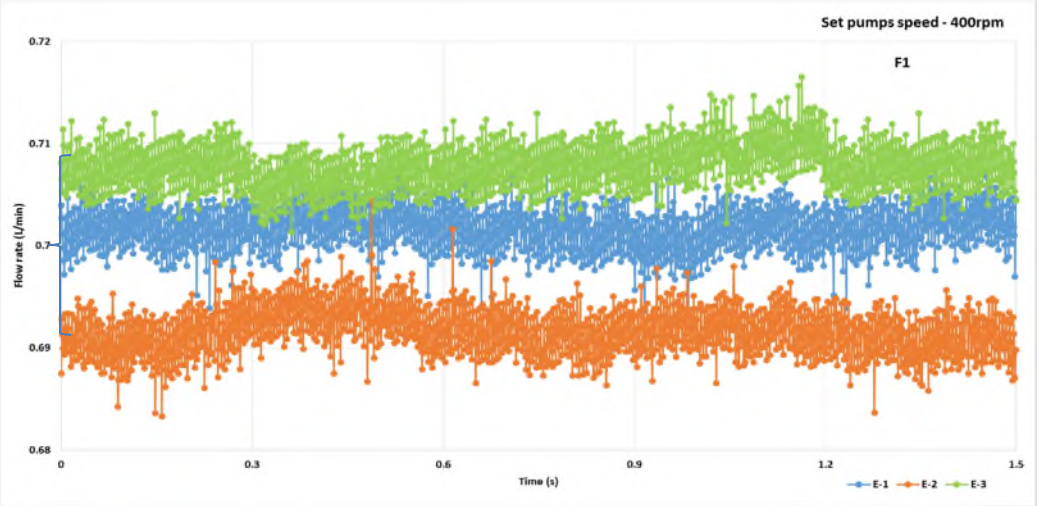


**Figure 4-18 Results from flow meter 1 when the pump speed is 400rpm**

The discrepancy of pressure and flow rate between different days' experiment at different pump speeds are shown in Table 4-8 and 4-9 respectively.

**Table 4-8 Discrepancy of pressure at different pump speeds**

| Set pump speed (rpm) | P1 | P2 | P3 | P4 | P5 | P6 | P7 | P8 | P9 | P10 |
|---|---|---|---|---|---|---|---|---|---|---|
| 200 | ±1.5% | ±2% | ±1.2% | ±1.1% | ±1% | ±1.2% | ±0.6% | ±0.5% | ±1.2% | ±0.5% |
| 300 | ±1.3% | ±1.5% | ±1.1% | ±1% | ±0.5% | ±1.1% | ±0.5% | ±0.6% | ±1.3% | ±0.5% |
| 400 | ±1.5% | ±2% | ±1% | ±1% | ±0.5% | ±1% | ±0.5% | ±0.5% | ±1% | ±0.5% |
| 500 | ±1% | ±1.6% | ±0.8% | ±1.2% | ±0.8% | ±1% | ±0.5% | ±0.7% | ±1% | ±0.6% |
| 600 | ±1.2% | ±2% | ±0.5% | ±0.7% | ±0.6% | ±0.5% | ±0.6% | ±0.8% | ±1.1% | ±0.6% |

**Table 4-9 Discrepancy of flow rate at different pump speeds**

| Set pump speed (rpm) | F1 | F2 | F4 | F5 |
|---|---|---|---|---|
| 200 | ±3% | ±2.5% | ±3% | ±3% |
| 300 | ±3% | ±2% | ±1.5% | ±2% |
| 400 | ±3% | ±2% | ±1.5% | ±1.5% |
| 500 | ±2% | ±1.5% | ±1.2% | ±1.5% |
| 600 | ±1.5% | ±1.5% | ±1.5% | ±1.2% |

It can be seen that the discrepancy between different days' experiment for the pressure measurements under different pump speeds is no more than ±2%. A slightly bigger discrepancy is observed in the flow rates with no more than ±3% discrepancy between different days' experiment. Both are acceptable in terms of repeatability.

**Simulation Model vs. Physical System Testing**

The testing is conducted by running both the rig and the physical simulation model under different test configurations and comparing them.

The physical simulation model of the rig is developed using a CAE (Computer-Aided Engineering) software tool – SimulationX™ from ITI. The SimulationX™ is a program package for the physical modelling and simulation of complex engineering systems such as hydraulic system and mechanical system. It offers a variety of model libraries from mechanics to hydraulics for designing and analysing the behaviour of an engineering system. The parameters of a component such as the tank capacity, pipe's length and diameter, pump characteristic, shut-off valve characteristic and DPV characteristic can be calibrated within the model library based on the user's requirement. After identifying the parameters of each component model, the overall system model can be created and the output from the system can be calculated through a computer-based simulation in no time. Figure 4-19 shows the simulation model of the fuel rig. The model is calibrated using data obtained from the experimental fuel rig.

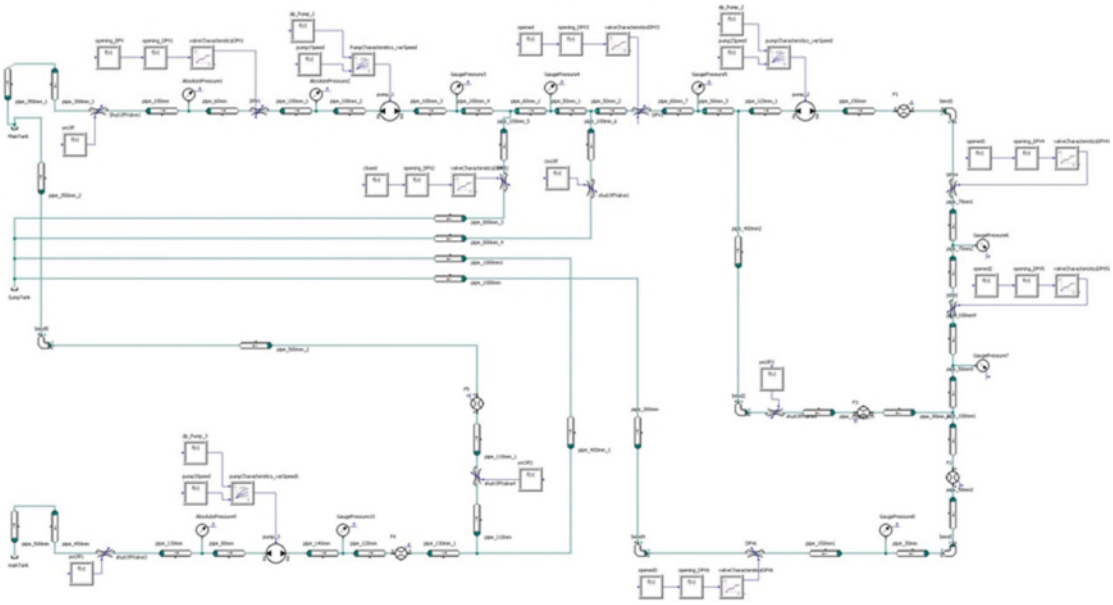

**Figure 4-19 Simulation model of the fuel rig**

The testing procedure is conducted for a range of pump speeds (from 200rpm to 600rpm). An example of the test configuration is shown in Table 4-10.

**Table 4-10 Test configuration**

| Degradation Valves | | | | | Gear Pumps | | | Other Valves | | | | | |
|---|---|---|---|---|---|---|---|---|---|---|---|---|---|
| DPV1 | DPV2 | DPV3 | DPV4 | DPV5 | 1 | 2 | 3 | SOV1 | SOV2 | PRV | SV | CFV | DPV6 |
| 100% Opening | 0% Opening | 100% Opening | 100% Opening | 100% Opening | 200 - 600 rpm | 200 - 600 rpm | 200 - 600 rpm | OPEN | OPEN | CLOSE | CLOSE | OPEN | 100% Opening |

The results from the pressure sensors and flow meters when the pump speed is 400rpm are selected as examples and shown in Figure 4-20 and Figure 4-21 respectively. The orange line represents the measured data from the rig, the green line represents the simulation data.

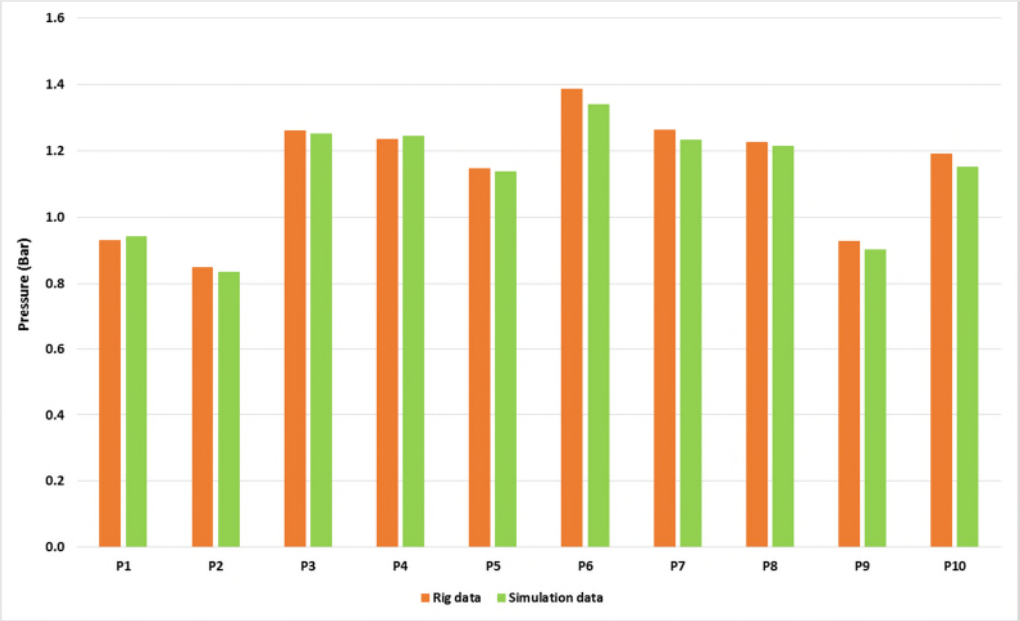


**Figure 4-20 Simulation data vs. rig data (pressure sensor)**

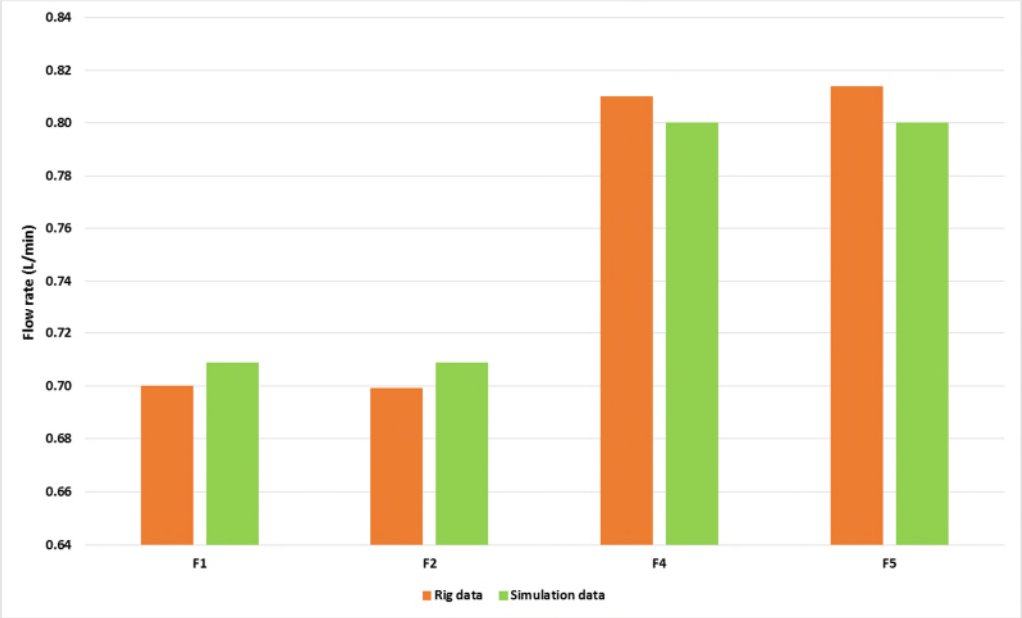


**Figure 4-21 Simulation data vs. rig data (flow meter)**

The discrepancy between the Simulation data and the measured data from the rig under the above test configuration is shown in Table 4-11 and 4-12 respectively. It should be noted here that the repeatability of the rig data for the pressure measurements and flow rates is within ±2% and ±3% respectively.

**Table 4-11 Discrepancy between the simulation data and rig data – pressure**

| Set pump speed (rpm) | P1 | P2 | P3 | P4 | P5 | P6 | P7 | P8 | P9 | P10 |
|---|---|---|---|---|---|---|---|---|---|---|
| 200 | -1.1% | -1.7% | 3.2% | 2.6% | 3.2% | 4.6% | 3.6% | 2.3% | 0.5% | 4.1% |
| 300 | 0.7% | 1.5% | 2.6% | 2.4% | 2.9% | 4.9% | 2.9% | 1.8% | 4.2% | 4.2% |
| 400 | -1.2% | 1.5% | 0.8% | -0.7% | 0.7% | 3.5% | 2.5% | 1.0% | 2.8% | 3.4% |
| 500 | -1.3% | 0.5% | 1.3% | 0.7% | 1.5% | 4.4% | 2.3% | 0.4% | 3.5% | 3.0% |
| 600 | -1.3% | 0.3% | 3.1% | 2.3% | 2.8% | 5.1% | 2.2% | 0.1% | 3.0% | 4.6% |

**Table 4-12 Discrepancy between the simulation data and rig data - flow rate**

| Set pump speed (rpm) | F1 | F2 | F4 | F5 |
|---|---|---|---|---|
| 200 | -4.6% | -3.6% | -4.5% | -3.0% |
| 300 | -1.5% | 0.8% | -1.6% | 1.6% |
| 400 | -1.3% | -1.4% | 1.3% | 1.7% |
| 500 | 1.7% | 2.4% | -1.4% | 0.7% |
| 600 | 0.6% | 2.2% | 2.6% | 3.4% |

It can be seen that the discrepancy between the simulation data and the rig data for the pressure measurements is less than 5% except the one for the pressure sensor 6 when the pump speed is 600rpm (the discrepancy is 5.1%). Flow rates calculated by the simulation model are also close to those obtained from the rig (having less than 5% discrepancy). Assessment was done for all the other test configurations and the discrepancies were acceptable as well. Overall, while the simulation model could be further improved, agreement was seen as satisfactory.

## 4.4 Configuration Management

Configuration management is the detailed recording of information that describes all the components used in an equipment. It is a typical system engineering practice for establishing and maintaining consistency of an equipment's performance, functional, and physical attributes and is modified over time as new components are installed. The configuration management

form produced for the experimental fuel rig is attached in Appendix A, which includes the description, manufacturer's information, quantity and cost of each component. In the future, if the rig needs to be repaired or upgraded, all these information can be used as a reference.

## 4.5 Operating Procedure

The operating procedure is a set of step-by-step instructions that helps the operators carry out routine operations. It aims to achieve safety, efficiency and repeatability of output, while reducing miscommunication to comply with the health and safety regulations. The operating procedure written for the experimental fuel rig is attached in Appendix B.

## 4.6 Experiments

This section introduces the experiments conducted on the experimental fuel rig for the implementation of the proposed method in Chapter 5. Table 4-13 shows the rig configuration of the experiments. For simplicity, all components will share the same degradation step, i.e., 10% for each step. All the sensor readings are collected at 1 kHz when the rig is running under steady state conditions.

**Table 4-13 Rig configuration of the experiments**

| Expt Name | Degradation Valves | | | | | Gear Pumps | | Other Valves | | | | | |
|---|---|---|---|---|---|---|---|---|---|---|---|---|---|
| | DPV1 | DPV2 | DPV3 | DPV4 | DPV5 | 1 | 2 | SOV1 | SOV2 | PRV | SV | CFV | DPV6 |
| Sticking Valve | 60-100% Opening | 0-20% Opening | 80-100% Opening | 80-100% Opening | 80-100% Opening | 400 rpm | 0.58L/min | OPEN | CLOSE | CLOSE | CLOSE | CLOSE | 100% Opening |
| Leaking Pipe | 80-100% Opening | 0-50% Opening | 80-100% Opening | 80-100% Opening | 80-100% Opening | 400 rpm | 0.7L/min | OPEN | CLOSE | CLOSE | CLOSE | CLOSE | 100% Opening |
| Clogged Filter | 80-100% Opening | 0-20% Opening | 60-100% Opening | 80-100% Opening | 80-100% Opening | 450 rpm | 0.66L/min | OPEN | CLOS | CLOS | CLOS | CLOS | 100% Opening |

| | | | | | | | | | | | | | |
|---|---|---|---|---|---|---|---|---|---|---|---|---|---|
| | | | | | | | | | E | E | E | E | |
| Blocked Flow Meter | 80-100% Opening | 0-20% Opening | 80-100% Opening | 60-100% Opening | 80-100% Opening | 300 rpm | 0.5L/min | OPEN | CLOSE | CLOSE | CLOSE | CLOSE | 100% Opening |
| Clogged Nozzle | 80-100% Opening | 0-20% Opening | 80-100% Opening | 80-100% Opening | 60-100% Opening | 300 rpm | 0.5L/min | OPEN | CLOSE | CLOSE | CLOSE | CLOSE | 100% Opening |

In the sticking valve experiment, the opening percentage of the DPV1 is varied from 60% to 100% representing the sticking valve fault with different degrees of severity. The opening percentage of the DPV2 is varied from 0% to 20% representing the degraded pipe with different degradation levels. The opening percentage of the DPV3, 4 and 5 is varied from 80% to 100% representing the degraded filter, flow meter and nozzle respectively.

In the leaking pipe experiment, the opening percentage of the DPV2 is varied from 0% to 50% representing the leaking pipe fault with different degrees of severity. The opening percentage of the DPV1, 3, 4 and 5 is varied from 80% to 100% representing the degraded valve, filter, flow meter and nozzle respectively.

In the clogged filter experiment, the opening percentage of the DPV3 is varied from 60% to 100% representing the clogged filter fault with different degrees of severity. The opening percentage of the DPV2 is varied from 0% to 20% representing the degraded pipe with different degradation levels. The opening percentage of the DPV1, 4 and 5 is varied from 80% to 100% representing the degraded valve, flow meter and nozzle respectively.

In the blocked flow meter experiment, the opening percentage of the DPV4 is varied from 60% to 100% representing the blocked flow meter fault with different degrees of severity. The opening percentage of the DPV2 is varied from 0% to 20% representing the degraded pipe with different degradation levels. The opening percentage of the DPV1, 3 and 5 is varied from 80% to 100% representing the degraded valve, filter and nozzle respectively.

In the clogged nozzle experiment, the opening percentage of the DPV5 is varied from 60% to 100% representing the clogged nozzle fault with different degrees of severity. The opening percentage of the DPV2 is varied from 0% to 20% representing the degraded pipe with different degradation levels. The opening percentage of the DPV1, 3 and 4 is varied from 80% to 100% representing the degraded valve, filter and flow meter respectively.

For all the five experiments, the gear pump 1 (serves as the low pressure pump) is controlled to run at a constant speed while the gear pump 2 (serves as the high pressure pump) is controlled to provide constant flow rate. The shut-off valve (SOV) 1 and the engine throttle valve (DPV6) are fully opened while other valves are closed.

### 4.6.1 Experimental Results

Figure 4-22 to 4-26 show the experimental data generated under each fault scenario without considering multi-component degradation. They will be analysed for extracting the key features of each fault scenario which are used to conduct the case analysis in Chapter 5.

**Sticking Valve**

For the sticking valve scenario (shown in Figure 4-22), the closing of DPV 1 to emulate a valve that is not closing properly leads to an increase in the pressure drop across the valve (shown in Figure 4-16). As the valve is located between the pressure sensor 1 and 2 (shown in Figure 4-7), the reading of the pressure sensor 2 will decrease correspondingly when the sticking fault occurs. Since the flow rate in the main line is controlled to be constant, the readings of the pressure sensor 3 to 5 will also decrease when the sticking fault occurs. The readings of the pressure sensor 6 to 8 will not change as they are determined by the atmosphere pressure at the output of the rig system. As the pressure ratio across the gear pump 2 increases, the speed of the pump will increase in order to provide constant flow rate (shown in Figure 4-14).

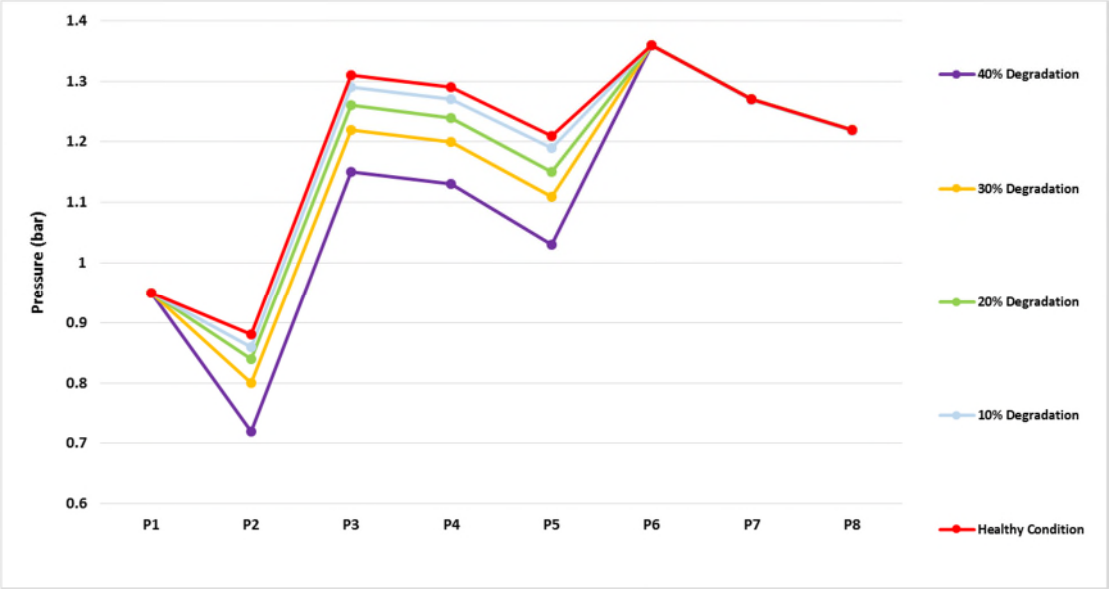


**Figure 4-22 Sensor reading (averaged) change under sticking valve scenario**

### Leaking Pipe

For the leaking pipe scenario (shown in Figure 4-23), as the leaking is injected by means of opening the DPV 2 which is located between the two gear pumps (shown in Figure 4-7), the leaking fault will lead to a decrease in the reading of the pressure sensor 3 to 5 when the flow rate in the main line is controlled to be constant. This is because the mass flow provided by the gear pump 1 needs to increase in order to maintain a constant flow rate in the main line, according to the continuity principle, but as the gear pump 1 is running at a constant speed, the pressure ratio across the pump needs to decrease as shown in Figure 4-14. The readings of pressure sensor 1 and 2 will not change as they are determined by the atmosphere pressure at the input of the rig system and the speed of the gear pump 1 which is constant. The readings of the pressure sensor 6 to 8 will not change as they are determined by the atmosphere pressure at the output of the rig system. The speed of the gear pump 2 will increase to compensate for the leaking pipe and keep the mass flow constant.

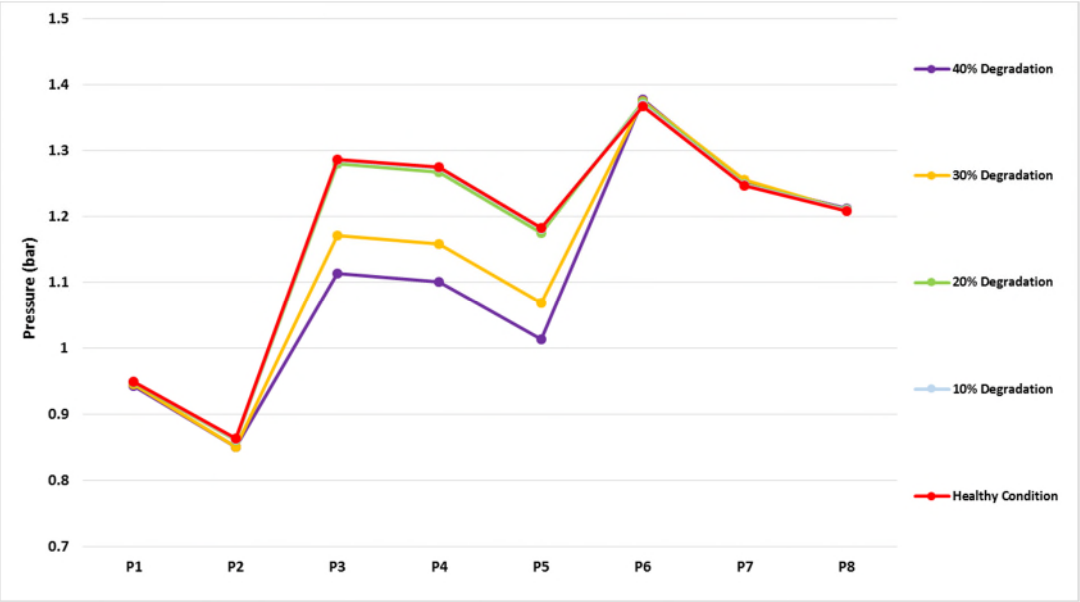


**Figure 4-23 Sensor reading (averaged) change under leaking pipe scenario**

### Clogged Filter

For the clogged filter scenario (shown in Figure 4-24), the closing of DPV 3 to emulate a clogged filter leads to an increase in the pressure drop across the valve (shown in Figure 4-16). As the DPV 3 is located between the pressure sensor 4 and 5 (shown in Figure 4-7), the reading of the pressure sensor 5 will decrease correspondingly when the clogging fault occurs. The readings of pressure sensor 1, 2, 6, 7 and 8 will not change for the same reason mentioned in the leaking pipe scenario. The readings of pressure sensor 3 and 4 will not change as the flow rate in the main line is controlled to be constant and the gear pump 1 is running at a constant speed. The speed of the gear pump 2 will increase for the same reason mentioned in the sticking valve scenario.

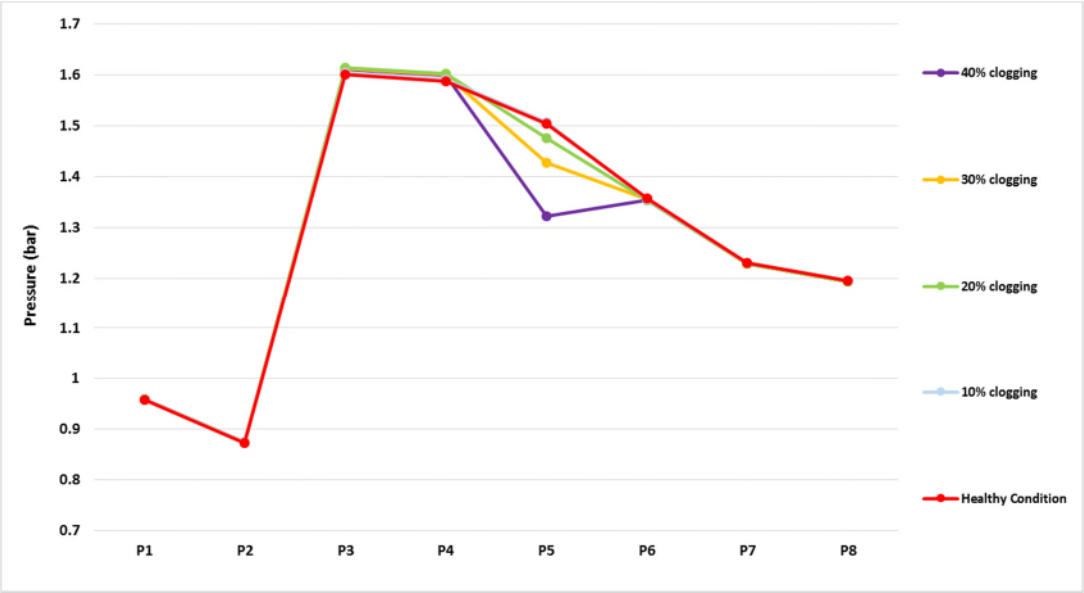


**Figure 4-24 Sensor reading (averaged) change under clogged filter scenario**

### Blocked Flow Meter

For the blocked flow meter scenario (shown in Figure 4-25), the closing of DPV 4 to emulate a blocked flow meter generates a backpressure to the gear pump 2. In order to maintain the constant flow rate in the main line, the speed of the gear pump 2 will increase. The readings of the pressure sensor 1, 2, 6, 7 and 8 will not change for the same reason mentioned in the leaking pipe scenario. As the flow rate in the main line is controlled to be constant and the speed of the gear pump 1 is constant, the readings of the pressure sensor 3 to 5 will not change either. Therefore it may be thought that the blocked flow meter has no effect. This is true for the observation made, but now if an imaginary pressure sensor (P*) is located between the gear pump 2 and the DPV 4, its pressure can be deduced according to the pump characteristic map (shown in Figure 4-14). As the pump speed and the flow rate are known, the pressure ratio across the pump can be determined. Given the reading of the pressure sensor 5 which is the inlet pressure of the pump, the reading of that imaginary pressure sensor (P*) can be obtained as shown by the dotted line in Figure 4-25.


**Figure 4-25 Sensor reading (averaged) change under blocked flow meter scenario**

### Clogged Nozzle

For the clogged nozzle scenario (shown in Figure 4-26), the closing of DPV 5 to emulate a clogged nozzle leads to an increase in the pressure drop across the valve (shown in Figure 4-16). As the DPV 5 is located after the pressure sensor 6 (shown in Figure 4-7), the reading of the pressure sensor 6 will increase correspondingly when the clogging fault occurs. The readings of the pressure sensor 1 to 5, 7 and 8 will not change for the same reason mentioned in the above fault scenarios. The speed of the gear pump 2 will increase in order to provide constant flow rate.


**Figure 4-26 Sensor reading (averaged) change under clogged nozzle scenario**

Based on the above experimental results, the key features (shown in Table 4-14) when a certain fault occurs without considering multi-component degradation can be extracted which will be used to conduct the case analysis in Chapter 5. Here the set allowable threshold level is 30% so if the degradation level reaches or exceeds this threshold level, the fault is considered to occur.

**Table 4-14 Key features of each fault scenario**

| Fault scenario | Key features |
|---|---|
| Sticking valve | The pressure drop across the sticking valve, i.e. the reading of pressure sensor 1 minus the reading of pressure sensor 2 should be no less than 0.17bar. |
| Leaking pipe | The reading of pressure sensor 3 to 5 should all decrease and the ratio of reading change of pressure sensor 2 should be less than 10%. |
| Clogged filter | The pressure drop across the clogged filter, i.e. the reading of pressure sensor 4 minus the reading of pressure sensor 5 should be no less than 0.17bar. |
| Blocked flow meter | The reading of pressure sensor 3 to 5 should all increase and the ratio of reading change of pressure sensor 6 should be less than 10%. |
| Clogged nozzle | The ratio of reading change of pressure sensor 6 should be no less than 10%. |

## 4.7 Summary

The whole development process of the experimental fuel rig and the experiments conducted for the implementation of the proposed method were introduced in this chapter. In the next chapter, the data generated from the experiments will be used to validate the proposed method.

# 5 Implementation of System Diagnosis on the Fuel Rig Data

Now that the experimental fuel rig has been constructed and validated, along with the simulation model, the rig can be used to produce the data of multi-component degradation on which various diagnostic approaches can be implemented. This chapter discusses the implementation of system diagnosis on the fuel rig data and is structured as follows. In Section 5.1, the workflow for the methods being used is introduced, followed by the description of the data-driven Bayesian method (both classic and modified) and neural network method. The neural network method is introduced in order to compare with the modified Bayesian method. Section 5.2 presents five different application scenarios, from the experimental work described in Section 4.6, that are used to validate the proposed Bayesian method and compare the diagnostic results. The discussion of the results from the five application scenarios is given in Section 5.3.

## 5.1 Diagnostic Approach

### 5.1.1 Workflow for the methods being used

This subsection introduces the workflow for the methods being used, and is shown in Figure 5-1.

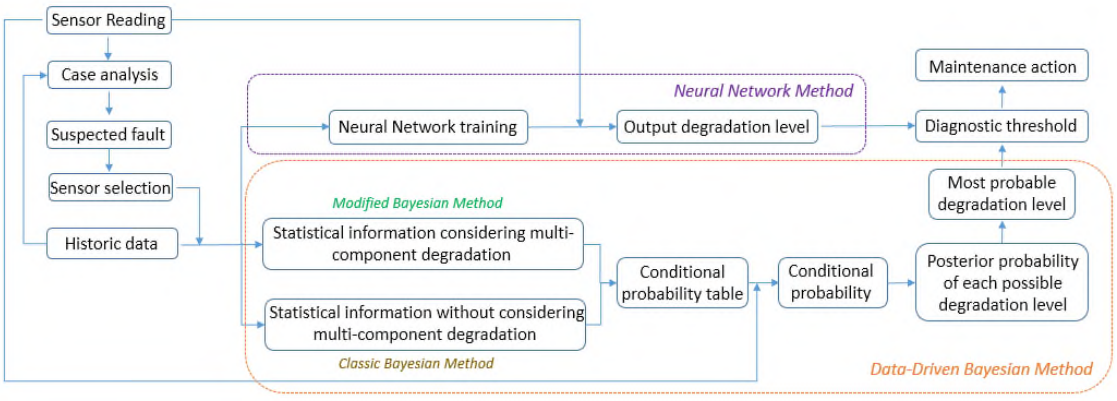


**Figure 5-1 Workflow for the methods being used**

In the workflow, first, when the current sensor readings come in, no matter which method is going to be used, a case analysis will take place to obtain the suspected fault based on the key features (shown in Table 4-14) extracted from the historic data generated under each fault scenario. By checking whether current sensor readings match the key features (shown in Table 4-14) or not, the suspected fault given current sensor readings can be obtained. With the suspected fault known, certain sensors will be selected based on the criteria that the ratio of that sensor reading change should be no less than 10% when the fault happens. Then for the data-driven Bayesian method, statistical information (i.e., the sensor reading distribution) from historic data will have been obtained for the suspected fault. Based on the sensor reading distribution, the conditional probability table for different degradation levels can be obtained by categorising the sensor reading into conditional probabilities (CP) of being in value ranges (very low-low-normal-high-very high). According to the conditional probability table, current sensor reading will be classified and the corresponding conditional probability can be obtained. Then based on the Bayesian formula, the probability of each possible degradation level will be calculated. Among all the possible degradation levels, the one that has the largest probability will be considered as the one that causes the current sensor reading. If that degradation level reaches or exceeds the allowable diagnostic threshold, the suspected fault is considered to occur and this result will be sent to maintainers to help them arrange their maintenance actions.

For the neural network method, the network will be trained for the suspected fault based on the historic data. After the training process, current sensor reading will be put into the network to obtain the corresponding output (i.e. the degradation level). If the output degradation level reaches or exceeds the allowable diagnostic threshold, the suspected fault is considered to occur and this result will be sent to maintainers to help them arrange their maintenance actions.

### 5.1.2 Data-Driven Bayesian Method

This subsection introduces the fundamental concept and formula of the Bayesian method (both classic and modified).

“The probability of any event is the ratio between the value at which an expectation depending on the happening of the event ought to be computed, and the value of the thing expected upon its happening.” -Thomas Bayes (1702-1761)

The fundamental concept behind Bayesian method is to update the current probability of an event given new or additional evidence. Assume that A represents an event and B represents an observable variable. If A and B occur independently in a system, it is able to calculate the probability of both occurring:

$$P(A\&B) = P(A)P(B) \tag{5-1}$$

If A occurs and given A has occurred then B occurs, the probability of A and B both occurring can be calculated as:

$$P(A\&B) = P(A)P(B|A) \tag{5-2}$$

P (B│A) is called conditional probability of B given A has occurred.

If B occurs and given B has occurred then A occurs, the probability of A and B both occurring can be calculated as:

$$P(A\&B) = P(B)P(A|B) \tag{5-3}$$

P (A│B) is called conditional probability of A given B has occurred.

From Eq. (5-2) and (5-3):

$$P(A\&B) = P(A)P(B|A) = P(B)P(A|B) \tag{5-4}$$

So the conditional probability of A given B has occurred can be written as:

$$P(A|B) = \frac{P(B|A)P(A)}{P(B)} \tag{5-5}$$

This simple but important expression allows us to form a hypothesis about an event based on the observable variable and a belief in the probability of that event.

One good and simple example of using this in real world is medical diagnosis. Suppose that a bacterial infection causes a fever 80% of the time, and now 5% patients are suffering from the fever. If a patient is selected randomly, there is 1% chance of that patient having a bacterial infection. Given all this information, the doctor can form a hypothesis that the probability of a bacterial infection given the patient having a fever is:

$$P(Infection|Fever) = \frac{P(Fever|Infection)P(Infection)}{P(Fever)} = \frac{80\% \times 1\%}{5\%} = 16\% \quad \textbf{(5-6)}$$

This result shows that if the patient has a fever, it is much more likely that the fever is not caused by a bacterial infection.

So in our case, based on current sensor reading $\boldsymbol{S}$ (a vector) from the target system, the probability of a certain degradation level L for the suspected faulty component can be written according to Bayes theory as:

$$P(L|\boldsymbol{S}) = \frac{P(\boldsymbol{S}|L)P(L)}{P(\boldsymbol{S})} \quad \textbf{(5-7)}$$

where P(L$\,|\,\boldsymbol{S}$) is the probability of a certain degradation level given the sensor reading; P($\boldsymbol{S}\,|\,$L) is the conditional probability of current sensor reading given a certain degradation level; P(L) is the prior probability of a certain degradation level; and P($\boldsymbol{S}$) is the prior probability of current sensor reading. Note that P(L) and P($\boldsymbol{S}$) are determined by a priori information (here we assume that the value used for P(L) and P($\boldsymbol{S}$) is 0.1), the probability of a certain degradation level in Eq. (5-7) can be denoted as:

$$P(L|\boldsymbol{S}) \propto P(\boldsymbol{S}|L) \quad \textbf{(5-8)}$$

Among all the possible degradation levels, the one that has the largest probability will be considered as the one that causes current sensor reading according to the Maximum Likelihood Estimate principle.

Thus, the main task for diagnosing the fault is to calculate the conditional probability P($\boldsymbol{S}$ | L) which can be computed as:

$$P(\boldsymbol{S}|L) = \prod_{i=1}^{n} P(S_i|L) \quad \textbf{(5-9)}$$

where P ($S_i$ | L) represents the conditional probability of ith sensor's reading under a certain degradation level, n is the number of selected sensors, Π is the symbol representing a product over a set of terms.

If the multi-component degradation is not taken into account, i.e. in classic Bayesian method, the probability of a certain degradation level would be expressed as:

$$P(L|\boldsymbol{S}) \propto P(\boldsymbol{S}|L) = \prod_{i=1}^{n} P(S_i|L) \quad \textbf{(5-10)}$$

When multi-component degradation is considered, one contribution from this research, the conditional probability P ($S_i$ | L) has been rewritten as P ($S_i$ | C), where C represents all the components' state in the system. This change means that the conditional probability of current sensor reading is not only dependent upon the faulty component but also the degraded components in the system. Figure 5-2 succinctly illustrates the relationship between the suspected faulty component, all the other degraded components in the system and current sensor reading. $F_C$ represents the suspected faulty component, $D_i$ (i=1, 2, …, m, m is the number of components) represents a certain degraded component in the system, $S_j$ (j=1, 2, …, n, n is the number of sensors) represents the current sensor reading, $L_k$ (k=1, 2, …, p, p is the number of possible degradation levels of the faulty component) represents the likelihood of a certain degradation level of the faulty component, CPT represents the conditional probability table.

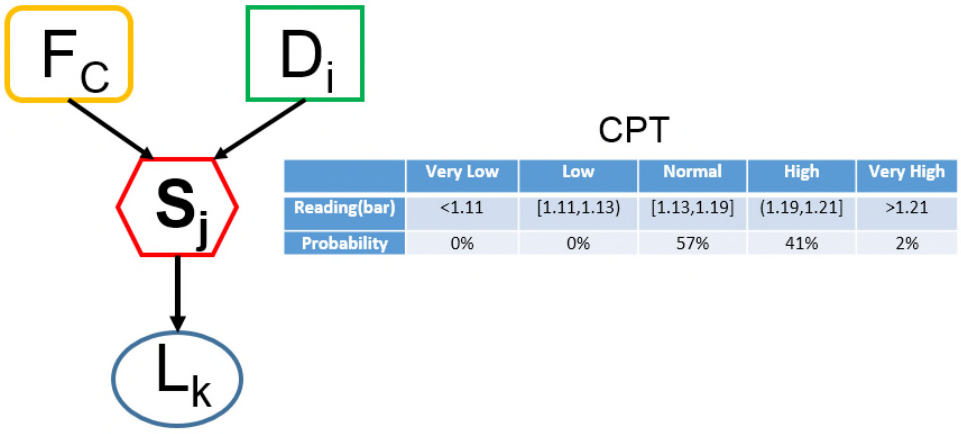


**Figure 5-2 Relationship between the suspected faulty component, all degraded components in the system and current sensor readings**

Thus, from Eq. (5-8) and (5-9):

$$P(C|\boldsymbol{S}) \propto P(\boldsymbol{S}|C) = \prod_{i=1}^{n} P(S_i|C) \tag{5-11}$$

It should be noted here that Eq. (5-11) is an improvement over Eq. (5-10) but requires the knowledge of the system in all of its degraded states.

### 5.1.3 Neural Network Method

The neural network used in our case is a typical three layer feed forward neural network (shown in Figure 5-3). The input data is the measured results (i.e. sensor readings) while the output is the degradation level.

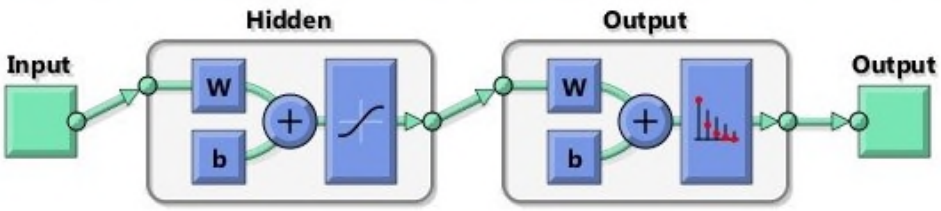


**Figure 5-3 Three layer feed forward neural network**

The fundamental concept of neural network method has been briefly introduced in Section 2.1.2. Here it is just used as a black box that deals with a vector of input (sensor readings) and provides a vector of output (degradation levels).

During the training process, the Neural Network Toolbox in Matlab is used and the training dataset for a certain degradation level of the faulty component is shown in Table 5-1. Each row in the table refers to the reading from a selected sensor and each column represents one set of sensor readings of the training dataset. After the training process, the current sensor readings can be put into the neural network to obtain the corresponding output degradation level of the faulty component.

**Table 5-1 Training dataset for a certain degradation level of the faulty component**

| Reading Set / Sensor | 1 | 2 | 3 | … | n |
|---|---|---|---|---|---|
| $S_1$ | $Reading_{1,1}$ | $Reading_{1,2}$ | $Reading_{1,3}$ | … | $Reading_{1,n}$ |
| $S_2$ | $Reading_{2,1}$ | $Reading_{2,2}$ | $Reading_{2,3}$ | … | $Reading_{2,n}$ |
| $S_3$ | $Reading_{3,1}$ | $Reading_{3,2}$ | $Reading_{3,3}$ | … | $Reading_{3,n}$ |
| … | … | … | … | … | … |
| $S_m$ | $Reading_{m,1}$ | $Reading_{m,2}$ | $Reading_{m,3}$ | … | $Reading_{m,n}$ |

### 5.1.4 Diagnostic Performance Assessment Metrics

In order to assess the proposed method and compare the results with other methods, this subsection introduces four metrics that are often used to assess the performance of a diagnostic method.

1. False positive (false alarm) rate: the ratio of cases in which an alarm is generated while no fault occurs.
2. False negative (missed alarm/missed detection) rate: the ratio of cases in which an alarm is not generated while a fault occurs. It is ideal to have low rate for both false positive and false negative, but in a practical case, there exists a trade-off between the two rates. A low diagnostic threshold will lead to a lot of false alarms which could mean that an engineering system goes to maintenance without needing to, while a high diagnostic

threshold will lead to missed alarms which means a damage may not be detected, i.e. the diagnostic method is essentially worthless.

3. Fault diagnostic rate: the ratio of cases in which an alarm is generated and a fault does occur. This metric is related to false negative rate. The sum of these two rates is equal to one so a lower false negative rate will lead to a higher fault diagnostic rate.
4. Fault diagnostic accuracy: the ratio of correct diagnostic results to the total number of cases. This metric is determined by both false positive and false negative rate. Lower false positive and false negative rate will lead to higher fault diagnostic accuracy which is desirable for a diagnostic method.

## 5.2 Case Studies

The data used for the case studies is generated from the experimental work described in Section 4.6. 3000 samples (i.e. 3 seconds of data taken at 1 kHz) are selected under each operating condition among which 2700 (i.e. 90%) are being used as historic data while the remaining 10% are used as test data.

### 5.2.1 Case Study 1: Leaking Pipe

In order to show how the proposed method works, two sets of sensor readings (instantaneous) are selected and serve as examples (shown in Table 5-2).

**Table 5-2 Two sets of sensor readings**

| Example | P1 | P2 | P3 | P4 | P5 | P6 | P7 | P8 | L2 |
|---|---|---|---|---|---|---|---|---|---|
| 1 | 0.94 bar | 0.83 bar | 1.21 bar | 1.21 bar | 1.10 bar | 1.39 bar | 1.25 bar | 1.22 bar | 423 rpm |
| 2 | 0.93 bar | 0.83 bar | 1.16 bar | 1.15 bar | 1.07 bar | 1.38 bar | 1.25 bar | 1.22 bar | 417 rpm |

For each example, after the case analysis (i.e. checking whether the sensor readings match the key features of a certain fault), the suspected fault can be obtained which is the leaking pipe fault in this case. For the leaking pipe fault, pressure sensor 3 to 5 and laser sensor 2 are selected as the indicator based

on the criteria that the ratio of sensor reading (averaged) change should be no less than 10% when the fault happens (shown in Figure 5-4). The fault is considered to happen when the degradation level (i.e. the opening percentage of the DPV 2) reaches or exceeds 30%.

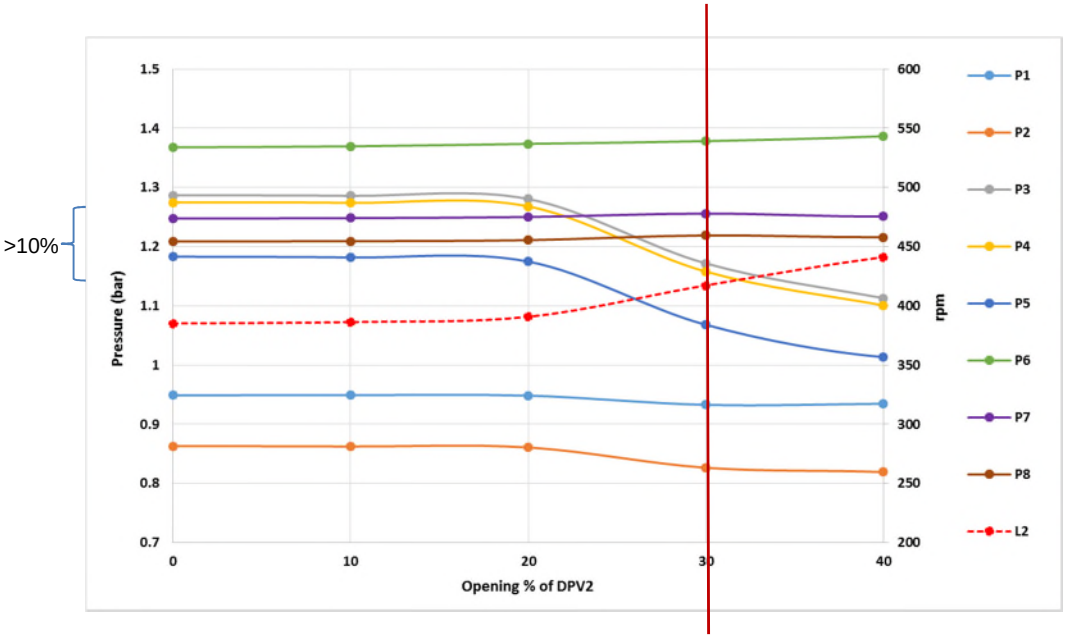


**Figure 5-4 Sensor reading change when the pipe leaking happens**

For the data-driven Bayesian method, based on the historic data, the reading distribution for each possible degradation level can be obtained. For example, Figure 5-5 shows the reading distribution of pressure sensor 4 when the pipe leaking is 30%, 40% and 50% with no other degraded component in the system, which will be used for the classic Bayesian method. Figure 5-6 shows the reading distribution (envelop plot) of pressure sensor 4 when the pipe leaking is 30%, 40% and 50% with all combinations of degraded components in the system, which will be used for the modified Bayesian method. It can be observed from Figures 5-5 and 5-6 that there exist some differences between the sensor reading distribution generated with and without the consideration of multi-component degradation. The sensor reading distribution generated with considering multi-component degradation covers a wider range than the sensor reading distribution generated without considering multi-component degradation. It can also be seen that the impact from the multi-component degradation in this case tends to shield the fault effect.

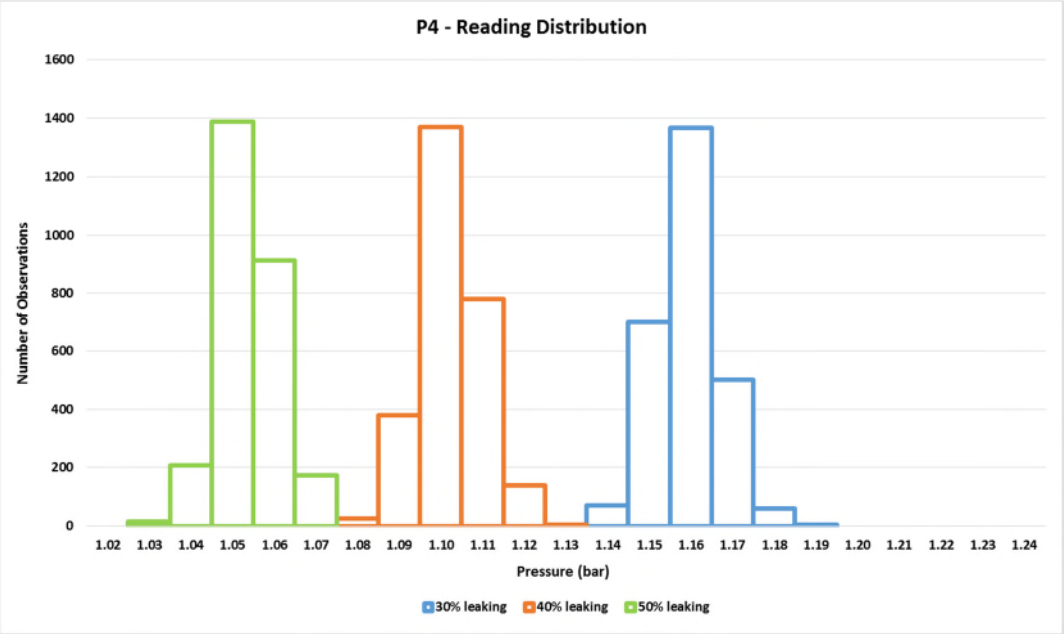


**Figure 5-5 Sensor reading distribution of pressure sensor 4 when the pipe leaking is 30%, 40% and 50% with no other degraded component ($P(S_4|L)$)**

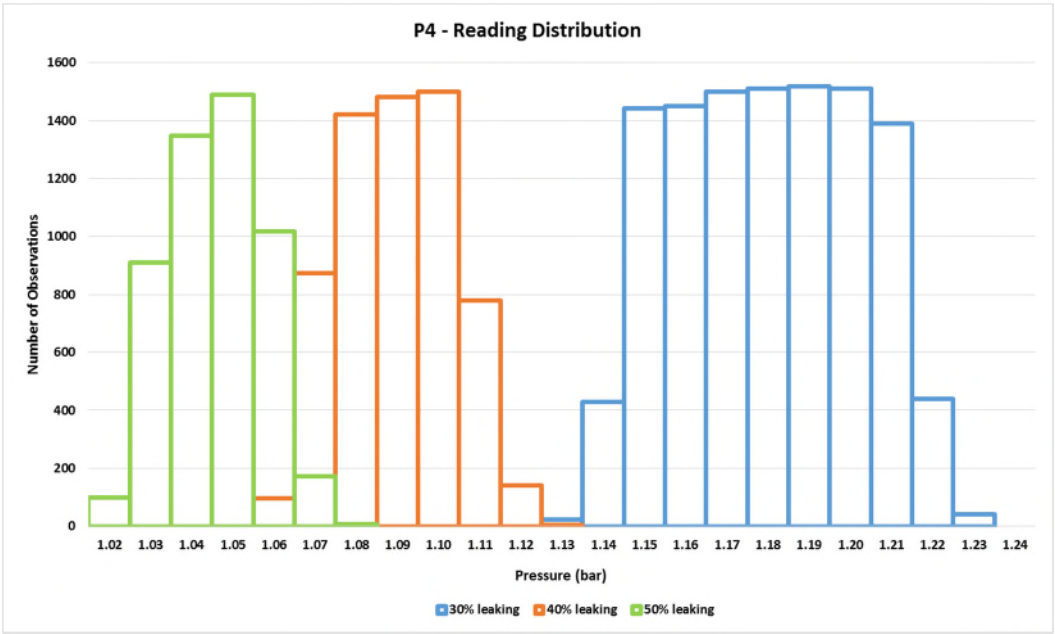


**Figure 5-6 Sensor reading distribution of pressure sensor 4 when the pipe leaking is 30%, 40% and 50% with all combinations of degraded components ($P(S_4|C)$)**

Based on the sensor reading distribution, the conditional probability table for each possible degradation level can be obtained by categorizing the sensor

reading into CP of being in value ranges (very low-low-normal-high-very high). The value range is chosen based on the principle that the normal range should cover all the historic data generated under a certain degradation level when there is no other degraded component in the system, and the low and high range should cover the data within 3σ away from the boundaries of the historic data generated under a certain degradation level when there is no other degraded component in the system. Table 5-3 shows the conditional probability table obtained from Figure 5-6 (the conditional probability of sensor readings within normal range would be 100% when there is no other degraded component in the system).

**Table 5-3 Conditional probability of readings from pressure sensor 4 when the pipe leaking is 30%, 40% and 50% with all combinations of degraded components**

| 30% Leaking | **Very Low** | **Low** | **Normal** | **High** | **Very High** |
|---|---|---|---|---|---|
| Reading(bar) | <1.11 | [1.11,1.13) | [1.13,1.19] | (1.19,1.21] | >1.21 |
| Probability | 0% | 0% | 57% | 41% | 2% |

| 40% Leaking | **Very Low** | **Low** | **Normal** | **High** | **Very High** |
|---|---|---|---|---|---|
| Reading(bar) | <1.05 | [1.05,1.07) | [1.07,1.13] | (1.13,1.15] | >1.15 |
| Probability | 0% | 2% | 98% | 0% | 0% |

| 50% Leaking | **Very Low** | **Low** | **Normal** | **High** | **Very High** |
|---|---|---|---|---|---|
| Reading(bar) | <1.00 | [1.00,1.02) | [1.02,1.08] | (1.08,1.10] | >1.10 |
| Probability | 0% | 0% | 100% | 0% | 0% |

For each selected sensor, based on the conditional probability tables, the current sensor reading can be classified and the corresponding conditional probability can be obtained given a certain degradation level. In Example 1, the conditional probabilities of current P4 reading (1.21bar) are 41%, 0% and 0% given 30%, 40% and 50% pipe leaking respectively according to Table 5-3. In Example 2, the conditional probabilities of current P4 reading (1.15bar) are 57%, 0% and 0% given 30%, 40% and 50% pipe leaking respectively according to Table 5-3.

Based on the conditional probabilities of current sensor readings, the probability of each possible degradation level can be calculated. For classic Bayesian method, the probability $P(L|\boldsymbol{S})$ is calculated using Eq. (5-10) while for the modified method, the probability $P(C|\boldsymbol{S})$ is calculated using Eq. (5-11). After the calculation, the most probable degradation level can be obtained by comparing the probability of each possible degradation level. The degradation level that has the largest probability will be considered as the most probable one that causes the current sensor reading.

Here the set allowable threshold level is 30% so if the most probable degradation level reaches or exceeds this threshold level, the fault is considered to occur. Compared with the actual state of the fault which is obtained by comparing the actual degradation level (the opening percentage of DPV 2) with the allowable threshold level (30%), whether or not the fault is correctly diagnosed can be known.

After running through all the test data generated under each possible degradation level (300×81), the overall decision matrix (shown in Table 5-4) for calculating the metrics that are used to assess the diagnostic performance can be obtained.

**Table 5-4 Overall decision matrix**

| Diagnostic Result / Actual State | Classic Bayesian method | | Modified Bayesian method | |
|---|---|---|---|---|
| | Alarm | No Alarm | Alarm | No Alarm |
| Fault | 63180 | 9720 | 72690 | 210 |
| No Fault | 486 | 72414 | 146 | 72754 |

Based on the overall decision matrix, the diagnostic performance assessment metrics can be calculated. Results are shown in Table 5-5.

**Table 5-5 Diagnostic performance assessment metrics (classic Bayesian method vs. modified Bayesian method)**

| | Classic Bayesian method | Modified Bayesian method |
|---|---|---|
| False positive rate | 0.7% | 0.2% |
| False negative rate | 13.3% | 0.3% |

| | | |
|---|---|---|
| Fault diagnostic rate | 86.7% | 99.7% |
| Fault diagnostic accuracy | 93.0% | 99.8% |

For the neural network method, based on the historic data of selected sensors, the neural network can be trained using the Neural Network Toolbox in Matlab. After the training process, the current sensor readings can be put into the neural network to obtain the output degradation level. If the output degradation level reaches or exceeds the allowable threshold level, which is 30%, the fault is considered to occur. Compared with the actual state of the fault, whether or not the fault is correctly diagnosed can be known.

After running through all the test data generated under each possible degradation level (300×81), the overall decision matrix (shown in Table 5-6) for calculating the metrics that are used to assess the diagnostic performance can be obtained.

**Table 5-6 Overall decision matrix**

| Diagnostic Result / Actual State | Alarm | No Alarm |
|---|---|---|
| Fault | 72535 | 365 |
| No Fault | 693 | 72207 |

Based on the overall decision matrix, the diagnostic performance assessment metrics can be calculated. Results are shown in Table 5-7.

**Table 5-7 Diagnostic performance assessment metrics**

| | |
|---|---|
| False positive rate | 1.0% |
| False negative rate | 0.5% |
| Fault diagnostic rate | 99.5% |
| Fault diagnostic accuracy | 99.3% |

### 5.2.2 Case Study 2: Clogged Filter

Same as the case study 1, the two sets of sensor readings (instantaneous) used as examples in this case are shown below.

**Table 5-8 Two sets of sensor readings**

| Example | P1 | P2 | P3 | P4 | P5 | P6 | P7 | P8 | L2 |
|---|---|---|---|---|---|---|---|---|---|
| 1 | 0.96 bar | 0.83 bar | 1.52 bar | 1.51 bar | 1.31 bar | 1.37 bar | 1.23 bar | 1.20 bar | 344 rpm |
| 2 | 0.96 bar | 0.86 bar | 1.55 bar | 1.52 bar | 1.35 bar | 1.42 bar | 1.24 bar | 1.21 bar | 346 rpm |

For each example, after the case analysis, the suspected fault can be obtained which is the clogged filter fault in this case. For the clogged filter fault, pressure sensor 5 and laser sensor 2 are selected as the indicator based on the criteria that the ratio of sensor reading (averaged) change should be no less than 10% when the fault happens (shown in Figure 5-7). The fault is considered to happen when the degradation level reaches or exceeds 30%.

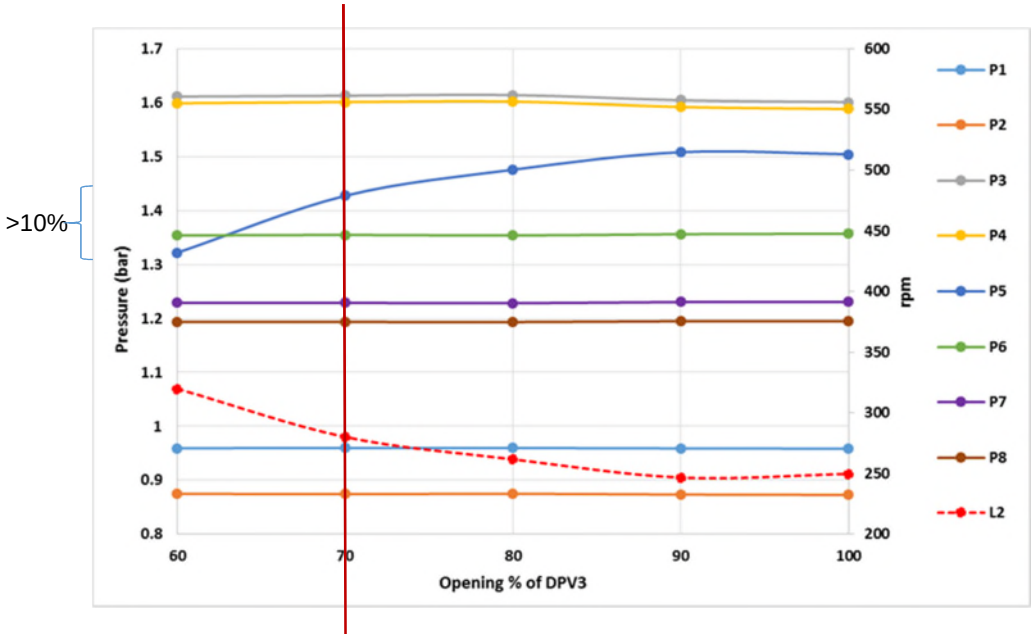


**Figure 5-7 Sensor reading change when the filter clogging happens**

For the data-driven Bayesian method, based on the historic data, the reading distribution for each possible degradation level can be obtained. For example, Figure 5-8 shows the reading distribution of pressure sensor 5 when the filter clogging is 20%, 30% and 40% with no other degraded component in the system. Figure 5-9 shows the reading distribution (envelop plot) of pressure sensor 5 when the filter clogging is 20%, 30% and 40% with all combinations of degraded components in the system. Similar to the case study 1, it can be

observed from Figures 5-8 and 5-9 that there exists a very big difference between the sensor reading distribution generated with and without the consideration of multi-component degradation. The sensor reading distribution generated with considering multi-component degradation covers a much wider range than the sensor reading distribution generated without considering multi-component degradation. It can also be seen that the impact from the multi-component degradation in this case tends to make the fault seem more severe.

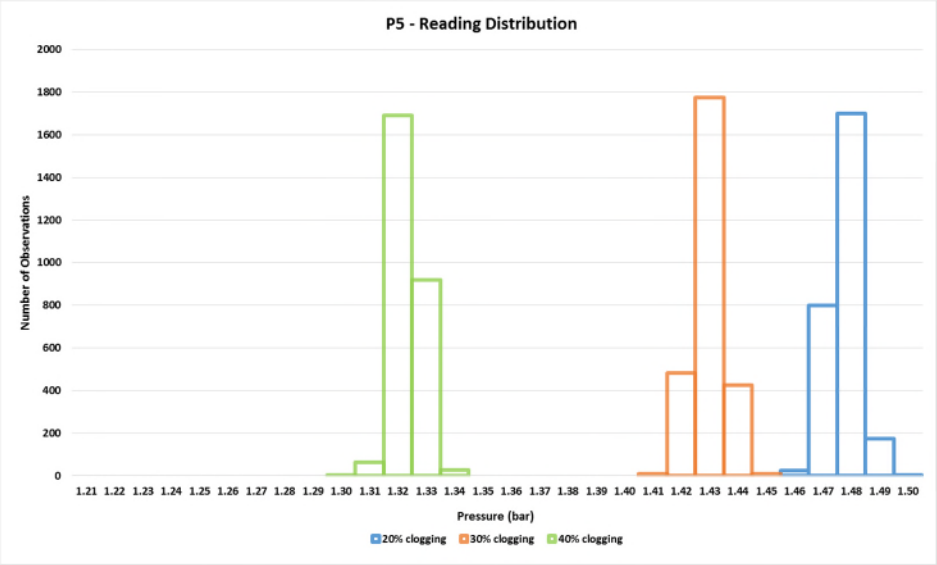


**Figure 5-8 Sensor reading distribution of pressure sensor 5 when the filter clogging is 20%, 30% and 40% with no other degraded component ($P(S_5|L)$)**

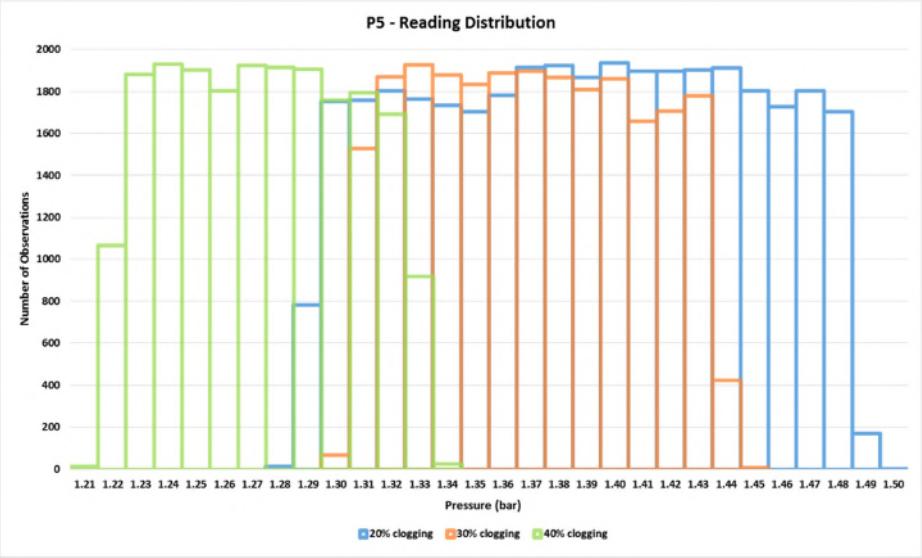


**Figure 5-9 Sensor reading distribution of pressure sensor 5 when the filter clogging is 20%, 30% and 40% with all combinations of degraded components ($P(S_5|C)$)**

Same as the case study 1, based on the sensor reading distribution, the conditional probability table for each possible degradation level can be obtained. Table 5-9 shows the conditional probability table obtained from Figure 5-9 (the conditional probability of sensor readings within normal range would be 100% when there is no other degraded component in the system).

**Table 5-9 Conditional probability for Pressure Sensor 5 when the filter clogging is 20%, 30% and 40% with all combinations of degraded components**

| 20% Clogging | **Very Low** | **Low** | **Normal** | **High** | **Very High** |
|---|---|---|---|---|---|
| Reading(bar) | <1.44 | [1.44,1.46) | [1.46,1.50] | (1.50,1.52] | >1.52 |
| Probability | 83% | 15% | 2% | 0% | 0% |

| 30% Clogging | **Very Low** | **Low** | **Normal** | **High** | **Very High** |
|---|---|---|---|---|---|
| Reading(bar) | <1.39 | [1.39,1.41) | [1.41,1.45] | (1.45,1.47] | >1.47 |
| Probability | 80% | 17% | 3% | 0% | 0% |

| 40% Clogging | **Very Low** | **Low** | **Normal** | **High** | **Very High** |
|---|---|---|---|---|---|
| Reading(bar) | <1.28 | [1.28,1.30) | [1.30,1.34] | (1.34,1.36] | >1.36 |
| Probability | 68% | 25% | 7% | 0% | 0% |

For each selected sensor, based on the conditional probability tables, the current sensor reading can be classified and the corresponding conditional probability can be obtained given a certain degradation level. In Example 1, the conditional probabilities of current P5 reading (1.31bar) are 83%, 80% and 7% given 20%, 30% and 40% clogging respectively according to Table 5-9. In Example 2, the conditional probabilities of current P5 reading (1.35bar) are 83%, 80% and 0% given 20%, 30% and 40% clogging respectively according to Table 5-9.

Based on the conditional probabilities of current sensor readings, the probability of each possible degradation level can be calculated as mentioned in case study 1. After the calculation, the most probable degradation level can be obtained by comparing the probability of each possible degradation level. The degradation level that has the largest probability will be considered as the most probable one that causes the current sensor reading.

As mentioned in case study 1, the set allowable threshold level is 30% so if the most probable degradation level reaches or exceeds this threshold level, the fault is considered to occur. Compared with the actual state of the fault which is obtained by comparing the actual degradation level (the opening percentage of DPV 3) with the allowable threshold level, whether or not the fault is correctly diagnosed can be known.

After running through all the test data generated under each possible degradation level, the overall decision matrix (shown in Table 5-10) for calculating the metrics that are used to assess the diagnostic performance can be obtained.

**Table 5-10 Overall decision matrix**

| Diagnostic Result / Actual State | Classic Bayesian method | | Modified Bayesian method | |
|---|---|---|---|---|
| | Alarm | No Alarm | Alarm | No Alarm |
| Fault | 33437 | 15163 | 45538 | 3062 |
| No Fault | 19464 | 53436 | 7873 | 65027 |

Based on the overall decision matrix, the diagnostic performance assessment metrics can be calculated. Results are shown in Table 5-11.

**Table 5-11 Diagnostic performance assessment metrics (classic Bayesian method vs. modified Bayesian method)**

| | Classic Bayesian method | Modified Bayesian method |
|---|---|---|
| False positive rate | 26.7% | 10.8% |
| False negative rate | 31.2% | 6.3% |
| Fault diagnostic rate | 68.8% | 93.7% |
| Fault diagnostic accuracy | 71.5% | 91.0% |

For the neural network method, following the same procedures mentioned in case study 1, after running through all the test data generated under each possible degradation level, the overall decision matrix (shown in Table 5-12) for calculating the metrics can be obtained.

**Table 5-12 Overall decision matrix**

| Diagnostic Result / Actual State | Alarm | No Alarm |
|---|---|---|
| Fault | 48472 | 128 |
| No Fault | 6218 | 66682 |

Based on the overall decision matrix, the diagnostic performance assessment metrics can be calculated. Results are shown in Table 5-13.

**Table 5-13 Diagnostic performance assessment metrics**

| | |
|---|---|
| False positive rate | 8.5% |
| False negative rate | 0.3% |
| Fault diagnostic rate | 99.7% |
| Fault diagnostic accuracy | 94.8% |

### 5.2.3 Case Study 3: Clogged Nozzle

Same as the case study 1, the two sets of sensor readings (instantaneous) used as examples in this case are shown below.

**Table 5-14 Two sets of sensor readings**

| Example | P1 | P2 | P3 | P4 | P5 | P6 | P7 | P8 | L2 |
|---|---|---|---|---|---|---|---|---|---|
| 1 | 0.96 bar | 0.92 bar | 1.29 bar | 1.28 bar | 1.20 bar | 1.41 bar | 1.15 bar | 1.12 bar | 351 rpm |
| 2 | 0.95 bar | 0.91 bar | 1.27 bar | 1.26 bar | 1.22 bar | 1.33 bar | 1.15 bar | 1.13 bar | 295 rpm |

For each example, after the case analysis, the suspected fault can be obtained which is the clogged nozzle fault in this case. For the clogged nozzle fault, pressure sensor 6 and laser sensor 2 are selected as the indicator based on the criteria that the ratio of sensor reading (averaged) change should be no less than 10% when the fault happens (shown in Figure 5-10). The fault is considered to happen when the degradation level reaches or exceeds 30%.

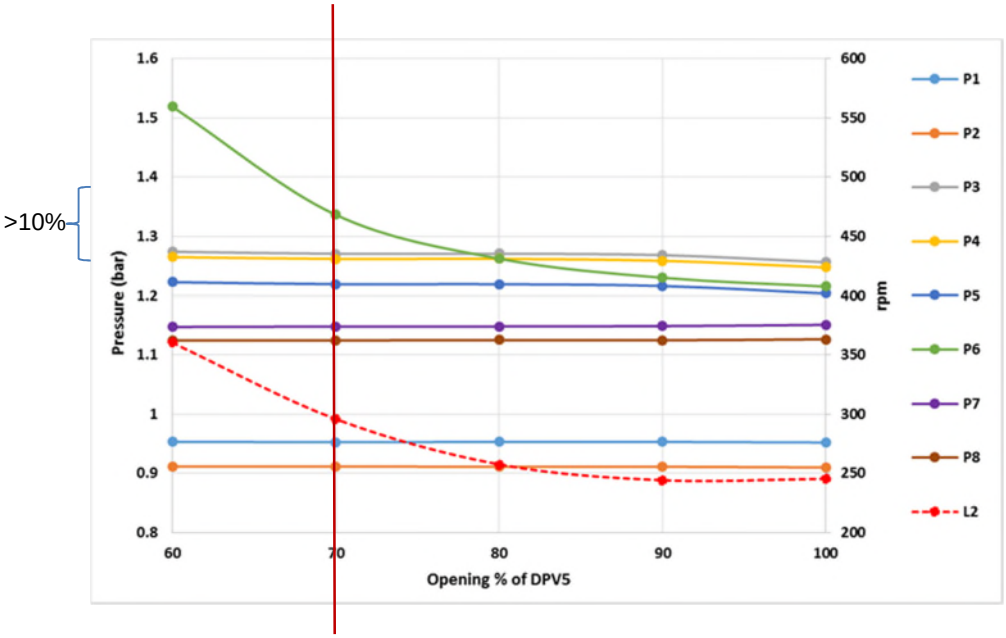


**Figure 5-10 Sensor reading change when the nozzle clogging happens**

For the data-driven Bayesian method, based on the historic data, the reading distribution for each possible degradation level can be obtained. For example, Figure 5-11 shows the reading distribution of pressure sensor 6 when the nozzle clogging is 10%, 20% and 30% with no other degraded component in the system, which will be used for the classic Bayesian method. Figure 5-12 shows the reading distribution (envelop plot) of pressure sensor 6 when the nozzle clogging is 10%, 20% and 30% with all combinations of degraded components in the system, which will be used for the modified Bayesian method. Again, it

can be observed from Figures 5-11 and 5-12 that there exists a very big difference between the sensor reading distribution generated with and without the consideration of multi-component degradation. The sensor reading distribution generated with considering multi-component degradation covers a much wider range than the sensor reading distribution generated without considering multi-component degradation. It can also be seen that the impact from the multi-component degradation sometimes shields the fault effect while sometimes makes the fault seem more severe. This is because the degraded components do not degrade equally so different combinations of the degraded components have different impacts on the fault effect.

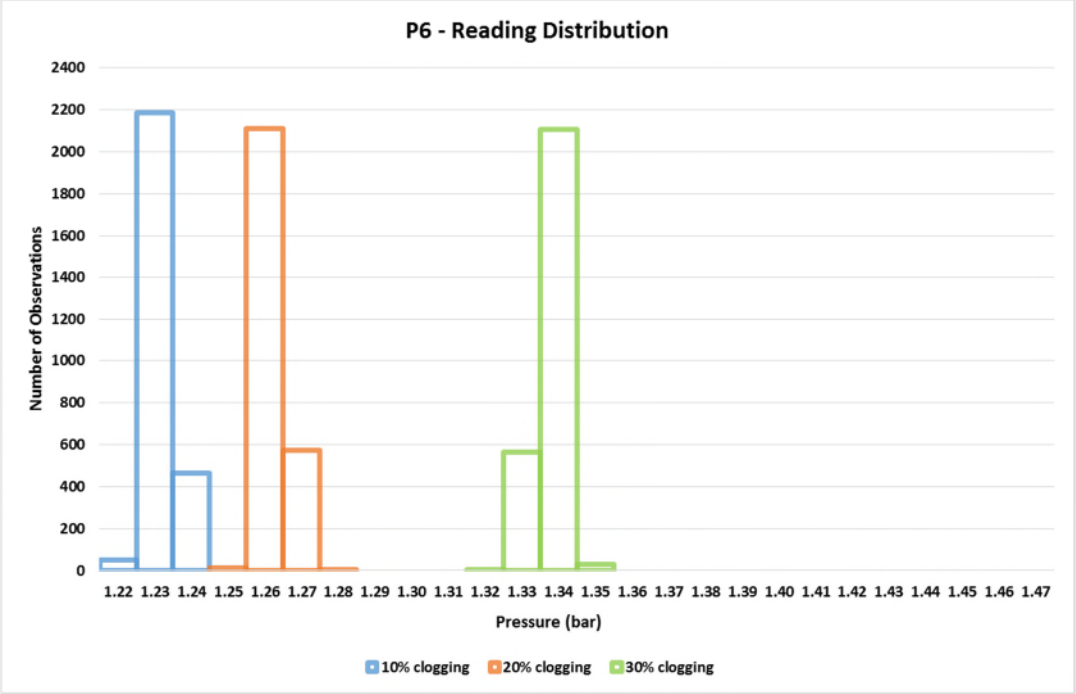


**Figure 5-11 Sensor reading distribution of pressure sensor 6 when the nozzle clogging is 10%, 20% and 30% with no other degraded component ($P(S_6|L)$)**

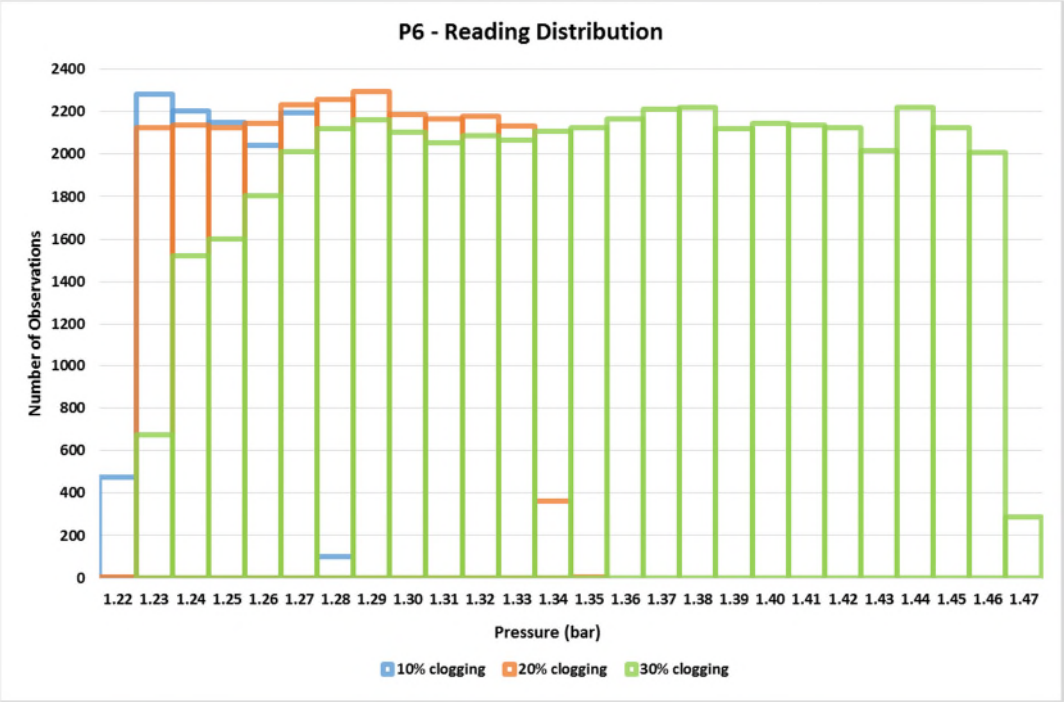


**Figure 5-12 Sensor reading distribution of pressure sensor 6 when the nozzle clogging is 10%, 20% and 30% with all combinations of degraded components ($P(S_6|C)$)**

Based on the sensor reading distribution, the conditional probability table for each possible degradation level can be obtained. Table 5-15 shows the conditional probability table obtained from Figure 5-12 (the conditional probability of sensor readings within normal range would be 100% when there is no other degraded component in the system).

**Table 5-15 Conditional probability of readings from pressure sensor 6 when the nozzle clogging is 10%, 20% and 30% with all combinations of degraded components**

| 10% Clogging | **Very Low** | **Low** | **Normal** | **High** | **Very High** |
|---|---|---|---|---|---|
| Reading(bar) | <1.21 | [1.21,1.22) | [1.22,1.25] | (1.25,1.26] | >1.26 |
| Probability | 0% | 0% | 69% | 28% | 3% |

| 20% Clogging | **Very Low** | **Low** | **Normal** | **High** | **Very High** |
|---|---|---|---|---|---|
| Reading(bar) | <1.24 | [1.24,1.25) | [1.25,1.28] | (1.28,1.29] | >1.29 |
| Probability | 1% | 9% | 39% | 11% | 40% |

| 30% Clogging | **Very Low** | **Low** | **Normal** | **High** | **Very High** |
|---|---|---|---|---|---|
| Reading(bar) | <1.31 | [1.31,1.32) | [1.32,1.35] | (1.35,1.36] | >1.36 |
| Probability | 32% | 3% | 18% | 5% | 42% |

For each selected sensor, based on the conditional probability tables, the current sensor reading can be classified and the corresponding conditional probability can be obtained given a certain degradation level. In Example 1, the conditional probabilities of current P6 reading (1.41bar) is 3%, 40% and 42% given 10%, 20% and 30% clogging respectively according to Table 5-15. In Example 2, the conditional probabilities of current P6 reading (1.33bar) is 3%, 40% and 18% given 10%, 20% and 30% clogging respectively according to Table 5-15.

Based on the conditional probabilities of current sensor readings, the probability of each possible degradation level can be calculated as mentioned in case study 1. After the calculation, the most probable degradation level can be obtained by comparing the probability of each possible degradation level. The degradation level that has the largest probability will be considered as the most probable one that causes the current sensor readings.

Here the set allowable threshold level is 30% so if the most probable degradation level reaches or exceeds this threshold level, the fault is considered to occur. Compared with the actual state of the fault which is obtained by comparing the actual degradation level (the opening percentage of DPV 5) with the allowable threshold level, whether or not the fault is correctly diagnosed can be known.

After running through all the test data generated under each possible degradation level, the overall decision matrix (shown in Table 5-16) for calculating the metrics that are used to assess the diagnostic performance can be obtained.

**Table 5-16 Overall decision matrix**

| Diagnostic Result / Actual State | Classic Bayesian method | | Modified Bayesian method | |
|---|---|---|---|---|
| | Alarm | No Alarm | Alarm | No Alarm |
| Fault | 29544 | 19056 | 45441 | 3159 |
| No Fault | 2625 | 70275 | 1385 | 71515 |

Based on the overall decision matrix, the diagnostic performance assessment metrics can be calculated. Results are shown in Table 5-17.

**Table 5-17 Diagnostic performance assessment metrics (classic Bayesian method vs. modified Bayesian method)**

| | Classic Bayesian method | Modified Bayesian method |
|---|---|---|
| False positive rate | 3.6% | 1.9% |
| False negative rate | 39.2% | 6.5% |
| Fault diagnostic rate | 60.8% | 93.5% |
| Fault diagnostic accuracy | 82.2% | 96.3% |

For the neural network method, following the same procedures mentioned in case study 1, after running through all the test data generated under each possible degradation level, the overall decision matrix (shown in Table 5-18) for calculating the metrics that are used to assess the diagnostic performance can be obtained.

**Table 5-18 Overall decision matrix**

| Diagnostic Result / Actual State | Alarm | No Alarm |
|---|---|---|
| Fault | 47725 | 875 |
| No Fault | 26635 | 46265 |

Based on the overall decision matrix, the diagnostic performance assessment metrics can be calculated. Results are shown in Table 5-19.

**Table 5-19 Diagnostic performance assessment metrics**

| | |
|---|---|
| False positive rate | 36.5% |
| False negative rate | 1.8% |
| Fault diagnostic rate | 98.2% |
| Fault diagnostic accuracy | 77.4% |

### 5.2.4 Case Study 4: Sticking Valve

As the fault scenario in this case study is similar to the one in case study 1, the data analysis procedure is not presented here but the diagnostic results are shown below.

For the data-driven Bayesian method, after running through all the test data generated under each possible degradation level, the overall decision matrix (shown in Table 5-20) for calculating the metrics that are used to assess the diagnostic performance is obtained.

**Table 5-20 Overall decision matrix**

| Diagnostic Result / Actual State | Classic Bayesian method | | Modified Bayesian method | |
|---|---|---|---|---|
| | Alarm | No Alarm | Alarm | No Alarm |
| Fault | 41553 | 7047 | 48357 | 243 |
| No Fault | 656 | 72244 | 218 | 72682 |

Based on the overall decision matrix, the diagnostic performance assessment metrics can be calculated. Results are shown in Table 5-21.

**Table 5-21 Diagnostic performance assessment metrics (classic Bayesian method vs. modified Bayesian method)**

| | Classic Bayesian method | Modified Bayesian method |
|---|---|---|
| False positive rate | 0.9% | 0.3% |
| False negative rate | 14.5% | 0.5% |
| Fault diagnostic rate | 85.5% | 99.5% |
| Fault diagnostic accuracy | 93.7% | 99.6% |

For the neural network method, following the same procedures mentioned in case study 1, after running through all the test data generated under each possible degradation level, the overall decision matrix (shown in Table 5-22) for calculating the metrics that are used to assess the diagnostic performance is obtained.

**Table 5-22 Overall decision matrix**

| Actual State \ Diagnostic Result | Alarm | No Alarm |
|---|---|---|
| Fault | 48259 | 341 |
| No Fault | 875 | 72025 |

Based on the overall decision matrix, the diagnostic performance assessment metrics can be calculated. Results are shown in Table 5-23.

**Table 5-23 Diagnostic performance assessment metrics**

| | |
|---|---|
| False positive rate | 1.2% |
| False negative rate | 0.7% |
| Fault diagnostic rate | 99.3% |
| Fault diagnostic accuracy | 99.0% |

### 5.2.5 Case Study 5: Blocked Flow Meter

As the fault scenario in this case study is similar to the one in case study 3, the data analysis procedure is not presented here but the diagnostic results are shown below.

For the data-driven Bayesian method, after running through all the test data generated under each possible degradation level, the overall decision matrix (shown in Table 5-24) for calculating the metrics that are used to assess the diagnostic performance is obtained.

**Table 5-24 Overall decision matrix**

| Actual State \ Diagnostic Result | Classic Bayesian method | | Modified Bayesian method | |
|---|---|---|---|---|
| | Alarm | No Alarm | Alarm | No Alarm |
| Fault | 29304 | 19296 | 45149 | 3451 |
| No Fault | 2770 | 70130 | 1895 | 71005 |

Based on the overall decision matrix, the diagnostic performance assessment metrics can be calculated. Results are shown in Table 5-25.

**Table 5-25 Diagnostic performance assessment metrics (classic Bayesian method vs. modified Bayesian method)**

| | Classic Bayesian method | Modified Bayesian method |
|---|---|---|
| False positive rate | 3.8% | 2.6% |
| False negative rate | 39.7% | 7.1% |
| Fault diagnostic rate | 60.3% | 92.9% |
| Fault diagnostic accuracy | 81.8% | 95.6% |

For the neural network method, following the same procedures mentioned in case study 1, after running through all the test data generated under each possible degradation level, the overall decision matrix (shown in Table 5-26) for calculating the metrics that are used to assess the diagnostic performance is obtained.

**Table 5-26 Overall decision matrix**

| Diagnostic Result / Actual State | Alarm | No Alarm |
|---|---|---|
| Fault | 47871 | 729 |
| No Fault | 27629 | 45271 |

Based on the overall decision matrix, the diagnostic performance assessment metrics can be calculated. Results are shown in Table 5-27.

**Table 5-27 Diagnostic performance assessment metrics**

| | |
|---|---|
| False positive rate | 37.9% |
| False negative rate | 1.5% |
| Fault diagnostic rate | 98.5% |
| Fault diagnostic accuracy | 76.7% |

## 5.3 Discussion of Diagnostic Performance Results

This section discusses the diagnostic performance results obtained from the above five case studies.

It should be noted here that because, for simplicity, all the components share the same degradation step (10%), this manually set step has some effect on the

diagnostic results, i.e., the false positive/negative rate can vary if the degradation step is changed.

### 5.3.1 The classic Bayesian method vs. modified Bayesian method

Table 5-28 shows the comparison of metrics of classic Bayesian (CB) method and the modified Bayesian (MB) method from the above five case studies.

**Table 5-28 A comparison of metrics of classic Bayesian method and the modified Bayesian method**

| | Case Study 1 | | Case Study 2 | | Case Study 3 | | Case Study 4 | | Case Study 5 | |
|---|---|---|---|---|---|---|---|---|---|---|
| | CB | MB | CB | MB | CB | MB | CB | MB | CB | MB |
| False positive rate | 0.7% | 0.2% | 26.7% | 10.8% | 3.6% | 1.9% | 0.9% | 0.3% | 3.8% | 2.6% |
| False negative rate | 13.3% | 0.3% | 31.2% | 6.3% | 39.2% | 6.5% | 14.5% | 0.5% | 39.7% | 7.1% |
| Fault diagnostic rate | 86.7% | 99.7% | 68.8% | 93.7% | 60.8% | 93.5% | 85.5% | 99.5% | 60.3% | 92.9% |
| Fault diagnostic accuracy | 93.0% | 99.8% | 71.5% | 91.0% | 82.2% | 96.3% | 93.7% | 99.6% | 81.8% | 95.6% |

Based on the definition of the metrics (Subsection 5.1.4), the higher false positive rate and false negative rate indicate poorer diagnostic performance while for the fault diagnostic rate and fault diagnostic accuracy, higher values indicate better diagnostic performance. For all the five case studies, it can be observed that due to the consideration of multi-component degradation, the diagnostic performance of the modified Bayesian method is much better than the classic Bayesian method. More specifically, in case study 1 and 4, it can be observed that the false negative rate of the classic Bayesian method is much higher than the modified Bayesian method while the false positive rates are relatively close. This is because the impact from the multi-component degradation in these two cases tends to shield the fault effect so the classic Bayesian method will sometimes fail to detect the fault based on the probabilistic knowledge without considering multi-component degradation. In case study 2, it can be observed that the false positive rate of the classic Bayesian method is much higher than the modified Bayesian method. This is because the impact from the multi-component degradation in this case tends to

make the fault seem more severe so the classic Bayesian method will sometimes overestimate the fault severity level. However, the false negative rate of the classic Bayesian method is also higher than the modified Bayesian method. This is because the historic data used by the classic Bayesian method only covers a very narrow range so the classic Bayesian method will fail to detect the fault when the current sensor reading is out of this range. In case study 3 and 5, it can be observed that both the false positive and false negative rate of the classic Bayesian method are higher than the modified Bayesian method. This is because the degraded components do not degrade equally so different combinations of degraded component have different impacts on the fault effect (some shield the fault effect while some make the fault seem more severe).

### 5.3.2 The modified Bayesian method vs. Neural Network method

Table 5-29 shows the comparison of metrics of the modified Bayesian (MB) method and neural network (NN) method from the above five case studies.

**Table 5-29 A comparison of metrics of the modified Bayesian method and neural network method**

| | Case Study 1 | | Case Study 2 | | Case Study 3 | | Case Study 4 | | Case Study 5 | |
|---|---|---|---|---|---|---|---|---|---|---|
| | MB | NN | MB | NN | MB | NN | MB | NN | MB | NN |
| False positive rate | 0.2% | 1.0% | 10.8% | 8.5% | 1.9% | 36.5% | 0.3% | 1.2% | 2.6% | 37.9% |
| False negative rate | 0.3% | 0.5% | 6.3% | 0.3% | 6.5% | 1.8% | 0.5% | 0.7% | 7.1% | 1.5% |
| Fault diagnostic rate | 99.7% | 99.5% | 93.7% | 99.7% | 93.5% | 98.2% | 99.5% | 99.3% | 92.9% | 98.5% |
| Fault diagnostic accuracy | 99.8% | 99.3% | 91.0% | 94.8% | 96.3% | 77.4% | 99.6% | 99.0% | 95.6% | 76.7% |

In case study 1 and 4, it can be observed that the diagnostic performance of the modified Bayesian method is better than the neural network method. This is because the neural network method requires the current sensor readings to

belong to the range of the historic data (i.e. training data) to obtain the estimated degradation level while the Bayesian method first classifies the current sensor readings into the defined value ranges (i.e. does not require the current sensor readings to belong to the range of the historic data) and then uses the corresponding conditional probabilities to calculate the probability of each possible degradation level. However, this difference does not always make the modified Bayesian method perform better than the neural network method which can be seen from case study 2 in which the diagnostic performance of the neural network method is better than the modified Bayesian method. This is because the neural network method can provide non-uniqueness outputs when the current sensor readings are included in the training data of different degradation levels while the Bayesian method only provides the most probable degradation level after comparing the probability of each possible degradation level. For the same reason, in case study 3 and 5, the false negative rate and fault diagnostic rate of the neural network method are better than the modified Bayesian method. However, as the impact from the multi-component degradation in these two cases can shield the fault effect, the neural network method will sometimes overestimate the fault severity level and therefore leads to a much higher false positive rate and lower fault diagnostic accuracy compared with the modified Bayesian method.

## 5.4 Conclusion

Overall speaking, due to the consideration of multi-component degradation, the modified Bayesian method has been found to have a much better diagnostic performance compared with the classic Bayesian method. However, compared with the neural network method, the modified Bayesian method still needs to be improved further in some cases but it should be noted here that the performance of the neural network method will decrease dramatically when it is used with the data that have not been trained on.

# 6 Conclusions and Future Work

## 6.1 Conclusions

In conclusion, the research aim of developing a fault diagnostic methodology for complex systems while considering multi-component degradation has been achieved through the accomplishment of five objectives which are laid out in Chapter 1 and reproduced below.

1. To conduct a full literature review on current fault diagnostic methods.

This objective has been accomplished by an extensive literature review on current fault diagnostic methods which is covered in Chapter 2. The advantages and disadvantages of current fault diagnostic methods are summarized, identifying the lack of consideration of multi-component degradation as the gaps in the knowledge. Also, by comparing different existing fault diagnostic methods, the Bayesian method is chosen as it has been used for system level diagnosis and can avoid the difficulty and time-consuming work from building physical models of the target system. The neural network method was chosen to compare with the proposed Bayesian method due to its broad application in the realm of fault diagnosis.

2. To develop a probabilistic framework from the classical Bayesian approach, considering multi-component degradation.

This objective has been accomplished by the development of a probabilistic framework from the classical Bayesian approach which is introduced in Chapter 5. The proposed framework established the link between the sensor reading and fault at the system level with the consideration of multi-component degradation and therefore provided a better diagnostic result compared to the existing methods which do not consider multi-component degradation.

3. To design, construct and validate an experimental fuel rig in order to produce benchmark datasets from a complex system.

This objective has been accomplished by the development of an experimental fuel rig which is covered in Chapter 4. The experimental fuel rig consists of an

array of pipes, valves and pumps with a control system representing those on the aircraft and is able to simulate the main functions of a real aircraft fuel system with the additional function of fault injection. It can produce benchmark datasets with high repeatability and accuracy, which can be used for other research projects as well.

4. To validate the proposed framework using data generated from the experimental fuel rig.

This objective has been accomplished by conducting five case studies, which are shown in Chapter 5, using data generated from the experimental fuel rig. The diagnostic results show that the proposed method has a better diagnostic performance compared with the classic Bayesian method due to the consideration of multi-component degradation.

5. To compare the proposed Bayesian method with another well-known method, in order to show the capabilities and imperfections of the proposed Bayesian method.

This objective has been accomplished by developing a neural network method and comparing the diagnostic results with the proposed method which is also covered in Chapter 5. The diagnostic results show that the proposed method still needs improvements in some cases compared with the neural network method, but the limitation of the neural network method is that its performance will decrease dramatically when using data it has not been trained on.

**Limitations**

As the proposed method in this research belongs to the class of data-driven methods, it is inevitable that a large amount of historic data is needed to derive a sensible diagnostic result. However, in a practical case, sometimes it might not be possible or feasible to have the historic data that covers all degraded states of the target system, especially for very large and complex systems that contains several hundred combinations of degraded components. However, if the simulation model of the target system is available, it could be used to generate the training data.

Also, from an engineering point of view, the limitation in terms of available sensors should be considered which could have a significant influence on the diagnostic result. This research just assumes that the sensors in the target system are sufficient for fault diagnosis.

In addition, this research only considers the faults that are already known by previous experience or knowledge (i.e., the historic data). The proposed method cannot deal with an unknown fault in the system.

## 6.2 Future Work

It should be noted that although the proposed method is validated using an experimental fuel rig in this research, its concept could definitely be applied to other engineering systems as well.

Several possible directions for future work are listed below.

1. The proposed Bayesian method can be combined with other methods, such as the fuzzy logic method, to further improve its diagnostic performance. An investigation on the reduction of the required amount of data will improve the applicability of the proposed method in a real world environment. Moreover, some future work can be done to use the Bayesian method to give fault and severity level directly.
2. More complex experiments can be conducted on the experimental fuel rig to generate the data for diagnosis. For example, the crossfeed line can be used to simulate the scenario when the weights of two wing tanks are unbalanced; the spill branch can be used to simulate the scenario when the engine requires less fuel from the aircraft fuel system.
3. The experimental fuel rig can be upgraded to provide more types of data. For example, more types of sensor can be installed on the experimental fuel rig such as level sensors and vibration sensors so that more failure indicators can be used for diagnostic methods to be tested on. Also, some future work can be done to explore the data collection mechanism.
4. In this research, the sensor degradation/drift in the system is not taken into account. Further research can be done to address this issue and

increase the technology readiness level of the proposed method. It is worth noting here that in reality sometimes it is very difficult to distinguish between sensor degradation/drift and sensor reading change caused by the degraded components.

5. This research only focuses on the system diagnosis, future work can be done on fault diagnosis at the vehicle level in which the interactions between different systems need to be considered.
6. The experiments conducted in this research are under steady state conditions. Future work can be done when the system is running under transient state conditions.
7. This research only focuses on the single independent fault, future work can be done on the multiple independent faults or cascade of faults in a system.

# REFERENCES

Abed, W., Sharma, S., & Sutton, R. (2014). Diagnosis of bearing fault of brushless DC motor based on dynamic neural network and orthogonal fuzzy neighborhood discriminant analysis. In Control (CONTROL), 2014 UKACC International Conference on (pp. 378-383). IEEE.

Ahooyi, T. M., Arbogast, J. E., Oktem, U. G., Seider, W. D., & Soroush, M. (2014). Estimation of complete discrete multivariate probability distributions from scarce data with application to risk assessment and fault detection. Industrial & Engineering Chemistry Research, 53(18), 7538-7547.

Ali, J. B., Fnaiech, N., Saidi, L., Chebel-Morello, B., & Fnaiech, F. (2015). Application of empirical mode decomposition and artificial neural network for automatic bearing fault diagnosis based on vibration signals. Applied Acoustics, 89, 16-27.

Alvarez, M. D. L., & Lane, D. M. (2016). A Hidden Markov Model application with Gaussian Mixture emissions for fault detection and diagnosis on a simulated AUV platform. In OCEANS MTS/IEEE Monterey (pp. 1-4). IEEE.

Amoozgar, M. H., Chamseddine, A., & Zhang, Y. (2013). Experimental test of a two-stage Kalman filter for actuator fault detection and diagnosis of an unmanned quadrotor helicopter. Journal of Intelligent & Robotic Systems, 1-11.

Armaki, M. G., & Roshanfekr, R. (2010). A new approach for fault detection of broken rotor bars in induction motor based on support vector machine. In Electrical Engineering (ICEE), 2010 18th Iranian Conference on (pp. 732-738). IEEE.

Askarian, M., Zarghami, R., Jalali-Farahani, F., & Mostoufi, N. (2016). Fault diagnosis of chemical processes considering fault frequency via Bayesian network. The Canadian Journal of Chemical Engineering, 94(12), 2315-2325.

Aslansefat, K., Latif-Shabgahi, G., & Kamarlouei, M. (2014). A strategy for reliability evaluation and fault diagnosis of Autonomous Underwater Gliding

Robot based on its Fault Tree. International Journal of Advances in Science Engineering and Technology, 2(4), 83-89.

Asr, M. Y., Ettefagh, M. M., Hassannejad, R., & Razavi, S. N. (2017). Diagnosis of combined faults in Rotary Machinery by Non-Naive Bayesian approach. Mechanical Systems and Signal Processing, 85, 56-70.

Boukhobza, T., Hamelin, F., & Canitrot, S. (2008). A graph-theoretic approach to fault detection and isolation for structured bilinear systems. International journal of control, 81(4), 661-678.

Bouzida, A., Touhami, O., Ibtiouen, R., Belouchrani, A., Fadel, M., & Rezzoug, A. (2011). Fault diagnosis in industrial induction machines through discrete wavelet transform. IEEE Transactions on Industrial Electronics, 58(9), 4385-4395.

Cabal-Yepez, E., Garcia-Ramirez, A. G., Romero-Troncoso, R. J., Garcia-Perez, A., & Osornio-Rios, R. A. (2013). Reconfigurable monitoring system for time-frequency analysis on industrial equipment through STFT and DWT. IEEE Transactions on Industrial Informatics, 9(2), 760-771.

Caliskan, F., Zhang, Y., Wu, N. E., & Shin, J. Y. (2014). Actuator fault diagnosis in a Boeing 747 model via adaptive modified two-stage Kalman filter. International Journal of Aerospace Engineering, 2014.

Cerrada, M., Zurita, G., Cabrera, D., Sánchez, R. V., Artés, M., & Li, C. (2016). Fault diagnosis in spur gears based on genetic algorithm and random forest. Mechanical Systems and Signal Processing, 70, 87-103.

Chen, A., Zhou, H., An, Y., & Sun, W. (2016). PCA and PLS monitoring approaches for fault detection of wastewater treatment process. In Industrial Electronics (ISIE), 2016 IEEE 25th International Symposium on (pp. 1022-1027). IEEE.

Chen, F., Tang, B., & Chen, R. (2013). A novel fault diagnosis model for gearbox based on wavelet support vector machine with immune genetic algorithm. Measurement, 46(1), 220-232.

Chen, J., & Patton, R. J. (2012). Robust model-based fault diagnosis for dynamic systems (Vol. 3). Springer Science & Business Media.

Chen, Y., Zhen, Z., Yu, H., & Xu, J. (2017). Application of Fault Tree Analysis and Fuzzy Neural Networks to Fault Diagnosis in the Internet of Things (IoT) for Aquaculture. Sensors, 17(1), 153.

Chiang, L. H., Russell, E. L., & Braatz, R. D. (2000). Fault diagnosis in chemical processes using Fisher discriminant analysis, discriminant partial least squares, and principal component analysis. Chemometrics and intelligent laboratory systems, 50(2), 243-252.

Chien, C. F., Chen, S. L., & Lin, Y. S. (2002). Using Bayesian network for fault location on distribution feeder. IEEE Transactions on Power Delivery, 17(3), 785-793.

Choqueuse, V., & Benbouzid, M. (2015). Induction machine faults detection using stator current parametric spectral estimation. Mechanical Systems and Signal Processing, 52, 447-464.

Codetta-Raiteri, D., & Portinale, L. (2015). Dynamic Bayesian networks for fault detection, identification, and recovery in autonomous spacecraft. IEEE Transactions on Systems, Man, and Cybernetics: Systems, 45(1), 13-24.

Dai, C., Cui, Y., & Liu, Z. (2014, July). The transformer fault diagnosis combing KPCA with PNN. In Neural Networks (IJCNN), 2014 International Joint Conference on (pp. 1314-1319). IEEE.

D'Angelo, M. F., Palhares, R. M., Takahashi, R. H., & Loschi, R. H. (2011). Fuzzy/Bayesian change point detection approach to incipient fault detection. IET control theory & applications, 5(4), 539-551.

D'Angelo, M. F., Palhares, R. M., Cosme, L. B., Aguiar, L. A., Fonseca, F. S., & Caminhas, W. M. (2014). Fault detection in dynamic systems by a Fuzzy/Bayesian network formulation. Applied Soft Computing, 21, 647-653.

Delgado-Aguiñaga, J. A., Besancon, G., Begovich, O., & Carvajal, J. E. (2016). Multi-leak diagnosis in pipelines based on Extended Kalman Filter. Control Engineering Practice, 49, 139-148.

Demetgul, M. (2013). Fault diagnosis on production systems with support vector machine and decision trees algorithms. The International Journal of Advanced Manufacturing Technology, 67(9-12), 2183-2194.

Dey, S., & Stori, J. A. (2005). A Bayesian network approach to root cause diagnosis of process variations. International Journal of Machine Tools and Manufacture, 45(1), 75-91.

Du, Z., Fan, B., Jin, X., & Chi, J. (2014). Fault detection and diagnosis for buildings and HVAC systems using combined neural networks and subtractive clustering analysis. Building and Environment, 73, 1-11.

Fernández-Cantí, R. M., Tornil-Sin, S., Blesa, J., & Puig, V. (2013). Nonlinear set-membership identification and fault detection using a Bayesian framework: Application to the wind turbine benchmark. In Decision and Control (CDC), 2013 IEEE 52nd Annual Conference on (pp. 496-501). IEEE.

Frost, M. (2015). Fuel & Inerting System Overview & Health Monitoring. IVHM Short Course, Cranfield.

Gertler J., & McAvoy T. J. (1997). Principal component analysis and parity relations–strong duality. IFAC Safe Process, 2, 837-842.

Ghate, V. N., & Dudul, S. V. (2011). Cascade neural-network-based fault classifier for three-phase induction motor. IEEE Transactions on Industrial Electronics, 58(5), 1555-1563.

Gritli, Y., Zarri, L., Rossi, C., Filippetti, F., Capolino, G. A., & Casadei, D. (2013). Advanced diagnosis of electrical faults in wound-rotor induction machines. IEEE Transactions on Industrial Electronics, 60(9), 4012-4024.

Gustafsson, F., & Gustafsson, F. (2000). Adaptive filtering and change detection (Vol. 1). New York: Wiley.

Hare, J., Gupta, S., Najjar, N., D'Orlando, P., & Walthall, R. (2015). System-level fault diagnosis with application to the environmental control system of an aircraft (No. 2015-01-2583). SAE Technical Paper.

Hocine, F., & Ahmed, F. (2016). Electric motor bearing diagnosis based on vibration signal analysis and artificial neural networks optimized by the genetic algorithm. In Advances in Condition Monitoring of Machinery in Non-Stationary Operations (pp. 277-289). Springer International Publishing.

Holbert, K. E., & Lin, K. (2012). Nuclear power plant instrumentation fault detection using fuzzy logic. Science and Technology of Nuclear Installations, 2012.

Hwang, W., & Huh, K. (2015). Fault detection and estimation for electromechanical brake systems using parity space approach. Journal of Dynamic Systems, Measurement, and Control, 137(1), 014504.

Jaber, A. A., & Bicker, R. (2016). Fault diagnosis of industrial robot gears based on discrete wavelet transform and artificial neural network. Insight-Non-Destructive Testing and Condition Monitoring, 58(4), 179-186.

Jackson, T., Austin, J., Fletcher, M., Jessop, M., Liang, B., Pasley, A., & Thompson, H. A. (2005). Distributed health monitoring for aero-engines on the GRID: DAME. In Aerospace Conference, 2005 IEEE (pp. 3738-3747). IEEE.

Jang, J. S. R., Sun, C. T., & Mizutani, E. (1997). Neuro-fuzzy and soft computing, a computational approach to learning and machine intelligence.

Jiang, P., Hu, Z., Liu, J., Yu, S., & Wu, F. (2016). Fault Diagnosis Based on Chemical Sensor Data with an Active Deep Neural Network. Sensors, 16(10), 1695.

Jiang, Q., Huang, B., Ding, S. X., & Yan, X. (2016). Bayesian Fault Diagnosis With Asynchronous Measurements and Its Application in Networked Distributed Monitoring. IEEE Transactions on Industrial Electronics, 63(10), 6316-6324.

Jiang, R., Yu, J., & Makis, V. (2012). Optimal Bayesian estimation and control scheme for gear shaft fault detection. Computers & Industrial Engineering, 63(4), 754-762.

Kadamb, A. (2003). Bayesian belief network for aero gas turbine module and system fault isolation' (Doctoral dissertation, MSc Thesis, School of Engineering, Cranfield University).

Kamal, M. M., & Yu, D. (2014, December). Online fault diagnosis of fuel cell systems using independent MLP neural network model. In Electrical, Electronics and System Engineering (ICEESE), 2014 International Conference on (pp. 38-41). IEEE.

Kankar, P. K., Sharma, S. C., & Harsha, S. P. (2011). Fault diagnosis of ball bearings using machine learning methods. Expert Systems with Applications, 38(3), 1876-1886.

Kobayashi, T., & Simon, D. L. (2005). Hybrid neural-network genetic-algorithm technique for aircraft engine performance diagnostics. Journal of Propulsion and Power, 21(4), 751-758.

Laamami, S., Ben, H. M., & Sbita, L. (2015, June). Fault detection for nonlinear systems: Parity space approach. In Information Technology and Computer Applications Congress (WCITCA), 2015 World Congress on (pp. 1-5). IEEE.

Langton, R., Clark, C., Hewitt, M., & Richards, L. (2009). Aircraft fuel systems. John Wiley & Sons, Ltd.

Laurentys, C. A., Bomfim, C. H. M., Menezes, B. R., & Caminhas, W. M. (2011). Design of a pipeline leakage detection using expert system: A novel approach. Applied Soft Computing, 11(1), 1057-1066.

Lee, K. W., & Lan, H. N. (2014). Fault Detection and Identification Using Neural Network and Fuzzy Logic. In IFAC Workshop (pp. 185-190).

Lee, W. Y., House, J. M., & Kyong, N. H. (2004). Subsystem level fault diagnosis of a building's air-handling unit using general regression neural networks. Applied Energy, 77(2), 153-170.

Lee, Y. K., Mavris, D. N., Volovoi, V. V., Yuan, M., & Fisher, T. (2010). A fault diagnosis method for industrial gas turbines using Bayesian data analysis. Journal of engineering for gas turbines and power, 132(4), 041602.

Li, B., Han, T., & Kang, F. (2013). Fault diagnosis expert system of semiconductor manufacturing equipment using a Bayesian network. International Journal of Computer Integrated Manufacturing, 26(12), 1161-1171.

Li, J., Zhang, Q., Wang, K., Wang, J., Zhou, T., & Zhang, Y. (2016). Optimal dissolved gas ratios selected by genetic algorithm for power transformer fault diagnosis based on support vector machine. IEEE Transactions on Dielectrics and Electrical Insulation, 23(2), 1198-1206.

Li, K., Zhang, Y. L., & Li, Z. X. (2012). Application research of Kalman filter and SVM applied to condition monitoring and fault diagnosis. In Applied Mechanics and Materials (Vol. 121, pp. 268-272). Trans Tech Publications.

Liao, S. H. (2005). Expert system methodologies and applications—a decade review from 1995 to 2004. Expert systems with applications, 28(1), 93-103.

Lin, Y., Skaf, Z., & Jennions, I. (2015). A Survey on Operational Safety Assessment in the Aviation Industry and its Link to IVHM (No. 2015-01-2590). SAE Technical Paper.

Lin, Y., Zakwan, S., & Jennions, I. (2017). A Bayesian approach to fault identification in the presence of multi-component degradation.

Liu, J., Liang, Y., & Sun, X. (2009). Application of Learning Vector Quantization network in fault diagnosis of power transformer. In Mechatronics and Automation, 2009. ICMA 2009. International Conference on (pp. 4435-4439). IEEE.

Liu, Y., Guo, L., Wang, Q., An, G., Guo, M., & Lian, H. (2010). Application to induction motor faults diagnosis of the amplitude recovery method combined with FFT. Mechanical Systems and Signal Processing, 24(8), 2961-2971.

Liu, Y., Xie, G., Yang, Y., Chen, Z., & Chai, Q. (2014, May). Hierarchical method of fault diagnosis based on extended SDG. In Control and Decision Conference (2014 CCDC), The 26th Chinese (pp. 3808-3812). IEEE.

Lo, C. H., Fung, E. H., & Wong, Y. K. (2009). Intelligent automatic fault detection for actuator failures in aircraft. IEEE Transactions on Industrial Informatics, 5(1), 50-55.

Loboda, I., & Olivares Robles, M. A. (2015). Gas turbine fault diagnosis using probabilistic neural networks. International Journal of Turbo & Jet-Engines, 32(2), 175-191.

Loboda, I., & Yepifanov, S. (2010). A mixed data-driven and model based fault classification for gas turbine diagnosis. In ASME Turbo Expo 2010: Power for Land, Sea, and Air (pp. 257-265). American Society of Mechanical Engineers.

Lu, L., Yan, J., & de Silva, C. W. (2015). Dominant feature selection for the fault diagnosis of rotary machines using modified genetic algorithm and empirical mode decomposition. Journal of Sound and Vibration, 344, 464-483.

Ma, D., Liang, Y., Zhao, X., Guan, R., & Shi, X. (2013). Multi-BP expert system for fault diagnosis of power system. Engineering Applications of Artificial Intelligence, 26(3), 937-944.

Ma, S., Li, S. M., & Xiong, Y. P. (2016). Uncertainty extraction based multi-fault diagnosis of rotating machinery. Journal of Vibroengineering, 18(1).

MacGregor, J. (1989). Multivariate statistical methods for monitoring large data sets from chemical processes. In AIChE Meeting.

Mack, D. L., Biswas, G., Koutsoukos, X. D., Mylaraswamy, D., & Hadden, G. (2011). Deriving Bayesian Classifiers from Flight Data to Enhance Aircraft

Diagnosis Models. In Annual Conference of the Prognostics and Health Management Society.

Maki, Y., & Loparo, K. A. (1997). A neural-network approach to fault detection and diagnosis in industrial processes. IEEE Transactions on Control Systems Technology, 5(6), 529-541.

Malik, H., & Mishra, S. (2015). Application of LVQ network in fault diagnosis of wind turbine using Turbsim, fast and simulink.

Malik, H., & Mishra, S. (2015). Application of Probabilistic Neural Network in Fault Diagnosis of Wind Turbine Using FAST, TurbSim and Simulink. Procedia Computer Science, 58, 186-193.

Mehranbod, N., Soroush, M., & Panjapornpon, C. (2005). A method of sensor fault detection and identification. Journal of Process Control, 15(3), 321-339.

Meskin, N., Naderi, E., & Khorasani, K. (2013). A multiple model-based approach for fault diagnosis of jet engines. IEEE Transactions on Control Systems Technology, 21(1), 254-262.

Michaels, K. (2016). MRO Industry Outlook. ICF International.

Mohammadi, E., & Montazeri-Gh, M. (2015). A fuzzy-based gas turbine fault detection and identification system for full and part-load performance deterioration. Aerospace Science and Technology, 46, 82-93.

Muralidharan V., & Sugumaran V. (2012). A comparative study of Naïve Bayes classifier and Bayes net classifier for fault diagnosis of monoblock centrifugal pump using wavelet analysis. Applied Soft Computing, 12(8), 2023-2029.

Nadarajan, S., Panda, S. K., Bhangu, B., & Gupta, A. K. (2016). Online model-based condition monitoring for brushless wound-field synchronous generator to detect and diagnose stator windings turn-to-turn shorts using extended Kalman filter. IEEE Transactions on Industrial Electronics, 63(5), 3228-3241.

Najjar, N., Hare, J., D'Orlando, P., Leaper, G., Pattipati, K., Silva, A., & Walthall, R. (2013). Heat exchanger fouling diagnosis for an aircraft air-conditioning system (No. 2013-01-2250). SAE Technical Paper.

Nasrolahzadeh, M., Mohammadpoory, Z., & Haddadnia, J. (2016). A novel method for early diagnosis of Alzheimer's disease based on higher-order spectral estimation of spontaneous speech signals. Cognitive neurodynamics, 10(6), 495-503.

Nguyen, P., Kang, M., Kim, J., Kim, J. M., Tan, A. C., & Kim, E. Y. (2014, December). Erratum: Reliable Fault Diagnosis of Low-Speed Bearing Defects Using a Genetic Algorithm. In Pacific Rim International Conference on Artificial Intelligence (pp. E1-E2). Springer International Publishing.

Niculita, O., Skaf, Z., & Jennions, I. K. (2014). The Application of Bayesian Change Point Detection in UAV Fuel Systems. Procedia CIRP, 22, 115-121.

Niida K. (1985). Expert system experiments in processing engineering. Proc. Inst. Chem. Eng. Symp. Series, 529-583.

Odendaal, H. M., & Jones, T. (2014). Actuator fault detection and isolation: An optimised parity space approach. Control Engineering Practice, 26, 222-232.

Ozturk, U. (2016). An intelligent fault diagnosis system on ship machinery systems based on support vector machine principles. In Risk, Reliability and Safety: Innovating Theory and Practice (pp. 1949-1953). CRC Press.

Palmé, T., Breuhaus, P., Assadi, M., Klein, A., & Kim, M. (2011). Early Warning of Gas Turbine Failure by Nonlinear Feature Extraction Using an Auto-Associative Neural Network Approach. In ASME 2011 Turbo Expo: Turbine Technical Conference and Exposition (pp. 293-304). American Society of Mechanical Engineers.

Payganeh, G. H., Khajavi, M. N., Ebrahimpour, R., & Babaei, E. (2012). Machine Fault Diagnosis Using MLPs and RBF Neural Networks. In Applied Mechanics and Materials (Vol. 110, pp. 5021-5028). Trans Tech Publications.

Picón, A., Ghita, O., Whelan, P. F., & Iriondo, P. M. (2009). Fuzzy spectral and spatial feature integration for classification of nonferrous materials in hyperspectral data. IEEE Transactions on Industrial Informatics, 5(4), 483-494.

Poon, J., Jain, P., Konstantakopoulos, I. C., Spanos, C., Panda, S. K., & Sanders, S. R. (2017). Model-based fault detection and identification for switching power converters. IEEE Transactions on Power Electronics, 32(2), 1419-1430.

Poon, J., Konstantakopoulos, I. C., Spanos, C., & Sanders, S. R. (2015). Real-time model-based fault diagnosis for switching power converters. In Applied Power Electronics Conference and Exposition (APEC), 2015 IEEE (pp. 358-364). IEEE.

Rahmoune, M. B., Hafaifa, A., & Guemana, M. (2017). Fault diagnosis in gas turbine based on neural networks: Vibrations Speed Application. In Advances in Acoustics and Vibration (pp. 1-11). Springer International Publishing.

Rajaraman, S., Hahn, J., & Mannan, M. S. (2004). A methodology for fault detection, isolation, and identification for nonlinear processes with parametric uncertainties. Industrial & engineering chemistry research, 43(21), 6774-6786.

Ramos, A. R., Acosta, C. D., Torres, P. J. R., Mercado, E. I. S., Baez, G. B., Rifón, L. A., & Llanes-Santiago, O. (2016). An approach to multiple fault diagnosis using fuzzy logic. Journal of Intelligent Manufacturing, 1-11.

Rodrigues, L. R., Gomes, J. P., Ferri, F. A., Medeiros, I. P., Galvão, R. K., & Júnior, C. L. N. (2015). Use of PHM information and system architecture for optimized aircraft maintenance planning. IEEE Systems Journal, 9(4), 1197-1207.

Romessis, C., Stamatis, A., & Mathioudakis, K. (2001). Setting up a belief network for turbofan diagnosis with the aid of an engine performance model. ISABE paper, 1032, 19-26.

Romessis, C., & Mathioudakis, K. (2002). Setting up of a probabilistic neural network for sensor fault detection including operation with component faults. In

ASME Turbo Expo 2002: Power for Land, Sea, and Air (pp. 101-108). American Society of Mechanical Engineers.

Romessis, C., & Mathioudakis, K. (2006). Bayesian network approach for gas path fault diagnosis. Journal of engineering for gas turbines and power, 128(1), 64-72.

Saha, B. (2008). A model-based reasoning architecture for system-level fault diagnosis. Georgia Institute of Technology.

Saimurugan, M., & Nithesh, R. (2016). Intelligent fault diagnosis model for rotating machinery based on fusion of sound signals. International Journal of Prognostics and Health Management, ISSN 2153-2648, 2016 018.

Sampath, S., & Singh, R. (2006). An integrated fault diagnostics model using genetic algorithm and neural networks. Journal of Engineering for Gas Turbines and Power, 128(1), 49-56.

Sankararaman, S., & Mahadevan, S. (2013). Bayesian methodology for diagnosis uncertainty quantification and health monitoring. Structural Control and Health Monitoring, 20(1), 88-106.

Santos, P., Villa, L. F., Reñones, A., Bustillo, A., & Maudes, J. (2015). An SVM-based solution for fault detection in wind turbines. Sensors, 15(3), 5627-5648.

Sapena-Bañó, A., Pineda-Sanchez, M., Puche-Panadero, R., Martinez-Roman, J., & Matić, D. (2015). Fault diagnosis of rotating electrical machines in transient regime using a single stator current's FFT. IEEE Transactions on Instrumentation and Measurement, 64(11), 3137-3146.

Saravanakumar, R., Manimozhi, M., Kothari, D. P., & Tejenosh, M. (2014). Simulation of sensor fault diagnosis for wind turbine generators DFIG and PMSM using Kalman filter. Energy Procedia, 54, 494-505.

Schein, J., & Bushby, S. T. (2006). A hierarchical rule-based fault detection and diagnostic method for HVAC systems. HVAC&R Research, 12(1), 111-125.

Seryasat, O. R., Honarvar, F., & Rahmani, A. (2010, October). Multi-fault diagnosis of ball bearing based on features extracted from time-domain and multi-class support vector machine (MSVM). In Systems Man and Cybernetics (SMC), 2010 IEEE International Conference on (pp. 4300-4303). IEEE.

Sheikh, F. R., & Patel, A. T. (2016). Fuzzy Logic Approach for Fault Diagnosis of Three Phase Transmission Line. Journal for Research, 2-03.

Sidhu, A., Izadian, A., & Anwar, S. (2015). Adaptive nonlinear model-based fault diagnosis of Li-ion batteries. IEEE Transactions on Industrial Electronics, 62(2), 1002-1011.

Singh, G. K., & Al Kazzaz, S. A. A. S. (2009). Isolation and identification of dry bearing faults in induction machine using wavelet transform. Tribology international, 42(6), 849-861.

Song, L., Xiu-ying, L., & Wen-xu, W. (2011, March). Fault diagnosis of transformer based on probabilistic neural network. In Intelligent Computation Technology and Automation (ICICTA), 2011 International Conference on (Vol. 1, pp. 128-131). IEEE.

Steinder, M., & Sethi, A. S. (2004). Probabilistic fault localization in communication systems using belief networks. IEEE/ACM transactions on networking, 12(5), 809-822.

Tao, E. P., Shen, W. H., Liu, T. L., & Chen, X. Q. (2013). Fault diagnosis based on PCA for sensors of laboratorial wastewater treatment process. Chemometrics and Intelligent Laboratory Systems, 128, 49-55.

Tayarani-Bathaie, S. S., Vanini, Z. S., & Khorasani, K. (2014). Dynamic neural network-based fault diagnosis of gas turbine engines. Neurocomputing, 125, 153-165.

Tian, J., Gao, M., Li, K., & Zhou, H. (2007). Fault detection of oil pump based on classify support vector machine. In Control and Automation, 2007. ICCA 2007. IEEE International Conference on (pp. 549-553). IEEE.

Trachi, Y., Elbouchikhi, E., Choqueuse, V., & Benbouzid, M. E. H. (2016). Induction machines fault detection based on subspace spectral estimation. IEEE Transactions on Industrial Electronics, 63(9), 5641-5651.

Tyagi, C. S. (2008). A comparative study of SVM classifiers and artificial neural networks application for rolling element bearing fault diagnosis using wavelet transform preprocessing. Neuron, 1, 309-317.

Unal, M., Onat, M., Demetgul, M., & Kucuk, H. (2014). Fault diagnosis of rolling bearings using a genetic algorithm optimized neural network. Measurement, 58, 187-196.

Vanini, Z. S., Khorasani, K., & Meskin, N. (2014). Fault detection and isolation of a dual spool gas turbine engine using dynamic neural networks and multiple model approach. Information Sciences, 259, 234-251.

Vapnik, V. N., & Vapnik, V. (1998). Statistical learning theory (Vol. 1). New York: Wiley.

Verbert, K., Babuška, R., & De Schutter, B. (2017). Bayesian and Dempster–Shafer reasoning for knowledge-based fault diagnosis–A comparative study. Engineering Applications of Artificial Intelligence, 60, 136-150.

Verbert, K., Babuška, R., & De Schutter, B. (2017). Combining knowledge and historical data for system-level fault diagnosis of HVAC systems. Engineering Applications of Artificial Intelligence, 59, 260-273.

Verron, S., Li, J., & Tiplica, T. (2010). Fault detection and isolation of faults in a multivariate process with Bayesian network. Journal of Process Control, 20(8), 902-911.

Vesely William et al. (2010). Fault tree handbook with aerospace applications-NASA.

Wang, B., Jiang, Q., & Yan, X. (2014). Fault detection and identification using a Kullback-Leibler divergence based multi-block principal component analysis and bayesian inference. Korean Journal of Chemical Engineering, 31(6), 930-943.

Wang, H., Chen, J., & Dong, G. (2014). Feature extraction of rolling bearing's early weak fault based on EEMD and tunable Q-factor wavelet transform. Mechanical Systems and Signal Processing, 48(1), 103-119.

Wang, H., & Chen, P. (2011). Fuzzy diagnosis method for rotating machinery in variable rotating speed. IEEE Sensors Journal, 11(1), 23-34.

Waqar, T., & Demetgul, M. (2016). Thermal analysis MLP neural network based fault diagnosis on worm gears. Measurement, 86, 56-66.

Wheeler, K. R., Kurtoglu, T., & Poll, S. D. (2010). A survey of health management user objectives in aerospace systems related to diagnostic and prognostic metrics. International Journal of Prognostics and Health Management. ISSN 2153-2648, 2010 003.

Willsky, A. S. (1976). A survey of design methods for failure detection in dynamic systems. Automatica 12, 601 /611.

Wu, C., Zhu, C., Ge, Y., & Zhao, Y. (2016). A diagnosis approach for typical faults of lithium-ion battery based on extended Kalman filter. Int. J. Electrochem. Sci, 11, 5289-5301.

Wu, K., An, S., Ma, G., & Tao, Y. (2012, March). Research and application of fuzzy expert system on transformer fault diagnosis. In Computer Science and Electronics Engineering (ICCSEE), 2012 International Conference on (Vol. 1, pp. 378-382). IEEE.

Wu, Y., Wang, Y., Jiang, Y., & Sun, Q. (2016). Multiple parametric faults diagnosis for power electronic circuits based on hybrid bond graph and genetic algorithm. Measurement, 92, 365-381.

Xiao, D., Jiang, J., Mao, Y., & Liu, X. (2016). Process Monitoring and Fault Diagnosis for Piercing Production of Seamless Tube. Mathematical Problems in Engineering, 2016.

Xu, L., & Zhou, Y. (2016). Fault diagnosis for BLDCM system used FFT algorithm and support vector machines. In Aircraft Utility Systems (AUS), IEEE International Conference on (pp. 384-387).

Yang, F., Shah, S., & Xiao, D. (2012). Signed directed graph based modeling and its validation from process knowledge and process data. International Journal of Applied Mathematics and Computer Science, 22(1), 41-53.

Yang, X. B., Jin, X. Q., Du, Z. M., & Zhu, Y. H. (2011). A novel model-based fault detection method for temperature sensor using fractal correlation dimension. Building and Environment, 46(4), 970-979.

Yin, H., Yang, S., Zhu, X., Jin, S., & Wang, X. (2014). Satellite fault diagnosis using support vector machines based on a hybrid voting mechanism. The Scientific World Journal, 2014.

Yu, J. (2013). A new fault diagnosis method of multimode processes using Bayesian inference based Gaussian mixture contribution decomposition. Engineering Applications of Artificial Intelligence, 26(1), 456-466.

Yu, J., & Rashid, M. M. (2013). A novel dynamic bayesian network-based networked process monitoring approach for fault detection, propagation identification, and root cause diagnosis. AIChE Journal, 59(7), 2348-2365.

Yuwono, M., Qin, Y., Zhou, J., Guo, Y., Celler, B. G., & Su, S. W. (2016). Automatic bearing fault diagnosis using particle swarm clustering and Hidden Markov Model. Engineering Applications of Artificial Intelligence, 47, 88-100.

Zarei, J., Arefi, M. M., & Hassani, H. (2015). Bearing fault detection based on interval type-2 fuzzy logic systems for support vector machines. In Modeling, Simulation, and Applied Optimization (ICMSAO), 2015 6th International Conference on (pp. 1-6). IEEE.

Zhang, C., Feng, Q., & Bai, Z. (2014). Probabilistic Neural Network Application in Fault Diagnosis of Airborne Fire Control System. In Proceedings of the First Symposium on Aviation Maintenance and Management-Volume I (pp. 235-242). Springer Berlin Heidelberg.

Zhang, J., Qi, M., & Li, B. (2016). Hybrid diagnosis of fault tree and Bayesian network in BIW automatic welding production line. In Advanced Information Management, Communicates, Electronic and Automation Control Conference (IMCEC), 2016 IEEE (pp. 297-300). IEEE.

Zhang, J., & Roberts, P. D. (1991). Process fault diagnosis with diagnostic rules based on structural decomposition. Journal of Process Control, 1(5), 259-269.

Zhang, J., Zhan, W., & Ehsani, M. (2016). On-line fault diagnosis of electric machine based on the Hidden Markov Model. In Transportation Electrification Conference and Expo (ITEC), 2016 IEEE (pp. 1-7). IEEE.

Zhang, X., Liang, Y., & Zhou, J. (2015). A novel bearing fault diagnosis model integrated permutation entropy, ensemble empirical mode decomposition and optimized SVM. Measurement, 69, 164-179.

Zhang, X., & Pisu, P. (2014). An Unscented Kalman Filter based on-line Diagnostic approach for PEM fuel cell Flooding. International Journal of Prognostics and Health Management, 5(1).

Zhang, X., & Zhou, J. (2013). Multi-fault diagnosis for rolling element bearings based on ensemble empirical mode decomposition and optimized support vector machines. Mechanical Systems and Signal Processing, 41(1), 127-140.

Zhao, Y., Xiao, F., & Wang, S. (2013). An intelligent chiller fault detection and diagnosis methodology using Bayesian belief network. Energy and Buildings, 57, 278-288.

Zhi-Ling, Y., Bin, W., Xing-Hui, D., & Hao, L. I. U. (2012). Expert system of fault diagnosis for gear box in wind turbine. Systems Engineering Procedia, 4, 189-195.

Zhong, M., Song, Y., & Ding, S. X. (2015). Parity space-based fault detection for linear discrete time-varying systems with unknown input. Automatica, 59, 120-126.

Zhou, S. G., Li, G. J., Luo, Z. F., & Zheng, Y. (2013). Analog circuit fault diagnosis based on LVQ neural network. In Applied Mechanics and Materials (Vol. 380, pp. 828-832). Trans Tech Publications.

Zidani, F., Diallo, D., Benbouzid, M. E. H., & Naït-Saïd, R. (2008). A fuzzy-based approach for the diagnosis of fault modes in a voltage-fed PWM inverter induction motor drive. IEEE Transactions on Industrial Electronics, 55(2), 586-593.

# APPENDICES

# Appendix A Configuration Management Form

### Table A-1 Configuration Management Form

| Configuration Management | | | | |
|---|---|---|---|---|
| ITEM | LINK | QUANTITY | PRICE EACH | TOTAL PRICE |
| NI Modules | | | | |
| NI 9205 32-Channel +/-10 V, 250 kS/s,16-Bit Analog Input Module | http://sine.ni.com/nips/cds/view/p/lang/en/nid/208800 | 1 | £634.50 | £634.50 |
| NI 9940 Strain relief & high voltage connector kit | http://sine.ni.com/nips/cds/view/p/lang/en/nid/987482 | 2 | £24.00 | £43.20 |
| NI 9264 16-Channel ±10 V, 25 kS/s,16-Bit, Analog Output Module | http://sine.ni.com/nips/cds/view/p/lang/en/nid/208807 | 1 | £711.00 | £711.00 |
| NI 9401 8-Channel, 100 ns, TTL Digital Input/Output Module | http://sine.ni.com/nips/cds/view/p/lang/en/nid/208809 | 3 | £216.00 | £648.00 |
| NI 9924 25 pin DSub terminal block for screw terminal connectivity | http://sine.ni.com/nips/cds/view/p/lang/en/nid/210162 | 3 | £71.10 | £213.30 |
| NI 9472 8-Channel 24 V, 100 us, Sourcing Digital Output Module | http://sine.ni.com/nips/cds/view/p/lang/en/nid/208822 | 3 | £79.00 | £213.30 |
| NI 9927, Strain Relief and Operator Protection | http://sine.ni.com/nips/cds/view/p/lang/en/nid/211677 | 3 | £23.00 | £62.10 |
| NI 9485 8-Ch, ±60 VDC, 750 mA (60V Ch-Ch, 250Vrms) | http://sine.ni.com/nips/cds/view/p/lang/en/nid/208828 | 1 | £252.00 | £252.00 |
| NI 9939 Strain relief & high voltage connector kit | http://sine.ni.com/nips/cds/view/p/lang/en/nid/211309 | 1 | £21.60 | £21.60 |
| | | SUBTOTAL | | £2,799.00 |
| Tray | | | | |
| Cranfield Workshop Charge | ___ | 1 | £125.00 | £125.00 |
| 2000 mm x 1000 mm x 1.5mm - 1050A | http://www.aluminiumwarehouse.co.uk/ | 2 | £39.64 | £79.28 |
| | | SUBTOTAL | | £204.28 |
| Mountings | | | | |
| 2 in x 2 in x 1/8 in x 1/8 in : Aluminium Channel | http://www.aluminiumwarehouse.co.uk/ | 1 | £25.86 | £25.86 |
| Aluminium Plate: 6082 T651 - 10.0 mm - 510mm x 250mm | http://www.aluminiumwarehouse.co.uk/ | 1 | £19.42 | £19.42 |
| Natural Rubber Work Bench Mat | http://uk.rs-online.com | 2 | £10.75 | £21.50 |
| | | SUBTOTAL | | £66.78 |
| Valves | | | | |
| Shut-off valve | http://uk.rs-online.com/web/p/solenoid-valves/6681848/ | 5 | £47.37 | £236.85 |
| Direct-proportional valve | http://www.burkert.com/en/type/8605 | 6 | £184.00 | £1,104 |
| Digital control electronics for proportional valves | http://www.burkert.com/en/type/8605 | 6 | £152.00 | £912 |
| | | SUBTOTAL | | £2,252.85 |
| Breadboard | | | | |
| Aluminium Optical Breadboard 1800 x 1100 x 55mm | http://www.thorlabs.com | 1 | £2,143.13 | £2,143.13 |
| Delivery and installation | http://www.thorlabs.com | 1 | £650.00 | £650.00 |
| | | SUBTOTAL | | £2,793.13 |
| Pumps & Motors | | | | |
| ABB ACS150-0.37kW Inverter Drive | www.inverterdrive.com | 3 | £85.00 | £255.00 |
| Motor (0.37kW, 4 Pole) | http://www.rotamec.co.uk | 3 | £105.00 | £315.00 |
| N999R Gear Pump | http://www.oberdorferpumps.com/ | 3 | £337.00 | £1,011 |
| Couple adaptor kit for connecting pump and motor | http://www.oberdorferpumps.com/ | 3 | £112.00 | £336 |
| | | SUBTOTAL | | £1,917.00 |
| Sensors & Power | | | | |
| IMP Industrial Pressure Sensor(Absolute) | http://www.sensorsone.co.uk | 3 | £139.80 | £419.40 |
| IMP Industrial Pressure Sensor(Gauge) | http://www.sensorsone.co.uk | 7 | £147.40 | £1,031.80 |
| Flow Meter | http://www.omega.com | 5 | £178.22 | £891.10 |
| P+F RETRO REFLECTIVE LASER SENSOR | http://www.pepperl-fuchs.co.uk | 3 | £361.88 | £1,085.64 |
| P+F CONNECTOR AND CABLE | http://www.pepperl-fuchs.co.uk | 3 | £13.19 | £39.57 |
| P+F Reflector Tape | http://www.pepperl-fuchs.co.uk | 1 | £25.64 | £25.64 |
| Aneroid barometer | http://www.barometerworld.co.uk | 1 | £110 | £110 |
| Power Supply | http://uk.rs-online.com/web/p/bench-power-supplies | 2 | £227 | £454.00 |
| | | SUBTOTAL | | £4,057.15 |
| Tube,Tanks & Adaptors | | | | |
| 6MM OD X 4MM ID POLYURETHANE TUBE | http://www.pneutrolspares.com/ | 1 | £12.47 | £12.47 |
| Water Tank | http://www.petsathome.com/ | 3 | £40 | £120 |
| Threaded-to-Tube Adapter | http://uk.rs-online.com | 15 | £1.42 | £21.33 |
| Adaptors(Male R Push In 1/4in) | http://uk.rs-online.com | 10 | £1.87 | £18.70 |
| Adaptors(3114 G 1/4 Female 20 bar) | http://uk.rs-online.com | 10 | £3.58 | £35.80 |
| Adaptors(1020 G 1/4 Male 15 bar) | http://uk.rs-online.com | 10 | £1.29 | £12.90 |
| Adaptors for connecting tube(STRAIGHT) | http://www.pneutrolspares.com/ | 10 | £2.10 | £21.00 |
| Adaptors for connecting tube(TEE) | http://www.pneutrolspares.com/ | 25 | £2.86 | £71.50 |
| | | SUBTOTAL | | £313.70 |
| PC, Screen & IO Combo | | | | |
| Lenovo ThinkCentre M900 Tiny PC | http://shop.lenovo.com/us/en/desktops/thinkcentre | 1 | £489.00 | £489.00 |
| DELL U2515H ADZG 25-Inch LCD Monitor | https://www.amazon.co.uk/gp/product | 1 | £259.99 | £259.99 |
| Logitech Wireless Combo MK620 UK Layout | https://www.amazon.co.uk/Logitech-Wireless-Combo | 1 | £59.95 | £59.95 |
| | | SUBTOTAL | | £808.94 |
| | | TOTAL | | £15,212.83 |

# Appendix B Operating Procedure

The rig contains two main tanks (each tank is about to contain 30 litres water) and a sump tank (under the bench), three gear pumps driven by external motors, five shut-off valves, six DPVs, three laser sensors, ten pressure sensors and five flow meters. A National Instruments LabVIEW application is installed on the PC positioned in front of the rig to control the system.

1. Before the rig is operating, the operator must make sure that:
    a. The two power supplies are switched on.
    b. The main tanks are filled a required quantity of water (visually inspect the tanks for its integrity and ensure the tanks are intact).
    c. The two CDAQ-9172 devices are switched on.
    d. The button for the motor drives (situated below the emergency button) is switched on.
2. Switch on the PC and launch LabVIEW (open the Main GUI screen in the Fuel rig system project folder):
    a. Before each experiment, run the system first to dispose air and bubbles.
    b. Click the record data button to start recording data.
    c. The five shut-off valves are initially closed.
    d. The three gear pumps can be controlled to run at constant speed. For gear pump 2, it can also be controlled to provide constant flow rate.
    e. The DPV 1, 3, 4, 5 and 6 are initially opened at 100%, the DPV 2 is initially closed. The knobs are used for setting the position (opening percentage) of the DPVs. The DPVs can be controlled manually or automatically. To control the DPVs automatically, open the block diagram and find the DPV mission control unit to load the control file through the ‘Read from Measurement File’ box.

**Emergency Shut Down**

**In the case of emergency push the emergency button on the left hand side.**

3. After experiment finished, the operator must make sure that:
    a. All the tanks are empty after experiment finished.
    b. Switch off both power supplies.
    c. Switch off the button for the drives (situated below the emergency button).
    d. Switch off the CDAQ-9172 devices.
    e. Switch off the PC.

**Protection Measures**

Administrative control measures:

a. Restricted access
b. Warning signs

If in doubt on any aspect of the system, an expert user must be consulted.